1975

The Geochemistry and Origin of Volcanic Features in the Quezaltenango Area

John R. Easter
Oberlin College

John R. Easter
May 8, 1975
Honors Research
Oberlin College

THE GEOCHEMISTRY AND ORIGIN OF VOLCANIC FEATURES IN THE QUEZALTENANGO AREA

Department of Geology
Oberlin College
Oberlin, Ohio 44074

INTRODUCTION

The city of Quezaltenango is located in southwestern Guatemala, approximately 100 kilometers WNW of Guatemala City (see figure 1). The volcanic features of this area represent a portion of the Central American Quaternary volcanic chain. This chain seems to be controlled by the underthrusting of the Cocos plate beneath the Americas and Carribean plates, which occurs in the Middle American trench. The two overriding plates are separated by a left lateral transform fault which, in the Carribean finds topographic expression in the Cayman Trough. Molnar and Sykes (1969) have suggested that faults in eastern Guatemala may represent the continental extension of the transform. Stoiber and Carr (1974) feel that this plate boundary is currently rather inactive. Thus, plate convergence in the Middle American Trench seems to be the dominant tectonic feature. Stoiber and Carr have shown that the associated seismic zone dips at an angle of 30° from the trench to a depth of 100 kilometers. At this point a drop in seismic activity occurs which they attribute to the beginning of melting in the subducted plate. Below 150 kilometers seismicity is evident again, but its position indicates a sharp increase in the dip of the seismic zone. They suggest that the steep dip at the depth where melting occurs may account for the linearity of the volcanic chain.

Stoiber and Carr have divided the Central American volcanic chain into seven segments utilizing differences in the strikes and positions of the volcanic lineaments. They suggest that the offset lineaments are produced by segmentation.

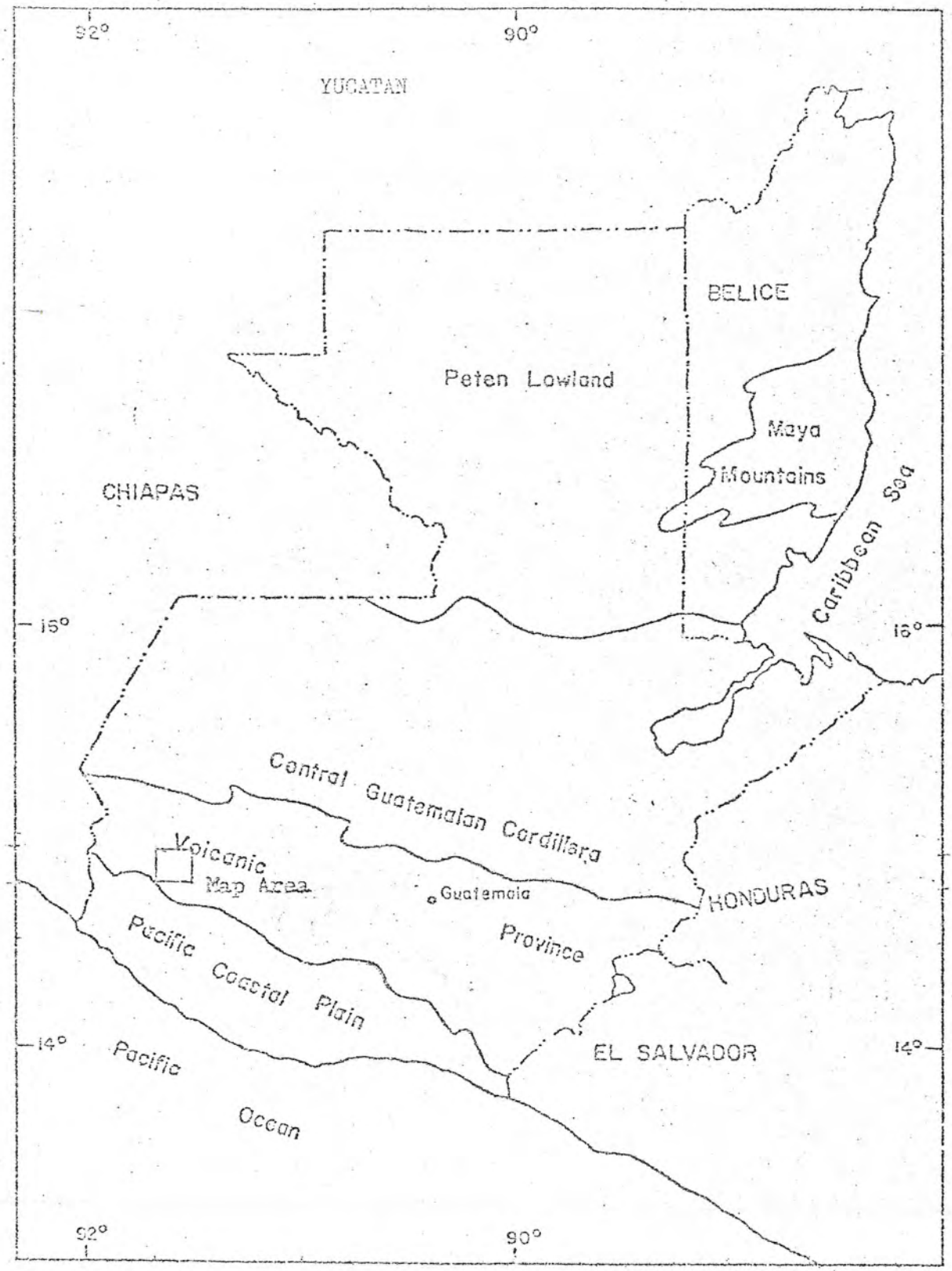

Figure 1 Physicgraphic provinces of Guatemala, from Bonis 1967.

in the underthrust slap. Each of these segments descends at a particular angle. Thus, the depth at which melting occurs can be reached at varying lateral distances from the trench. When the melts rise to the surface, the volcanic chain will appear as a series of offset lineaments. Stoiber and Carr also suggest that the boundary regions between segments are volcanically the most active. These areas are represented by a volcanic sequence alligned perpendicular to the major chain.

The volcanic features of the Quezaltenango area lie in one of the transverse boundary regions defined by Stoiber and Carr. The single dominant linear structure is the Zunil fault.(see fig. 2). In the Quezaltenango area this fault is actually a one kilometer wide zone (Johns 1975). Associated with this zone is the caldera which forms the Almolonga valley. Farther west, the volcanic vents are aligned parallel to the fault zone. This line runs from Cerro Quemado in the north through Volcan de Valle, Santa Maria and finally Santiaguito in the southwest. North of Cerro Quemado lies the flows and domes of La Pedrera and the underlying flows of Llano del Pinal. West of the main transverse trend lies the breached composite cone of Siete Orejas. To the north of all the volcanic vents lies the Quezaltenango valley ignimbrite. Johns has established the relative ages of these units: Siete Orejas, Santa Maria, Volcan de Valle, Volcan de Almolonga, Quezaltenango ignimbrite, Llano del Pinal, La Pedrera, and Cerro Quemado (listed by decreasing age). Each of these units and the Santiaguito dome were examined geochemically, except Volcan de Valle and Volcan de Almolonga. In addition, Siete Orejas will not be discussed here because it does not seem to be associated with the same sequence.

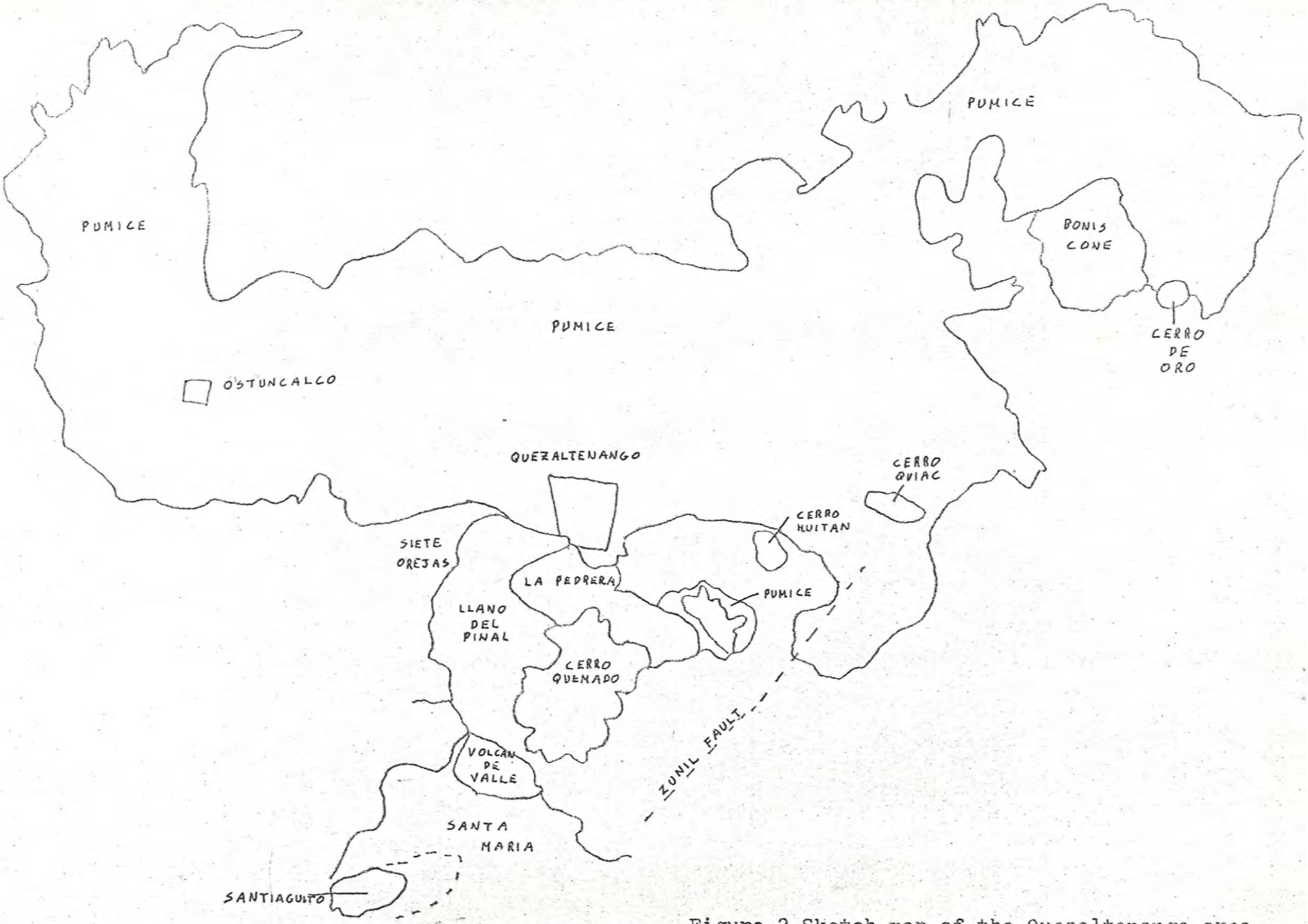

(after Johns, 1975 and MacGinitie 1973)

Figure 2 Sketch map of the Quezaltenango area, showing major volcanic features.

Santa Maria is the largest volcanic structure in the Quezaltenango area, rising to 3772 meters. It is a composite cone which until 1902 was highly symmetrical. In that year an explosive eruption blasted a crater in the southwestern side of the cone and produced an estimated 5.5 cubic kilometers of pumice. It covered a 155 square kilometer area with a 1 meter thick blanket (Sapper 1903 in Rose 1972:35). This material is mostly glass but it contains a few crystal fragments of plagioclase and green hornblende (Rose 1972). According to Johns, the flows within the main cone are basaltic-andesites. They contain plagioclase, olivine, and two pyroxenes (Rose 1975, personal communication).

In 1922, the dacite dome of Santiaguito began to grow in the explosion crater of Santa Maria. Lavas contain plagioclase, hypersthene, oxyhornblende, augite, tridymite, and opaques, but are 70% groundmass (Rose 1972). Two vents - Caliente and El Brujo - are currently active, also producing ash eruptions, nuee ardentes, and fumarolic activity.

Northeast of Santa Maria lies the Cerro Quemado complex which covers 8.5 square kilometers. Johns has distinguished eight flows and two domes and assigned relative ages to them. He describes the lavas as andesites having ten to fifteen percent plagioclase phenocrysts, varying amounts of hornblende and biotite, scattered rounded quartz grains which are occassionally ringed with augite laths, and heavily corroded olivine, in a vesicular to massive groundamss.

Between Cerro Quemado and the city of Quezaltenango lies the La Pedrera complex of domes and flows. The main La Pedrera flow

is a steep sided dacite which covers 2.6 square kilometers and is capped by an andesite plug (Johns 1975). A glassy groundmass is dominant, but phenocrysts of plagioclase, quartz, amphibole, and pyroxene are also present. Due south of and underlying this flow is a fine-grained vesicular hornblende andesite which Johns thinks flowed from the La Pedrera vent. Southeast of the La Pedrera unit lies a rhyolitic flow in which Johns recognized alternating bands of pumice with elongated vesicles and small glass grains grading into a more granular base with glass grains about four millimeters in diameter. He has suggested that Cerro de Sud - a generally rhyolitic dome with a late dacitic stage - may be the source for this flow.

Underlying the La Pedrera units is the porphyritic hornblende andesitic flow of the Llano del Pinal valley. It is a flat lying flow, averaging ten meters in thickness, and covers over ten square kilometers (Johns 1975). This unit overlies the main valley ignimbrite.

The ignimbrite which fills the Quezaltenango valley is a Quaternary rhyolitic pumice. The maximum thickness of the pumice is uncertain, but rivers and road cuts expose over 75 meters of material, while drill holes of 180 meters have failed to reach basement in some areas. Whims (1974) has suggested that the valley formed as a down-dropped graben like block which was later filled with pumice. Charred trees found in the lower part of this sequence have been dated at 35,000 $\pm$ 3000 years (Bonis 1965 in Whims 1974:11). This age has recently been recalculated as 45,000 years (Rose 1975, personal communication).

The dominant unit in the ignimbrite is the flow pumice.

These units represent the high energy eruption of a volatile rich magma. When pressure in the chamber exceeds confining pressure, the magma is erupted explosively with the heavier material given buoyancy by the gaseous phase. This turbulent gaseous cloud then moves downslope as a nuee ardente and deposits its unsorted debris. The bulk of the flow pumice is a friable glassy debris. However, larger more cohesive, white to tan pumice fragments which are sparsely porphyritic are also common. Plagioclase is the most common phenocryst in these fragments. Quartz and small amounts of amphibole and biotite also occur. The flow pumices also contain lithic fragments which range up to one foot in diameter. The upper portions of the flow pumice have been reworked by water.

Above and below the flow material lie units of white airfall pumice. These units exhibit good sorting. The lower unit is topped by a brown soil layer which clearly marks the unconformity below the flow pumice. This layer demonstrates the lack of a close relationship between the two types of pumice. This idea is also borne out by the geochemistry (Easter, 1974).

The problem of identifying the source of the Quezaltenango valley ignimbrite is still unsolved. Gest and Grant (1973) and MacGinitie (1973) have attempted to solve this problem by carefully identifying the extent of the ignimbrite, its exact stratigraphic relationship to other features in the area, and its time relationship to other events. Gest and Grant have identified three possible sources - Siete Orejas, an area south of Totanicapan near Cerro de Oro, and an area north of Cajola and south of Sibilia near the coordinates 54N x 50E (this material

is hypothesized to have flowed northeast toward San Carlos Sija and toward San Francisco et Alto). These conclusions are based on the assumption that the upper surface elevations of the pumice would rise toward the source. Williams (1960) however, suggests only two of these sources - Siete Orejas and the Cerro de Oro area. He found pumice high up on Siete Orejas, far above the valley floor, which suggested an origin there. However, Rose (1972) feels that this is airfall pumice due to the 1902 explosion of Santa Maria. Koch and McLean (1975) suggest that the Quezaltenango ignimbrite is actually only a portion of a much more widespread ash flow covering at least 16,000 square kilometers. They suggest a source in the Quezaltenango-Totanicapan or Lake Atitlan area. Eastward increasing size of lithic fragments in the Quezaltenango ignimbrite suggests a source to the east (Rose, volcanic conference, Oberlin College, 1974). Rose is currently investigating the possibility of a source east of Totanicapan and north of Lake Atitlan.

EXPERIMENTAL METHODS

Preparation of rock powders was done at Michigan Technological University by William Rose, Jr. Major element analyses for SiO_2, Al_2O_3, Fe_2O_3, MgO, CaO, K_2O, H_2O, and TiO_2 were also carried out there. Determinations of Rb, Sr, Zr, Ni, Cr, Ce, Mn, Fe_2O_3, and TiO_2 were made at Oberlin College. Jeff Stein and Katya Levin did much of the work on the Cerro Quemado samples. Katya Levin also analyzed the Santiaguito samples and a few of the ignimbrites for Rb, Sr, Zr, and Ni. The remainder of the approximately 150 samples was run by the author.

Samples analyzed at Oberlin were pressed into powder pellets and run on a General Electric XRD-5 diffraction unit operating at 50 KVP and 40 MA for Molybdenum and Tungsten target tubes. Mass absorption coefficients were determined from the Compton scattering and FeKα peaks according to Reynolds (1963, 1967) and Walker (in press). U. S. G. S. standards DTS-1, G-2, AGV-1, W-1, and BCR-1 were used to determine Compton scattering. GSP-1 was used as the standard for Rb, Sr, and Zr runs, W-1 for the Ni peak, and both GSP-1 and W-1 for the Fe, Mn, Cr, Ce, and Ti determinations. At least every second run, a standard was also run as an unknown to check the accuracy of the method. The results are shown in table 1 of appendix II. This data shows determinations of Rb, Sr, Zr, Fe_2O_3, and TiO_2 to have adequate accuracy. The inaccuracy in determinations of Cr, Ce, and Ni is probably related to their relatively low concentrations. The cause of the moderate inaccuracy in Mn is not evident

Threee FORTRAN IV computer programs written at Oberlin

College were used to compute peak heights and calculate element concentrations. The results for all of the samples are included in table 2 of appendix II. The Fe_2O_3 and TiO_2 data produced at Oberlin seemed somewhat superior to that done at Michigan Technological University, so that it has been used in this paper. A fourth computer program was used to plot the variation diagrams used in this paper. These have been reduced and included in appendix I.

Three parameters - Rb, Sr, and $K_2O/(K_2O + Na_2O)$ - were chosen initially for use in plots against all other elements. Sr correlations provided superior results, probably because of the importance of the crystallization of plagioclase in the chemical evolution of the area. Rb gave decidedly inferior correlations. $K_2O/(K_2O + Na_2O)$ correlations were not as good as Sr, but gross trends could still be recongnized. Figures 3 and 4 show each of these parameters plotted against SiO_2. Note that in each a field of andesite (blue) and dacite (green) can be clearly distinguished, but that the bimodal distribution of the pumice fragments (red) can only be seen in the Sr graph. This bimodality has been shown to be evident for most elements, but not for $K_2O/(K_2O + Na_2O)$ (Easter 1974). Thus the additional scatter of figure 4 can be seen to be critical. Moreover, Bowles, Jack and Carmichael (1973) have shown trace elements to be better indicators in their study of ignimbrites on the ocean floor west of Guatemala. For these reasons, Sr was selected as the key parameter.

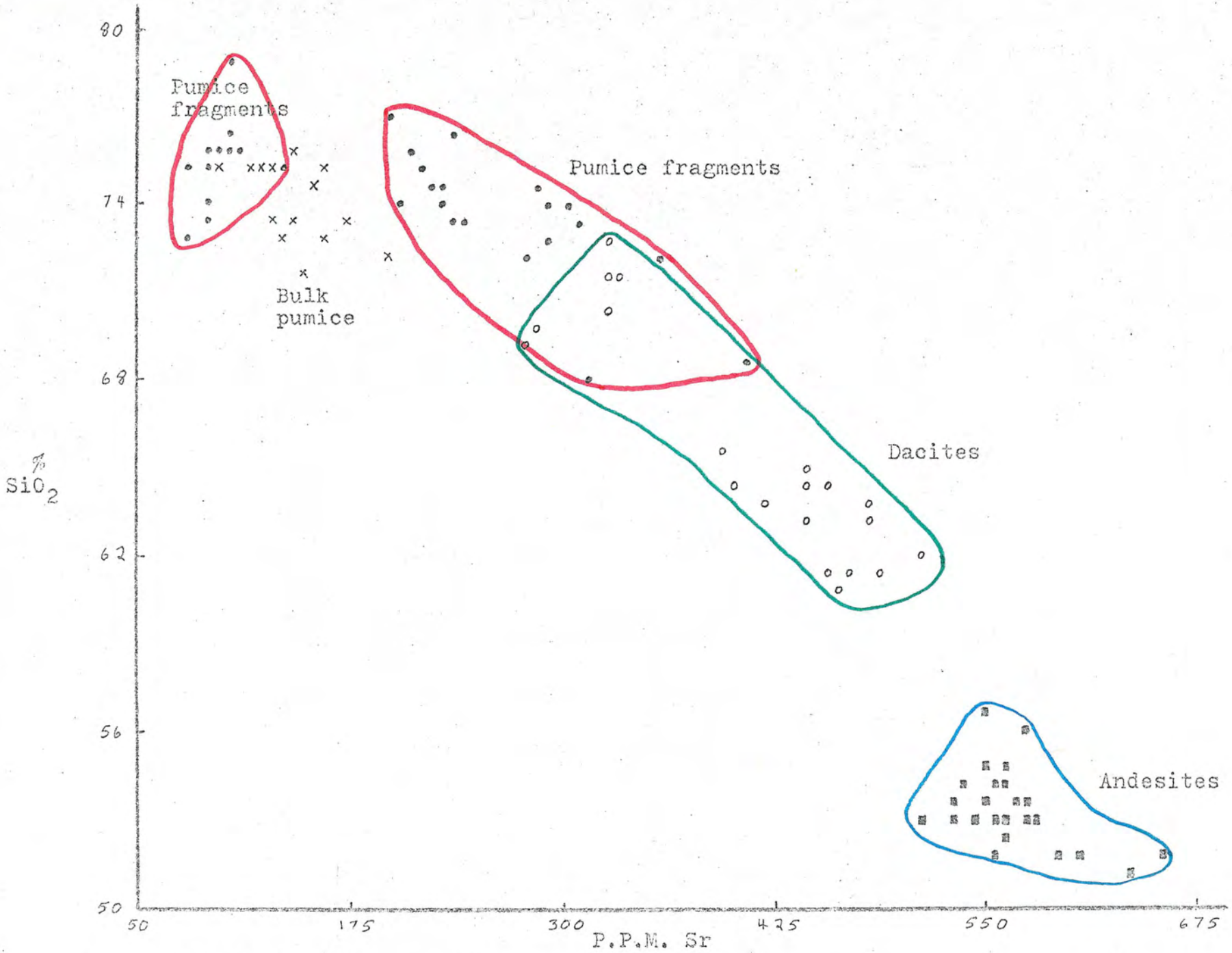

Figure 3 Variation diagram of Sr vs. SiO_2

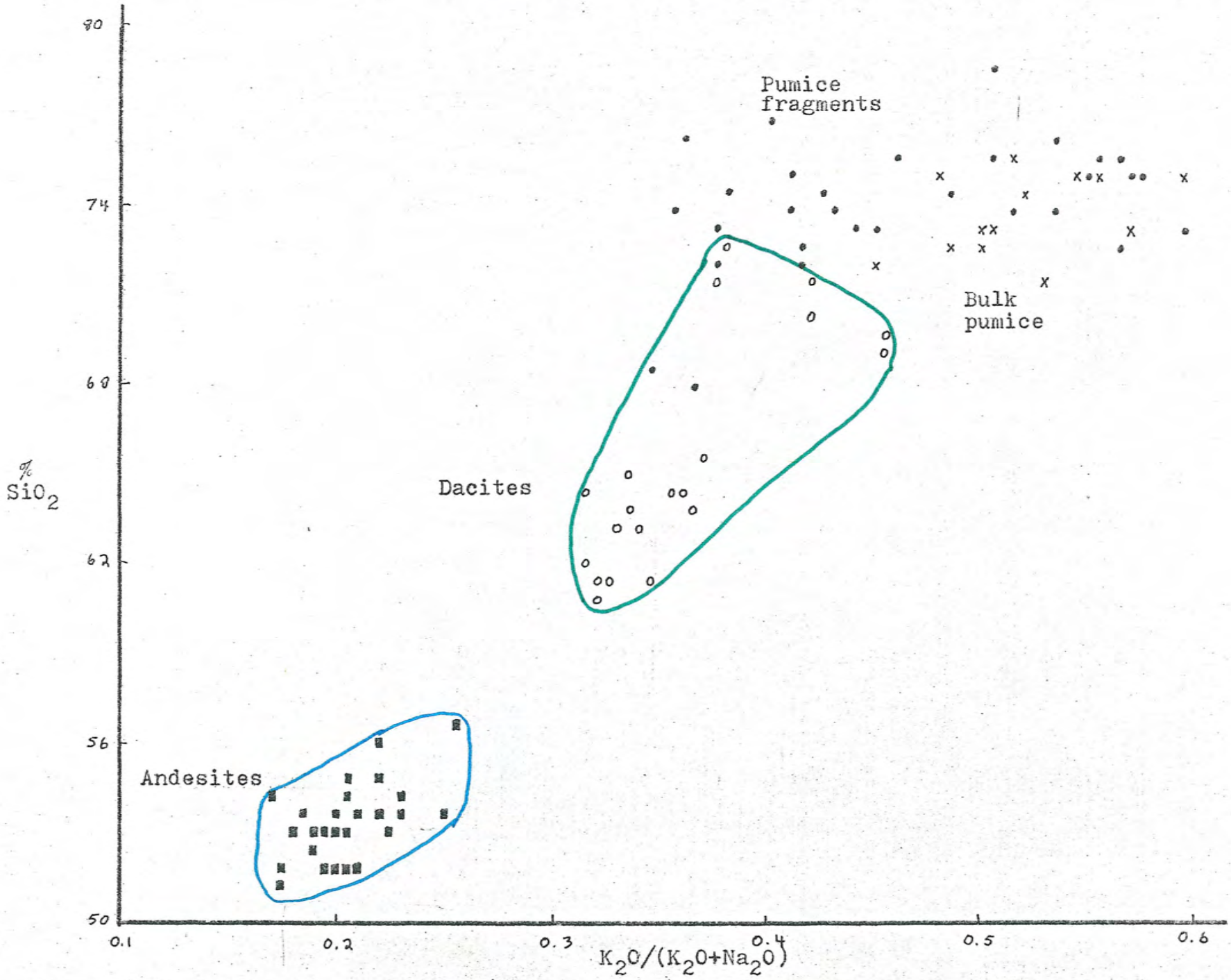

Figure 4 Variation diagram of $K_2O/(K_2O+Na_2O)$ vs. SiO_2

GEOCHEMISTRY

Valley Pumices

Analysis of all the flow pumice samples is represented by the Sr vs. CaO variation diagram of figure 5. Plots for all other elements are on pages 1-3 of appendix I. In these diagrams, two separate fields of pumice fragments can be distinguished. The bulk pumices lie within a relatively limited compositional range which lies between the two fragment fields. It has been shown that the composition of both types of pumice is independent of geographic locality (Easter 1974). It was also shown that the mean composition of the fragments corresponds rather closely to the mean composition of the bulk pumices(Easter, 1974, Rose, memo, October 1974). It therefore seems quite possible that the bulk pumice represents a homogenization of the fragment compositions. A mechanical mixture of two liquids within a turbulent nuee ardente could produce such a distribution. Those small cohesive portions in the nuee which were not mixed would maintain their original chemical identity, producing the chemically bimodal pumice fragments. Most of the material however, would be mixed, giving it a composition closer to the mean for the entire cloud.

Figure 6 illustrates the chemical variation in a stratigraphic section through a single unit of bulk pumice west of Totanicapan. The plots of CaO, Fe_2O_3, Rb, and Sr show a distinct vertical variation. The significance of these elements will be discussed later. At this point it should simply be noted that there is a vertical zonation and that the uppermost material is enriched in CaO, Fe_2O_3, and Sr, and depleted in Rb. Interpretation of this

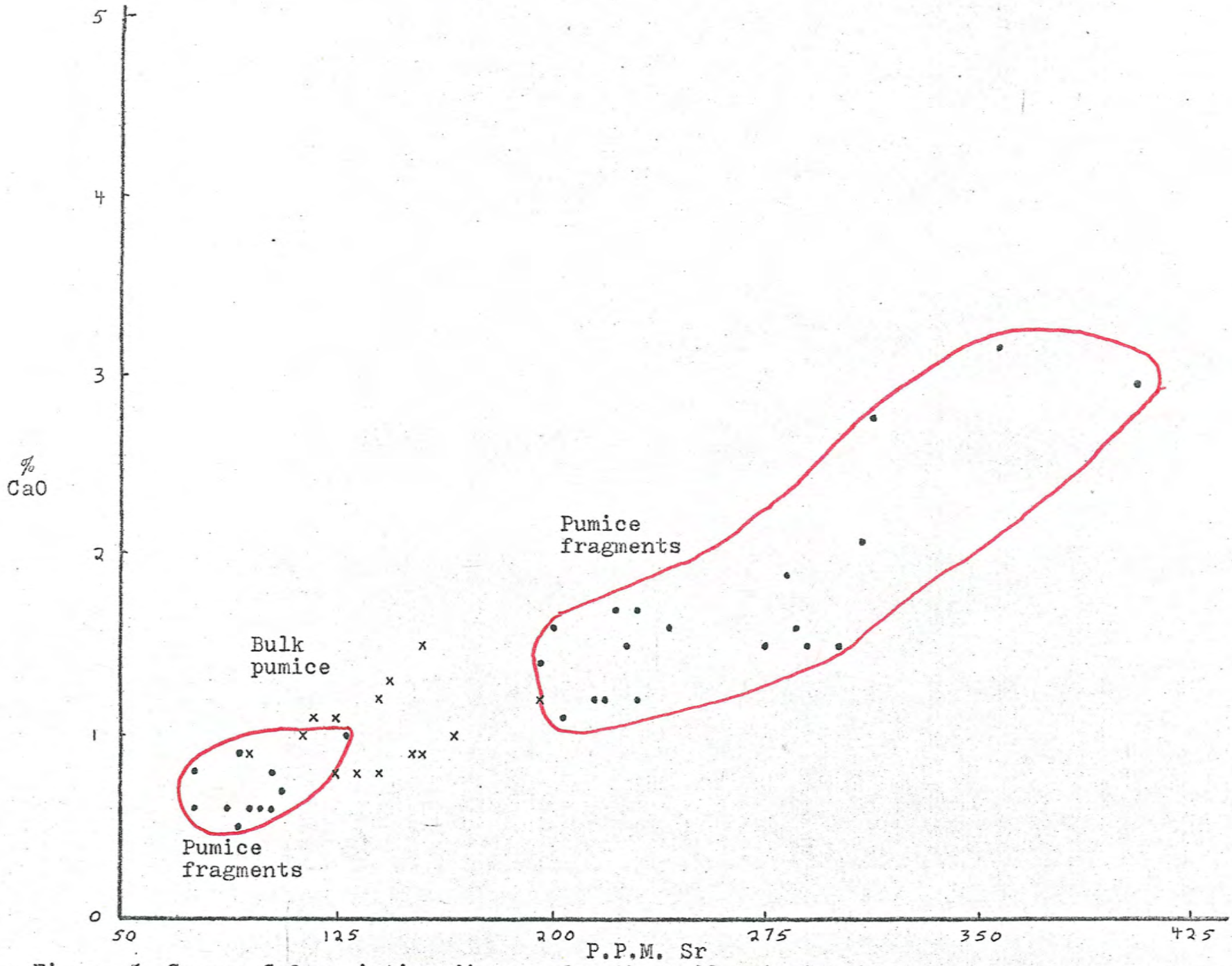

Figure 5 Sr vs. CaO variation diagram for the valley ignimbrites.

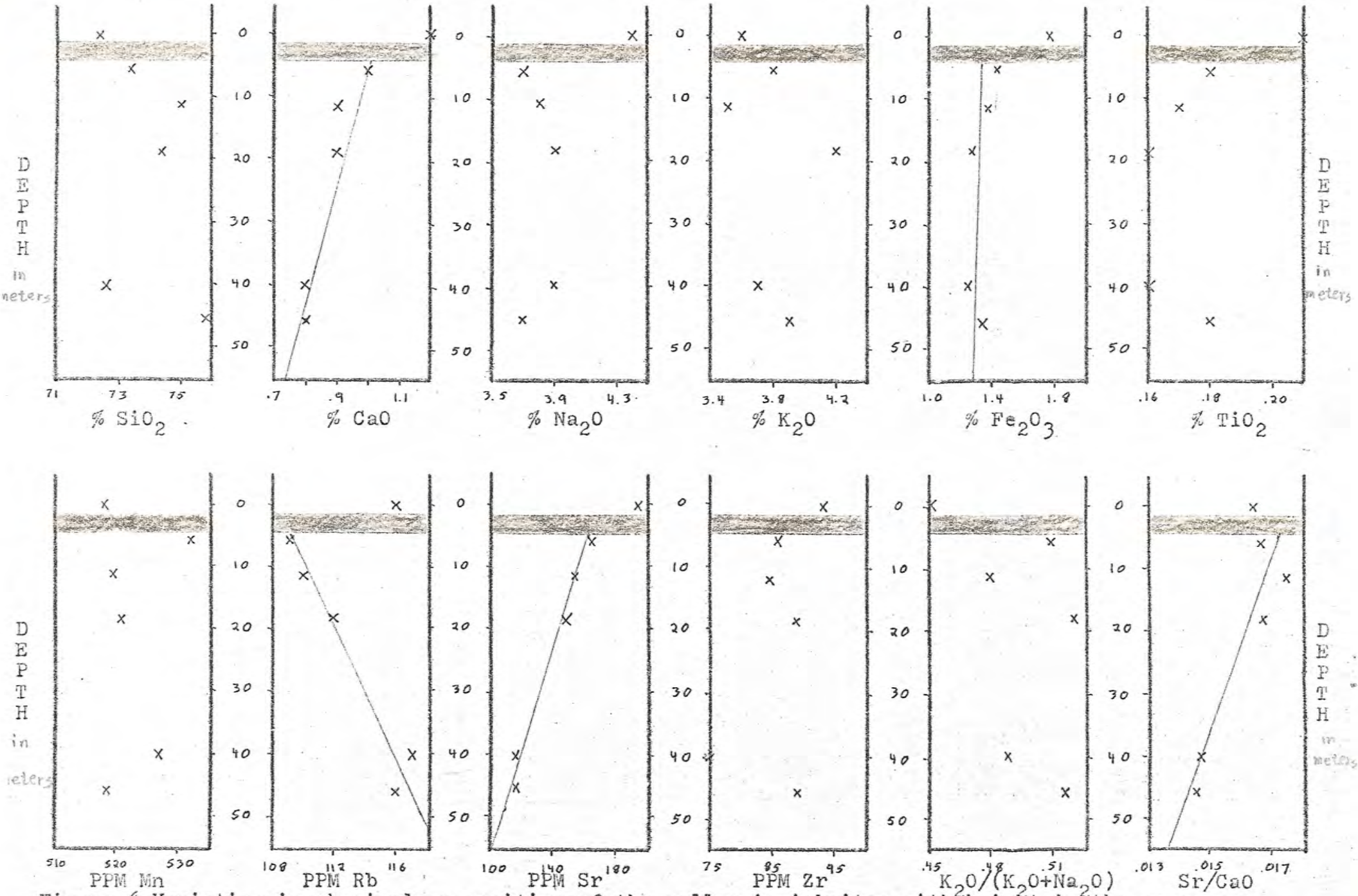

Figure 6 Variation in chemical composition of the valley ignimbrites with height in the sequence. The top sample is separated from the lower unit by a zone of reworked material.

data depends on the significance of height in the sequence. If the material is deposited from different portions of the nuee as they pass over, then the vertical variation reflects change in composition from the first part of the cloud to the last. If, however, all of the ignimbrite unit is deposited at one instant in time by a single portion of the nuee, there is probably little significance to this chemical variation. In fact, it is difficult to see how it was produced. Thus, it seems that the vertical variation does represent a change in composition through time. Moreover, if the composition of the bulk pumice depends on the mixture of two chemically distinct liquids, then the relative amounts of the two liquids must also have varied through time.

Cerro Quemado, La Pedrera, and Llano del Pinal Dacites

A Sr versus SiO_2 variation diagram for samples from Cerro Quemado, La Pedrera, and Llano del Pinal is shown in figure 7 (other examples appear on pages 4-6 of appendix I). It can be seen that there is a gross linear array. The older La Pedrera samples plot at the high silica - low Sr part of the diagram, while the younger Cerro Quemado rocks plot in the opposite corner, suggesting the possibility of chemical evolution. Figure 8 shows further evidence in support of this hypothesis. It is a series of plots of element concentrations against relative age, as determined by Johns for the Cerro Quemado complex. SiO_2 and CaO show distinct trends, and MgO, Fe_2O_3, TiO_2, Rb, Zr, and Sr suggest trends. These trends are in agreement with those suggested by chemical differences between Cerro Quemado and La Pedrera. Such evidence for differentiation of a parent magma has also been given by Levin (1974) and

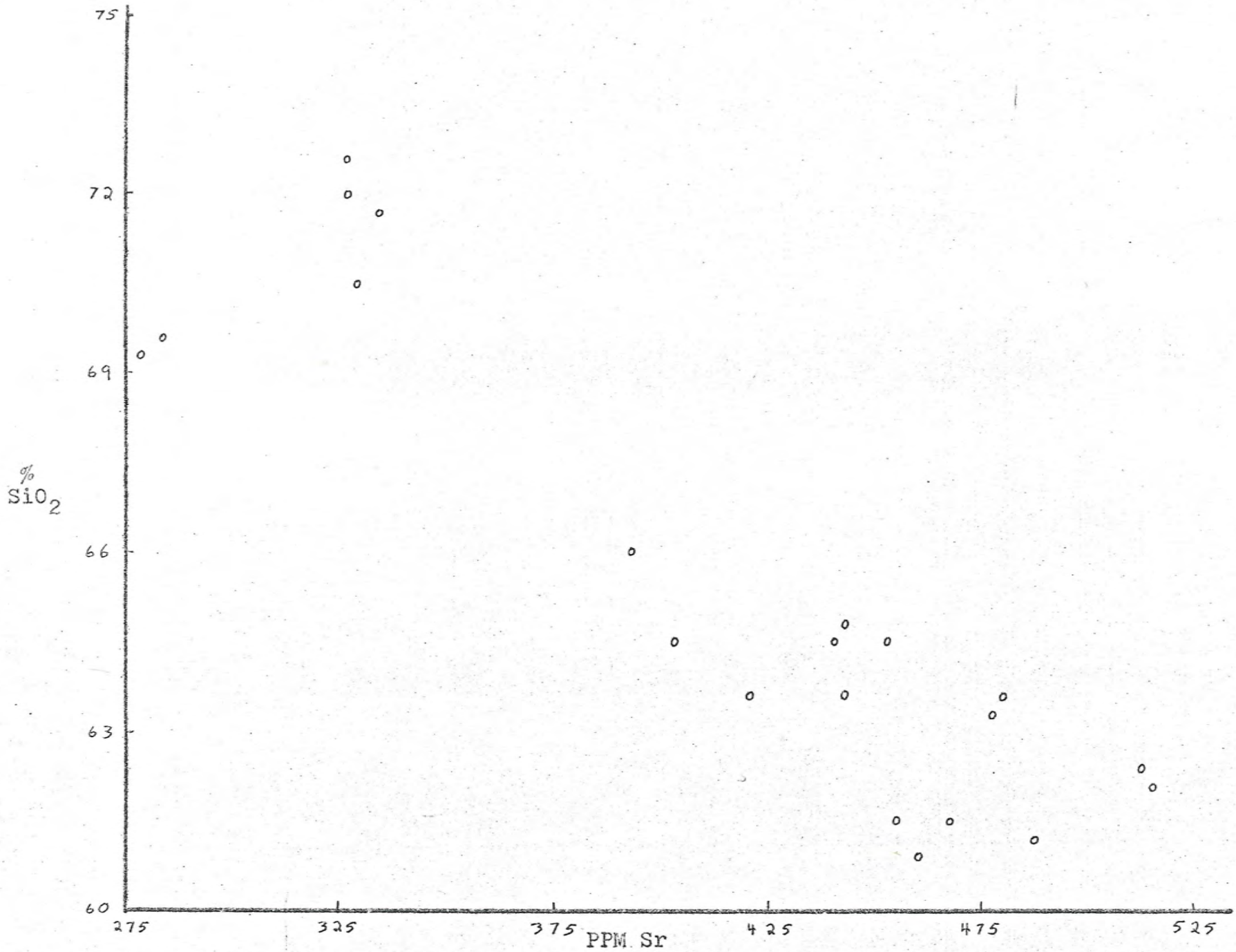

Figure 7 Variation diagram of Sr vs. SiO_2 for the Cerro Quemado, La Pedrera, and Llano del Pinal dacites.

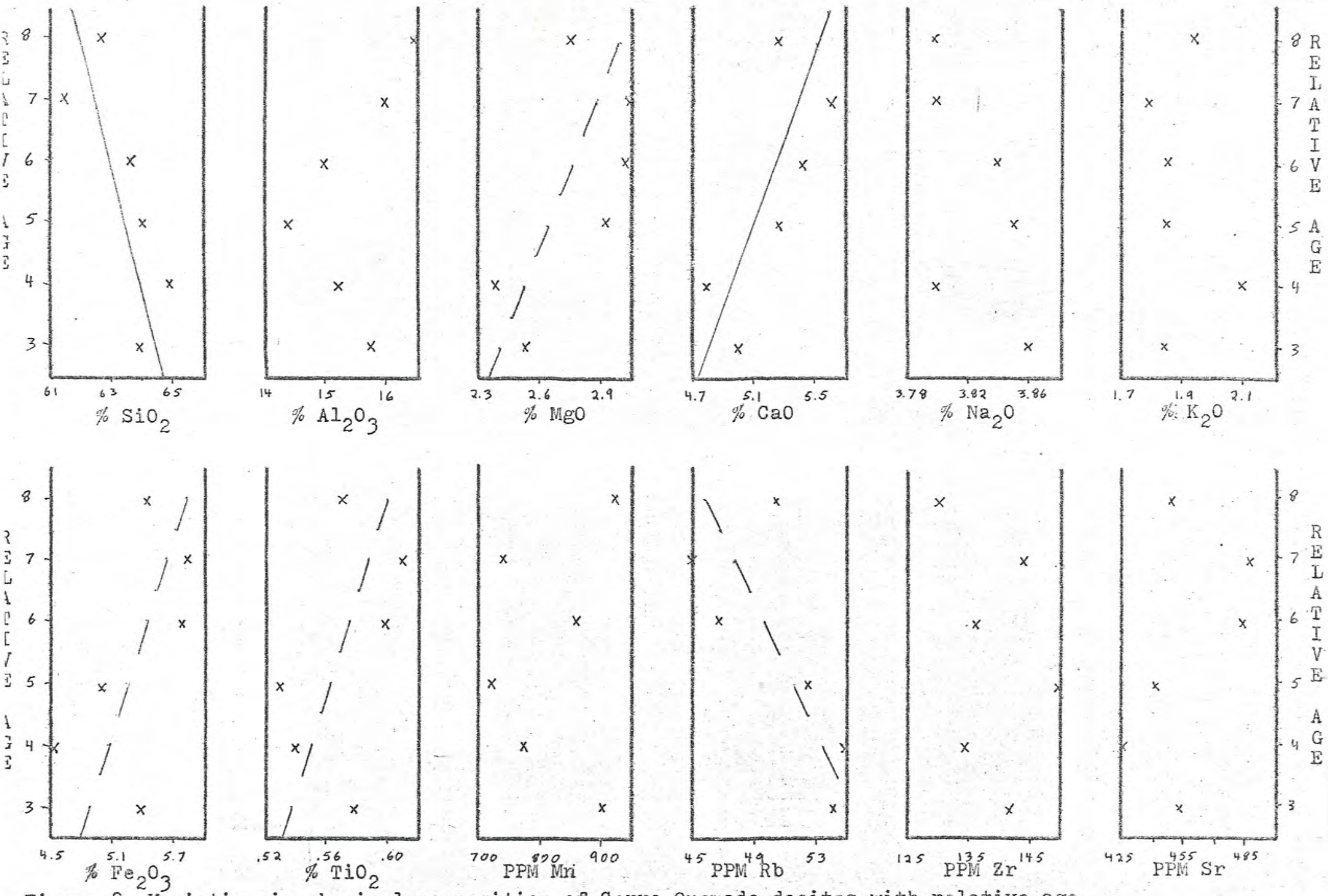

Figure 8 Variation in chemical composition of Cerro Quemado dacites with relative age.

Johns (1975).

The acceptability of a crystal fractionation model to account for the variation was tested utilizing a technique which Noble and Korringa (1974) used in the Quaternary lavas of Oregon. Phenocrysts were separated from six Cerro Quemado whole rock samples. Element concentrations were then calculated for the phenocryst and groundmass phases. The results are illustrated in figures 9 and 10. (Other examples appear on pages 7 and 8 of appendix I.) These diagrams show the whole rock samples for all of the dacite samples and the phenocryst and groundmass compositions for the six separated samples. Tie lines drawn from the whole rock samples to the groundmass represent the chemical evolution of the residual liquid during crystallization. Parallelism between these tie lines and the entire field suggest that the whole rock field has also developed by fractional crystallization. Such parallelism is evident in the plots of CaO, K_2O, and Rb against Sr. Other plots such as that of Fe_2O_3 versus Sr (figure 10) show no parallelism between tie lines and whole rock fields. This shows that partitioning of these elements between the liquid and crystal phases was not particularly significant. The behaviour of those elements which are significant can be explained by the crystallization of plagioclase. The relative ages of the dacites show that the most differentiated magma is the earliest to be erupted. This suggests a fractionating magma column, zoned by gravitational setting, in which the most differentiated liquid is at the top. The magma is tapped intermittently each time drawing from a lower portion of the zoned magma. In this way, the extrusive units become more mafic through time,

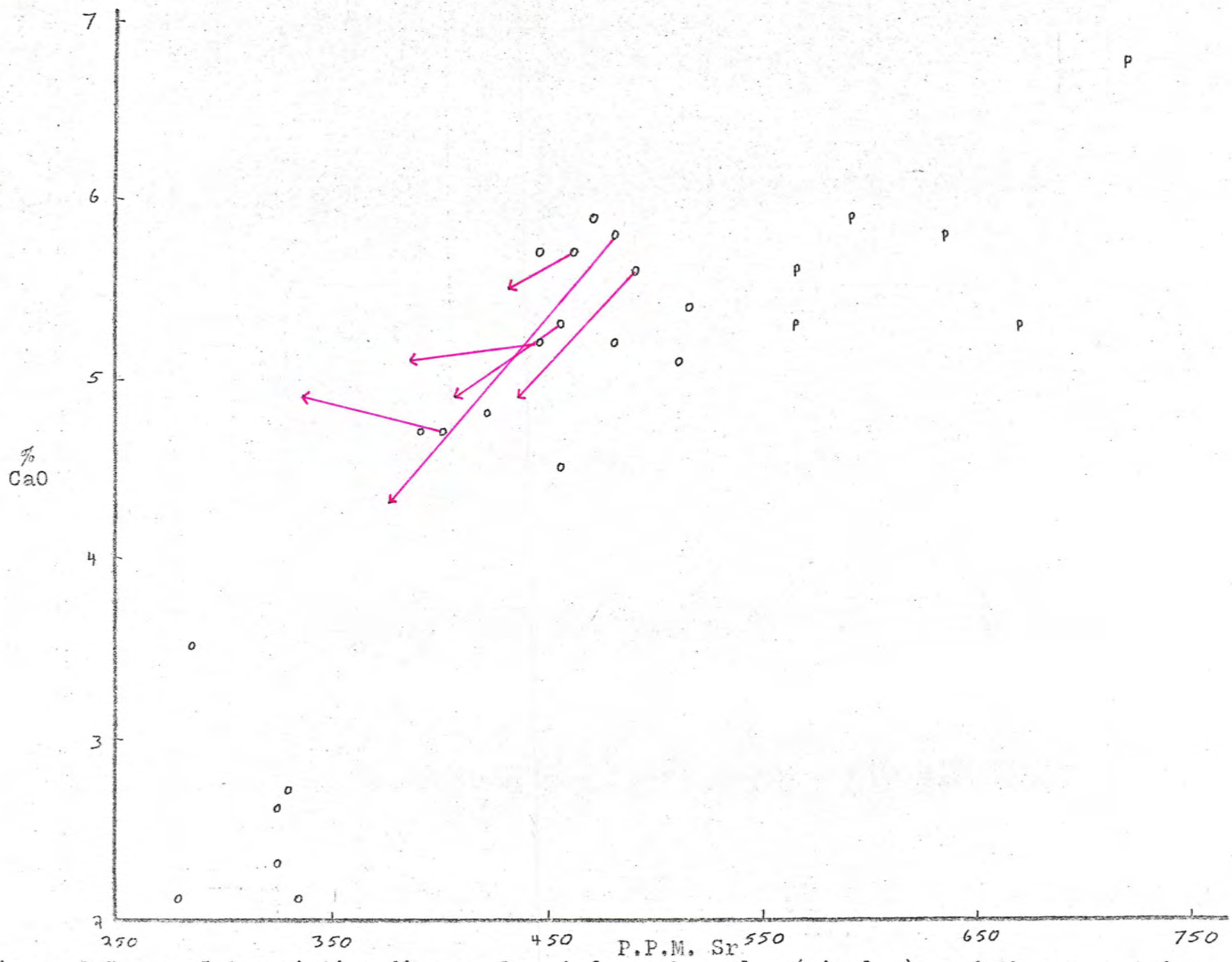

Figure 9 Sr vs. CaO variation diagram for whole rock smples (circles), and the separated groundmass (tip of arrow) and phenocryst phases (P) from the Cerro Quemado and La Pedrera dacites. Tie lines indicate compositional evolution of the residual liquid.

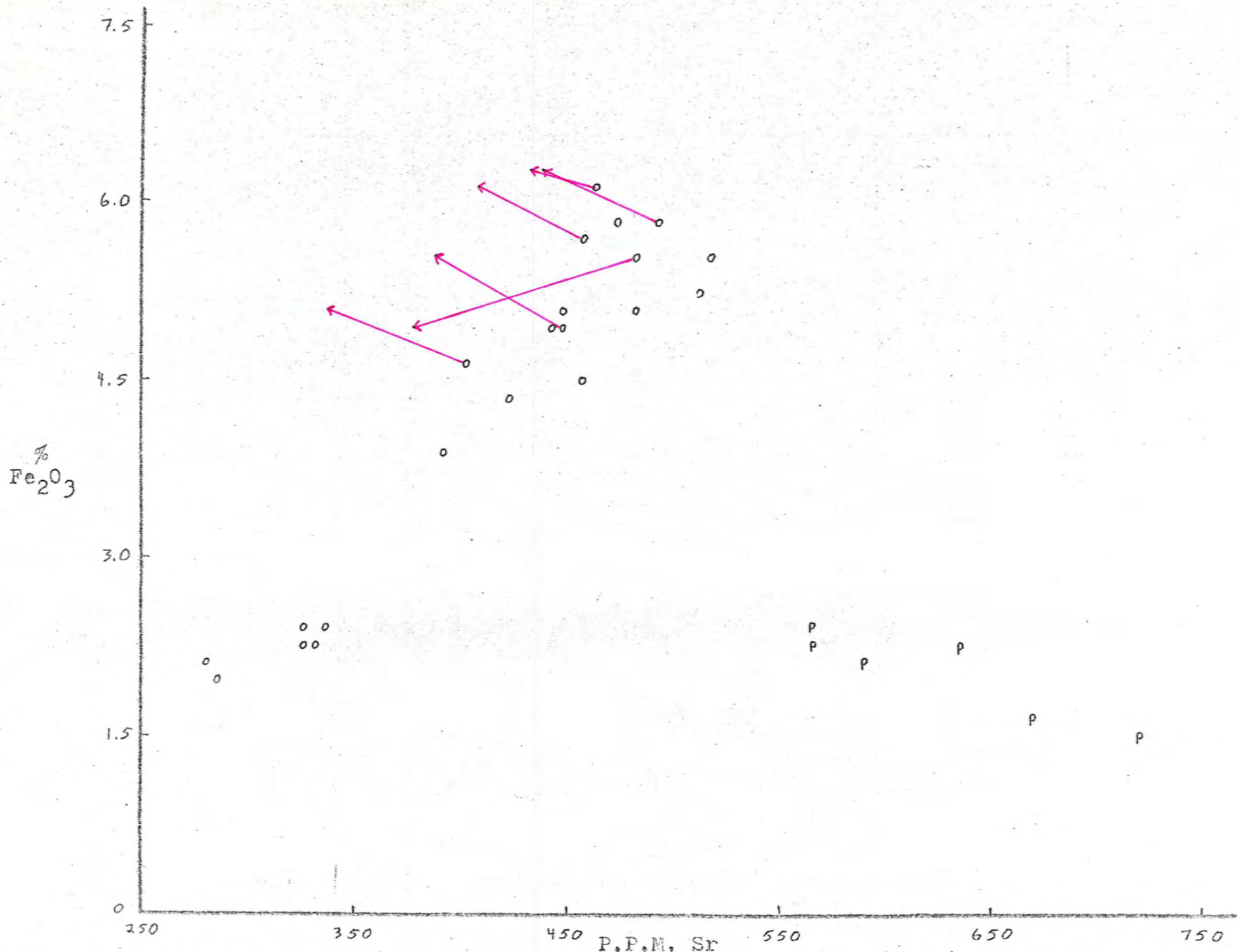

Figure 10 Sr vs. Fe_2O_3 variation diagram for whole rock samples (dots) and the separated groundmass (tip of arrow) and phenocryst (P) phases from Cerro Quemado and La Pedrera. Tie lines indicate compositional evolution of the residual liquid.

the later liquids being enriched in Al_2O_3, MgO, CaO, Fe_2O_3, TiO_2 and Mn and depleted in SiO_2, K_2O, Rb, and Zr.

Santa Maria Andesite

The structure of Santa Maria's cone is dissected by the large 1902 explosion scar. Twenty-six flows from the wall of the crater were sampled. These flows represent about 1/3 of the exposed material, the remainder being composed of pyroclastic materials. This section of the cone represents 40% of the total volume (Rose, memo, January 1974). However, no consistent geochemical variation can be recognized in this stratigraphic section. Rather, the andesite seems to be chemically monotonous, causing all samples to plot in a small field (see figures 11, 12, and 13).

Andesites, Dacites, and Rhyolitic Pumices - A Model

The common occurrence of andesitic volcanoes, dacitic domes, and ignimbrites in close proximity to one another suggests that they may be genetically related. With this possibility in mind, variation diagrams incorporating all of the samples discussed were drawn. In the plot of Sr against K_2O (figure 11) it can be seen that all four sample types - pumice fragments, bulk pumices, dacites and andesites - lie along a linear trend. The graph of Sr against Fe_2O_3 (figure 12) shows the andesites and dacites lying along one line and the pumices lying along a different line. The two trends intersect at one end of the compositionally more variable pumice fragments group and form an angle of approximately 30°. In the diagram of Sr against Zr (figure 13) two distinct trends are again evident, but in this case their directions differ by 90°, again they intersect at the end of one of the fragment groups. Further examples of these variation

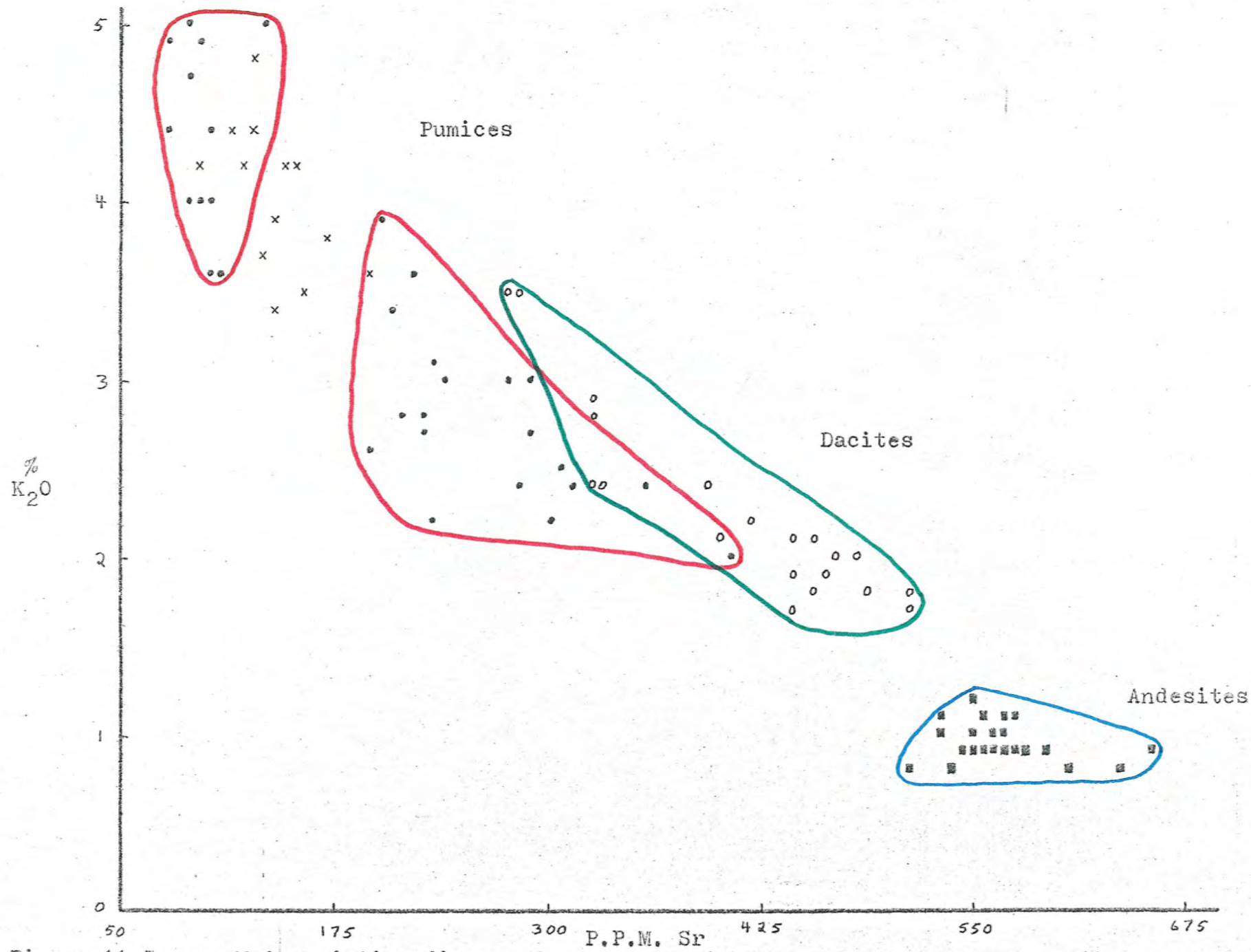

Figure 11 Sr vs. K_2O variation diagram for Santa Maria andesite, Cerro Quemado and La Pedrera dacites, and the rhyolitic valley pumice.

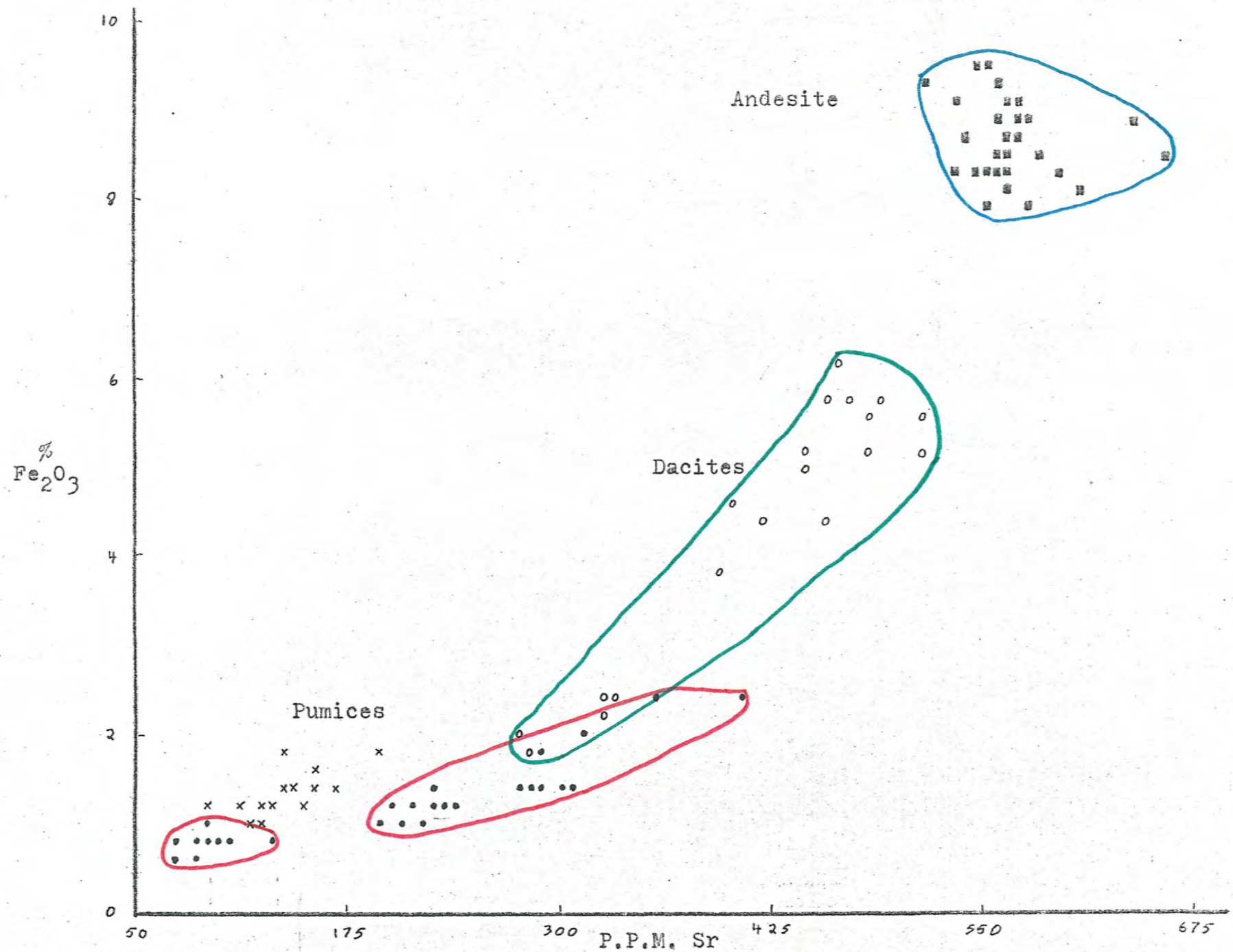

Figure 12 Sr vs. Fe_2O_3 variation diagram for Santa Maria andesite, Cerro Quemado and La Pedrera dacites, and the rhyolitic valley pumice.

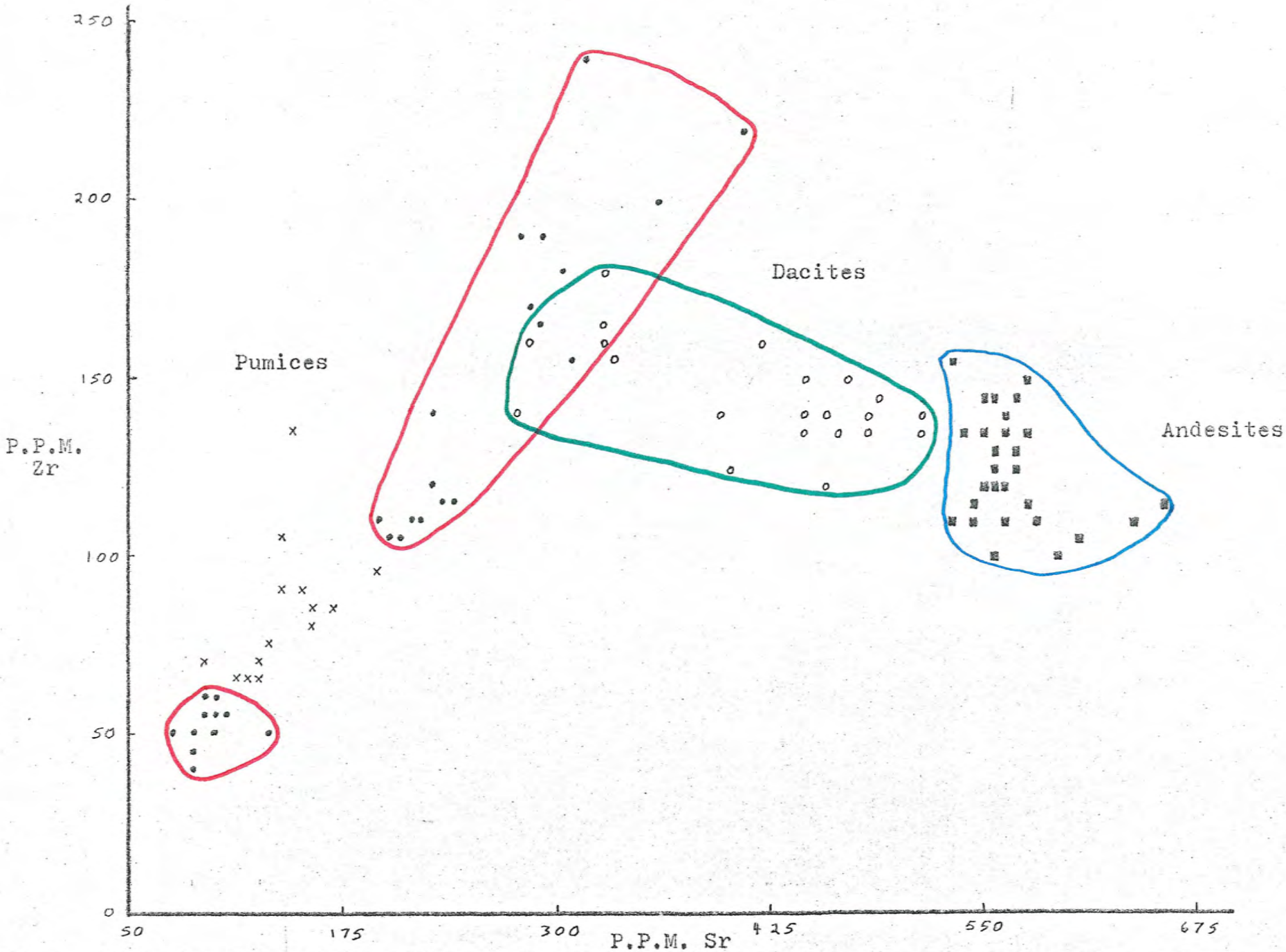

Figure 13 Sr vs. Zr variation diagram for Santa Maria andesite, Cerro Quemado and La Pedrera dacites, and the rhyolitic valley pumices.

diagrams are given on pages 9-11 of appendix I. It has already been shown that the compositional evolution of the dacites is due to fractional crystallization. The colinear relationship of the andesites to the dacites suggests that they also represent a portion of the zoned magma. They are more mafic and clearly therefore originated lower in the column. It is obvious that the pumice compositions cannot be explained by the same simple fractionation model. It would not provide two chemically distinct magmas, and cannot explain the discrepant trends unless a new mineral phase had begun to crystallize. The influence of plagioclase on the composition of both pumices and dacites has already been demonstrated. The inabundance of other phenocryst mineral phases relative to plagioclase suggests that no sharp break in the chemical trends would be expected. Thus, another mechanism must be found.

Several pumice fragments show signs of immiscibility on a very small scale -1/10 micron (Rose 1975, personal communication). This suggests the possibility that the chemically bimodal distribution of the fragments may represent two immiscible liquids. Figure 14 shows two sketches of hypothetical phase diagrams for the system. A liquid of initial composition L_1 (figure 14A) evolves through fractional crystallization of B toward point C. At this invariant point the following reaction occurs:

Liquid (C) $\rightarrow$ B + Liquid D

During the course of this reaction, two immiscible liquids coexist. This model explains both the fractionation trend of the dacites and andesites and the bimodal chemistry of pumice

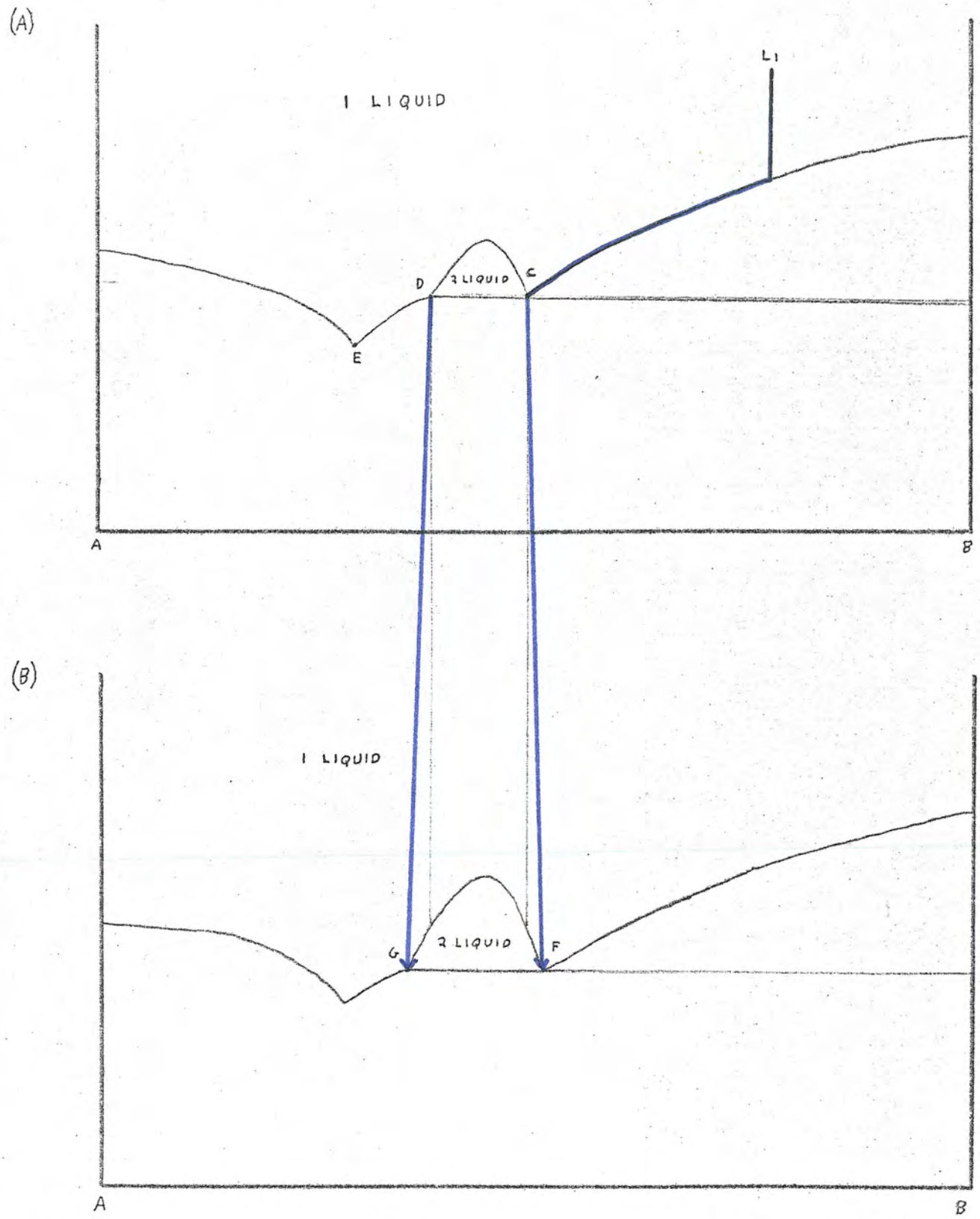

Figure 14 Two hypothetical phase diagrams showing the compositional evolution (blue line) of the parent magma due to fractional crystallization and immiscibility. The cross-section of the two liquid field in figure A shows the two liquids C and D to be more similar in composition than liquids F and G of figure B.

fragments. It can also be seen that the vertical zoning of the bulk pumices is accounted for. The uppermost portion of the zoned magma column represents the most evolved liquid. This liquid may even have completed the reaction at C, and therefore shows no signs of immiscibility. Liquid slightly lower in the column would not have completed the reaction, however, and would actually consist of two immiscible liquids C and D. The lower the initial liquid is in the column, the less the extent of reaction and the smaller the amount of liquid D and the greater the amount of liquid C. Clearly, the bulk composition of the pumices which has been shown to be a mechanical mixture of these two liquids must reflect their relative proportions, thus producing the vertical variation. Preservation of this vertical variation also shows that the immiscible liquids have not separated into discreet layers, but have simply formed blebs.

It must be remembered that representation of the system by this simple two component phase diagram is a great oversimplification. Consideration of a third dimension provides some insight into the small-scale immiscibility found by Rose. If, after the liquid has separated into the two immiscible phases C and D of figure 14A crystallization of another phase drives them down thermal valleys toward F and G (figure 14B), it is clear that further immiscibility will result. The cross section of the two liquid field shown in figure 14B shows the two immiscible liquids to differ more in composition than do the earlier immiscible liquids C and D of figure 14A. If each bleb behaved as a closed system, the immisciblity would be preserved, producing the signs of unmixing which Rose observed.

The model proposed here accounts for the chemical bimodality of the pumice fragments, the signs of immisciblity found in them, and the compositional zoning of the bulk pumices. It explains the lack of colinearity between the pumice trends and the andesite-dacite trend in variation diagrams. Clearly, the distribution coefficients between two immiscible liquids will not be the same as those between the crystal and liquid phases of the fractionation system. It also explains the continuity of the variation curve inspite of the break in slope between the two trends. In fact, it isn't apparent where the fractionation sequence ends and the immiscibility begins. In any of the variation diagrams, some of the pumice fragments lie at the intersection of the trends and could have been produced by either process. However, in the phase diagram of 14A, the compositon of liquid C which makes the border between the fractionation and immiscibility systems, is produced by fractionation. It therefore seems r reasonable that the composition of some of the pumice fragments is due only to crystal fractionation and not to liquid immiscibility (see figure 15). This also places the bulk pumices closer to the edge of the fractionation field, and, as the model predicts, shows their compostional range to approximate that delineated by the two immiscible liquids (pumice fragments).

Santa Maria Andesite, Santiaguito Dacite, and the Pumice from the 1902 Explosion

As was mentioned in the introduction, the composite cone of Santa Maria was disrupted by an energetic eruption in 1902. This activity produced the explosion crater on the southwest side of the cone and spread pumice over a reasonably widespread

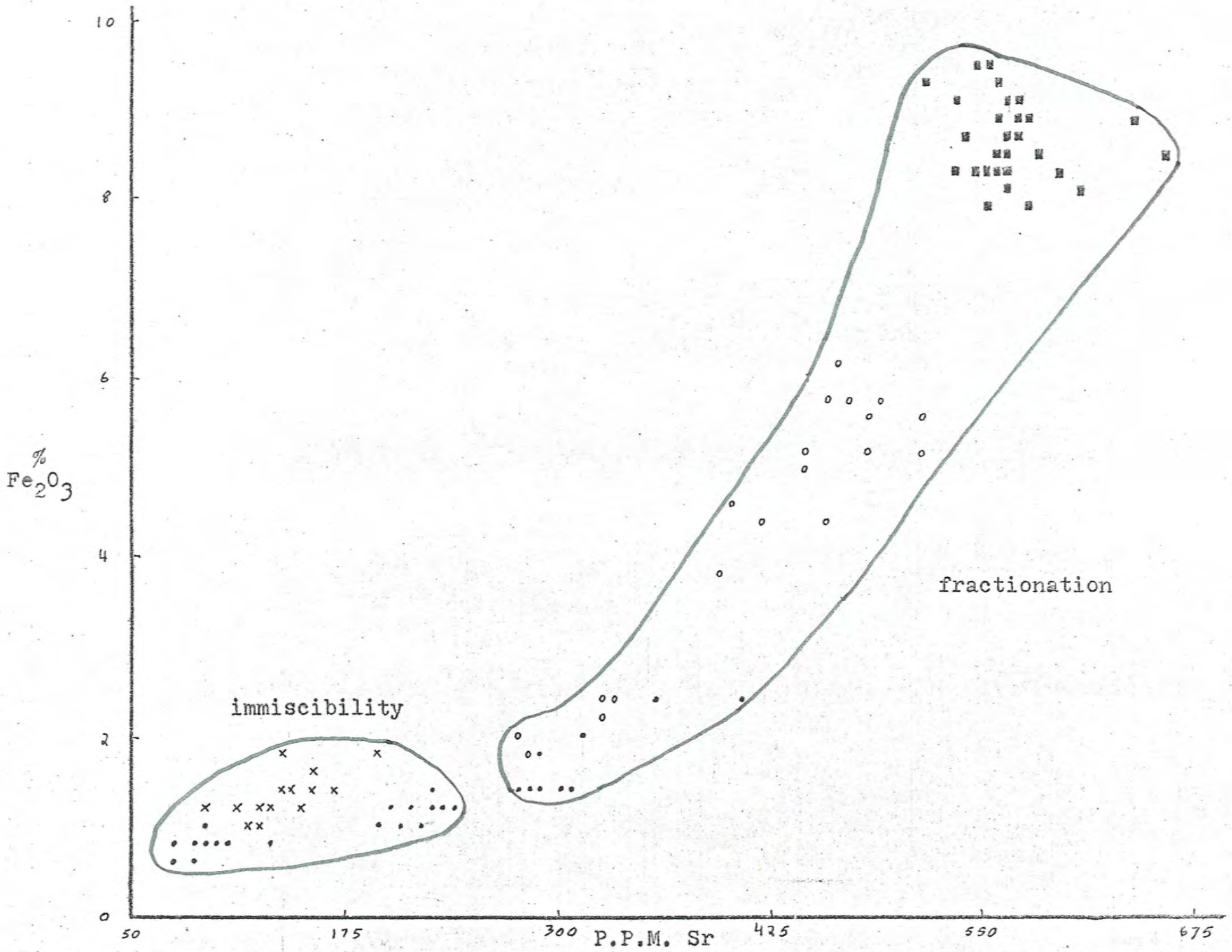

Figure 15 Sr vs. Fe_2O_3 diagram for Santa Maria, Cerro Quemado, La Pedrera, and the valley pumice, showing which compositions result from immiscibility and which were produced by fractional crystallization.

area. In 1922, the crater became the site of extrusion of the Santiaguito dacite dome. Figure 16 shows a Sr against Fe_2O_3 variation diagram for samples of these three units (other diagrams appear on pages 12-14 of appendix I). Comparison of this plot with that for Santa Maria, Cerro Quemado, and La Pedrera (figure 12) shows an incredible similarity in trends. The 1902 pumice field is compositionally restricted because it has been determined by a single sample. The compositional evolution of the dacite is severely restricted because the succession represents only 53 years. Thus, the major difference between the two plots is the compositional range of the overall sequence, which is more restricted in the case of Santa Maria, Santaiguito, and the 1902 pumice. Therefore, it seems that this suite may represent a similar fractionation sequence but that differentiation of the upper liquids in the column did not proceed as far.

Cerro Quemado, La Pedrera, and Llano del Pinal

When these dacites were considered earlier, it was shown that they represented a fractionation suite and that this expected compositional evolution was found from the relatively older feature, La Pedrera, to the younger domes and flows of Cerro Quemado. However, there is an additional subtlety to this evolution of the dacites. The Llano del Pinal flows undelie and, therefore, predate the La Pedrera flows. Yet in figure 17 it can be seen that the two Llano delPinal samples lie in the middle of the Cerro Quemado field and are therefore similar to this late feature while the La Pedrera rocks of an intermediate age are less mafic (other variation diagrmas are shown on pages 4-6 of appendix I). This chemical evolution is also shown by the

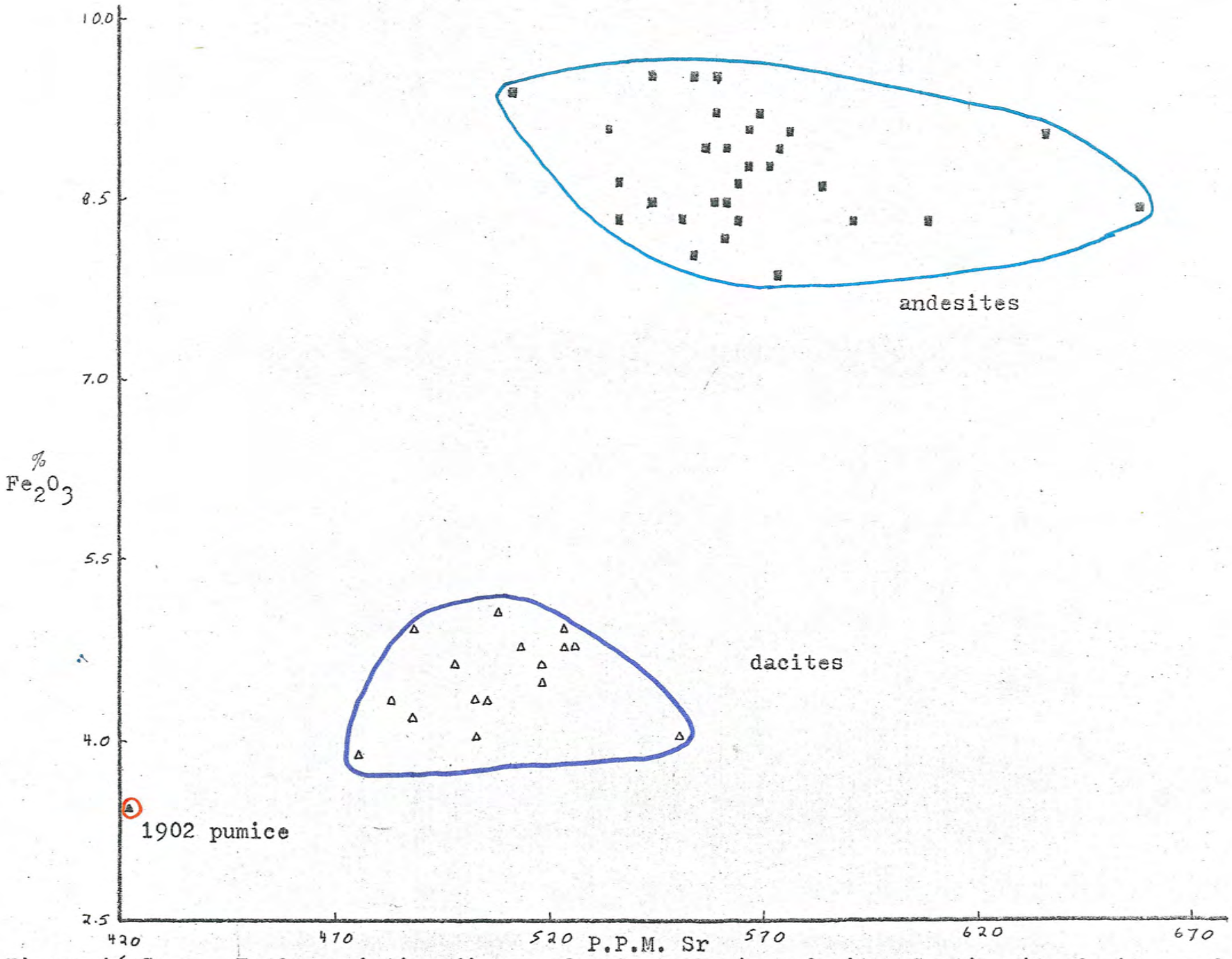

Figure 16 Sr vs. Fe_2O_3 variation diagram for Santa Maria andesite, Santiaguito dacite, and 1902 pumice.

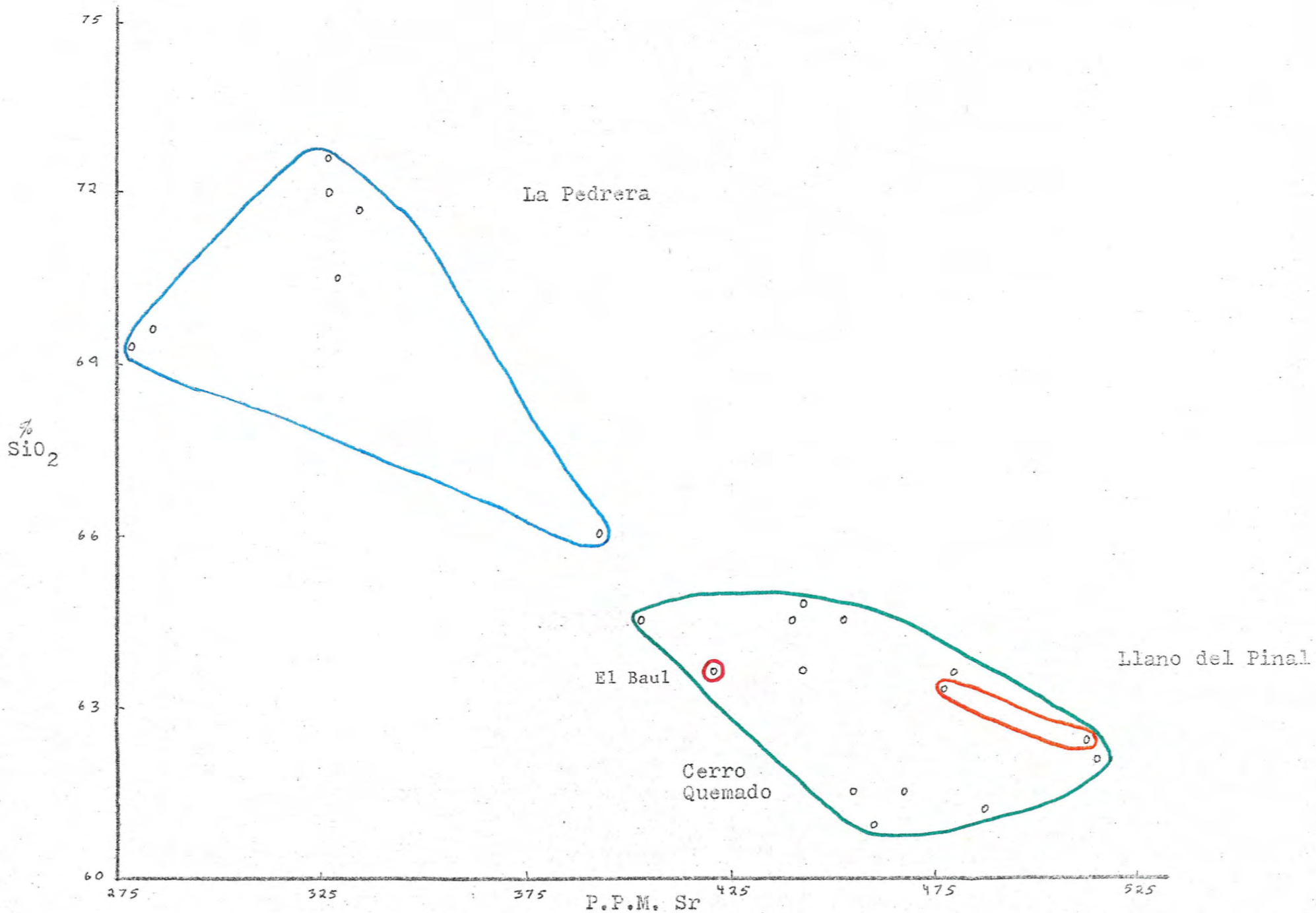

Figure 17 Sr vs. SiO_2 diagram for Llano del Pinal, La Pedrera, and Cerro Quemado dacites.

classification of Johns. He considers the Llano del Pinal flows to be andesitic, the lower La Pedrera flows and domes to be pumiceous rhyolite, the upper La Pedrera flows and domes to be dacitic and the Cerro Quemado complex to be andesitic. It seems that this sequence may be a smaller scale example of fractionation. A magma of composition similar to that of Llano del Pinal differentiated through crystal fractionation and settling, producing a zoned column. The upper part of this liquid was tapped first, producing the rhyolite. Subsequent eruptions extruded the more mafic magma from lower in the chamber. Thus, the composition evolved back to that of Cerro Quemado.

SUMMARY AND CONCLUSIONS

Samples from the Quezaltenango area have been separated into three sequences, each of which has been considered separately. It has been shown that the geochemistry of the area has been dominated by the process of fractional crystallization, followed by a gravitational settling of crystals. This conclusion is based on the general linearity of the dacite-andesite trend, and the parallelism between this trend and the whole rock-groundmass tie lines, which can be seen in some variation diagrams. Only in the case of the valley ignimbrites is it necessary to invoke another mechanism. In these rocks the chemically bimodal distribution of the cohesive pumice fragments and the correspondence of their mean composition to the mean composition for the smaller friable debris suggests mechanical mixing of the fragments to form the bulk pumice. The two liquids represented by the pumice fragments were probably produced in the upper portion of the magma chamber by liquid immiscibility. Vertical compositional variations in the bulk pumice, similar to those in other uints of the area suggest that the immiscible liquids of the magma simply represent a further evolved portion of the fractionation series.

Very little has been said about the mineralogy of the crystallizing phases because very few samples were available for thin sections. In general, however, simple correlations can be made between the geochemical parameters which show good correlation in a rock unit and the mineralogy of the phenocrysts. The distribution of CaO, Sr, and Fe_2O_3 in the ignimbrites are probably related to the abundance of plagioclase and lesser

amounts of amphibole and biotite. In the dacites SiO_2, CaO, MgO, Fe_2O_3, TiO_2, Rb, and Sr show correlations, and the stable phenocrysts include plagioclase, quartz, hornblende, augite, and biotite. The differentiation which has occurred between phenocrysts and groundmass in the dacites, causing depletion of Sr and CaO in the final liquid and enrichment in K_2O and Rb, suggests that crystallization of plagioclase is dominant in the late stages. Although no chemical trends were observed in the andesites, their chemistry almost certainly depends on crystallization of plagioclase, olivine, and two pyroxenes.

The samples from Santa Maria were used in this paper in two sets of graphs. They represent the youngest member of the valley ignimbrite - La Pedrera - Cerro Quemado - Santa Maria series and the oldest member of the Santa Maria - 1902 pumice - Santiaguito sequence. These two groups can be put together, giving a single volcanic sequence. The variation diagrams of figures 18 and 19 show the overall geochemical evolution of the Quezaltenango area. It can be seenthat crystal fractionation has occurred within the magma chamber on two separate occasions. The first magma which probably originated as a partial melt associated with subduction, rose to the chamber. There it was chemically zoned by crystal fractionation. This source was intermittently tapped by the overlying volcanoes, each subsequent eruption extruding liquid from lower in the zoned sequence. As the chamber was emptied from the top, new melts entered from the underlying subduction zone. These were also fractionated, either during their rise to the surface, or while they sat in the chamber. Portions of this sequence are currently being

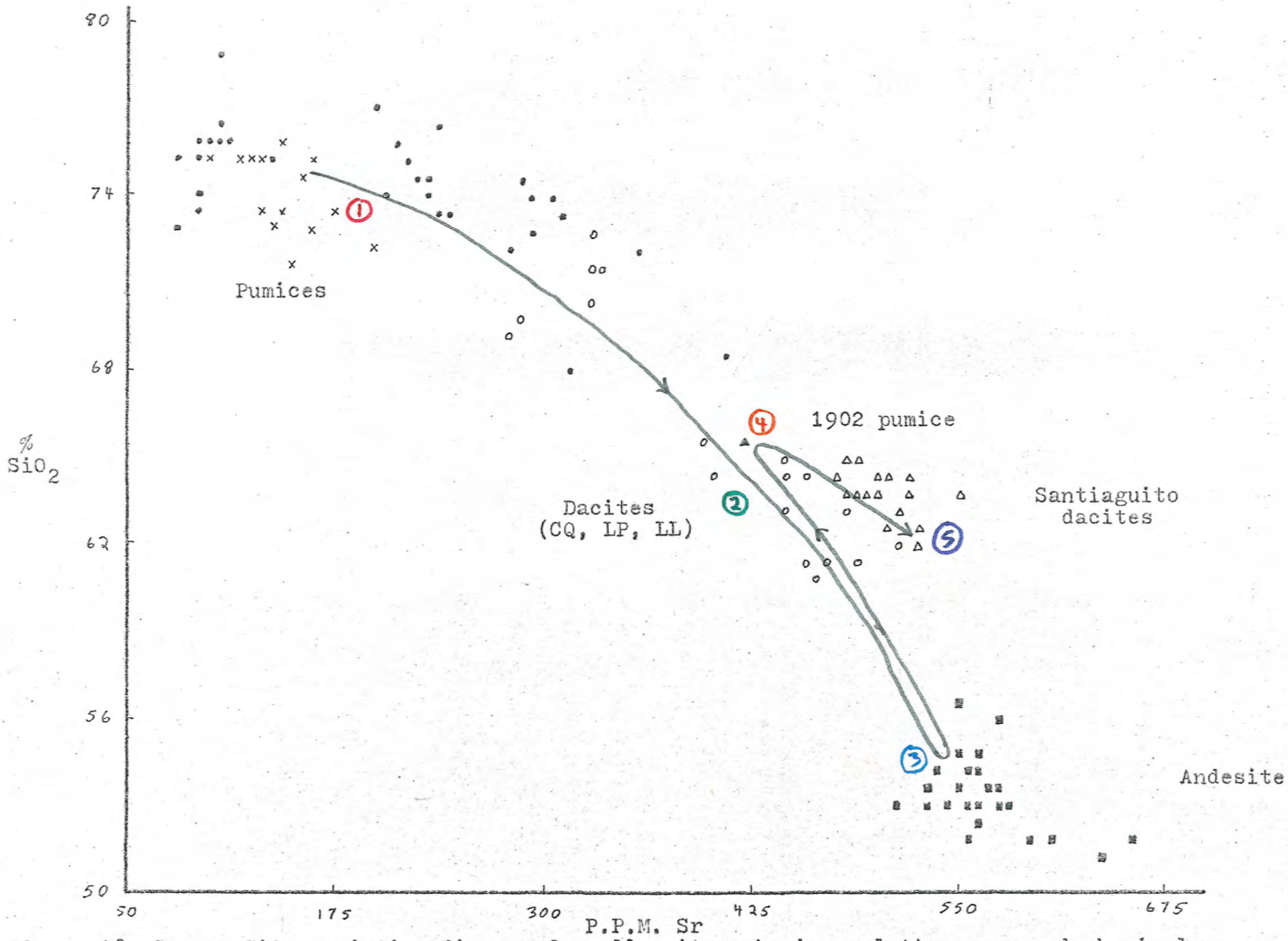

Figure 18 Sr vs. SiO_2 variation diagram for all units, showing relative ages and chemical evolution.

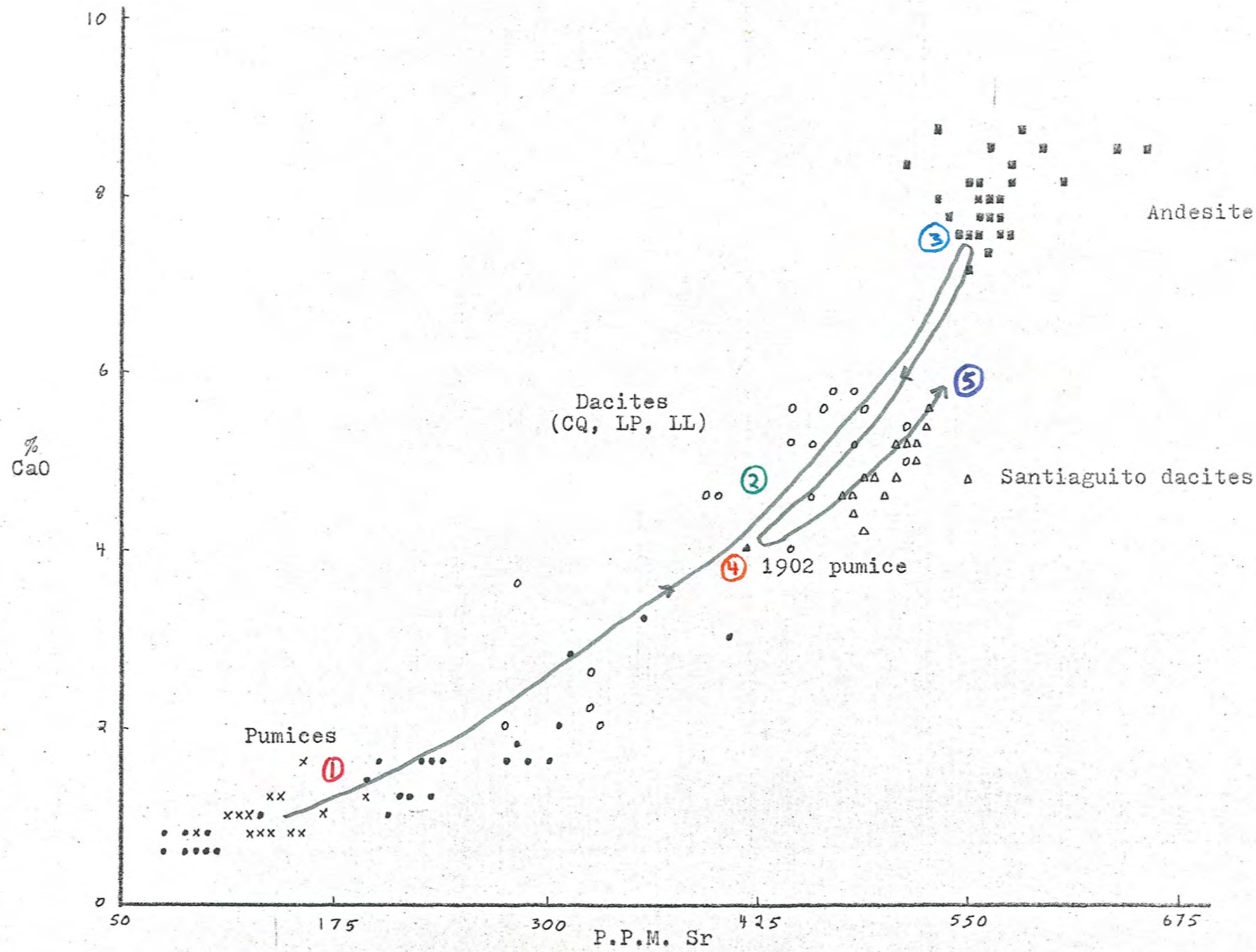

Figure 19 Sr vs. CaO variation diagram for all units, showing relative ages and chemical gross chemical evolution.

extruded by Santiaguito. It is also possible that the Llano del Pinal - La Pedrera - Cerro Quemado sequence may represent a smaller scale example of zoning in the parent magma. A significant amount of differentiation may have occurred in the upper levels of the magma chamber, if extrusion of the valley ignimbrites was followed by a relatively long quiescent period.

ACKNOWLEDGEMENTS

I wish to thank Norman Grant for his suggestions and encouragement during the preparation of this paper. The contributions of Bill Rose in the form of major element chemical data and field observations are gratefully acknowledged. Thanks are due to Hubert Bates, Katya Levin, and Jeff Stein for their aid in the trace element analyses. Thanks also go to Abbi Goldin for her constant encouragement and stenographic services.

BIBLIOGRAPHY

Bowles, F. A., Jack, R. N., and Carmichael, I. S. E., (1973) "Investigation of Deep-Sea Volcanic Ash Layers from Equatorial Pacific Cores" Geol. Soc. Am. Bull. v. 84, pp. 2371-2388.

Easter, J. R., (1974), "Geochemistry and Origin of the Quezaltenango Valley Ignimbrites" unpublished report, Oberlin College.

Gest, D., and Grant, N., (1973), "The Volcanic Geology of the Quezaltenango Valley" unpublished report, Oberlin College.

Johns, G. W., (1975), "Geology of the Cerro Quemado Volcanic Dome Complex Guatemala" unpublished report, Michigan Technological University.

Koch, A. J., and McLean, H., (1975) "Pleistocene Tephra and Ash-Flow Deposits in the Volcanic Highlands of Guatemala" Geol. Soc. Am. Bull. v. 86, pp. 529-541.

Levin, K. A. (1974) "Geochemistry of Three Quaternary Dacite Domes of the Guatemalan Highlands" unpublished report, Oberlin College.

MacGinitie, M., (1973) "Photogeology of the Quezaltenango Area, Guatemalan Highlands" unpublished report, Oberlin College.

Molnar, P., and Sykes, G. R., (1969) "Tectonics of the Carribean and Middle America Regions from Focal Mechanisms and Seismicity" Geol. Soc. Am. Bull. v. 80, pp. 1639-1684.

Noble, D. R., and Korringa, M. K., (1974) "Strontium, Rubidium, Potassium, and Calcium Variations in Quaternary Lava, Crater Lake, Oregon, and their Residual Glasses" Geology v. 2 pp. 187-190.

Reynolds, R. C. Jr., (1963) "Matrix Corrections in Trace Element Analysis by X-Ray Fluorescence: Estimation of the Mass Absorption Coeffecient by Compton Scattering" Am. Min. v. 48, pp. 1133-1143.

_____, (1967) "Estimations of Mass Absorption Coefficients by Compton Scattering: Improvements and Extensions of the Method" Am. Min. v. 52, pp. 1493-1502.

Rose, W. I. Jr., (1972) "Santiaguito Volcanic Dome, Guatemala" Geol. Soc. of Am. Bull. v. 83, pp. 1413-1434.

_____, (1972) "Notes on the 1902 Eruption of Santa Maria, Guatemala" Bull. Volcanologique v. 36, pp. 29-45.

Stoiber, R. E., and Carr, M. J., (1973) "Quaternary Volcanic and Tectonic Segmentation of Central America" Bull. Volcanologique v. 37, pp. 304-325.

Walker, D., (in press) "Behaviour of X-Ray Mass Absorption Coefficients near Absorption Edges: Reynolds Method Revisited" in press.

Whims, M., (1974) "Report of a Joint Geological - Geophysical Survey in Guatemala" unpublished report, Michigan Technological University.

Williams, H., (1960) "Volcanic History of the Guatemalan Highlands" University of California Publications in Geological Sciences, v.38, number 1, pp. 1-86.

APPENDIX I

Key to Graphs

×	Bulk pumice
⊙	Pumice fragment
▣	Santa Maria andesite
○	Cerro Quemado, La Pedrera, and Llano del Pinal dacite
▲	1902 pumice
△	Santiaguito dacite
P	Separated phenocryst phase
tip of arrow	Separated groundmass phase

A DIFFERENT COLOR SCHEME IS USED ON PAGES 4-6.

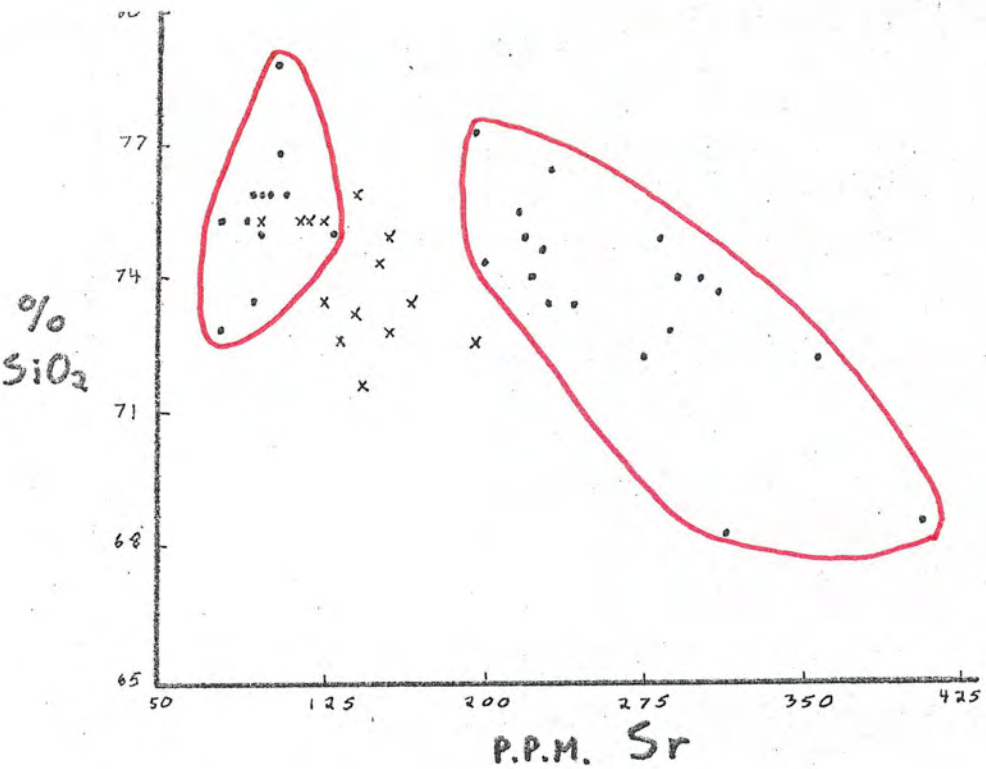
% SiO_2
77
74
71
68
65
50
125
200
275
350
425
P.P.M. Sr

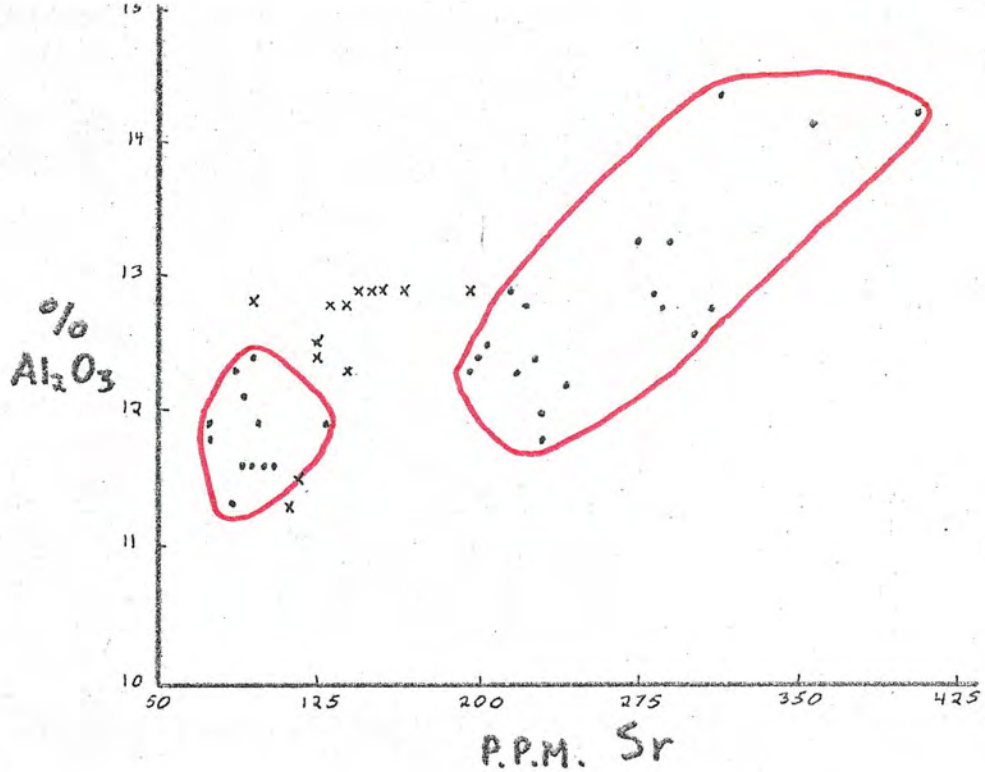
% Al_2O_3
14
13
12
11
10
50
125
200
275
350
425
P.P.M. Sr

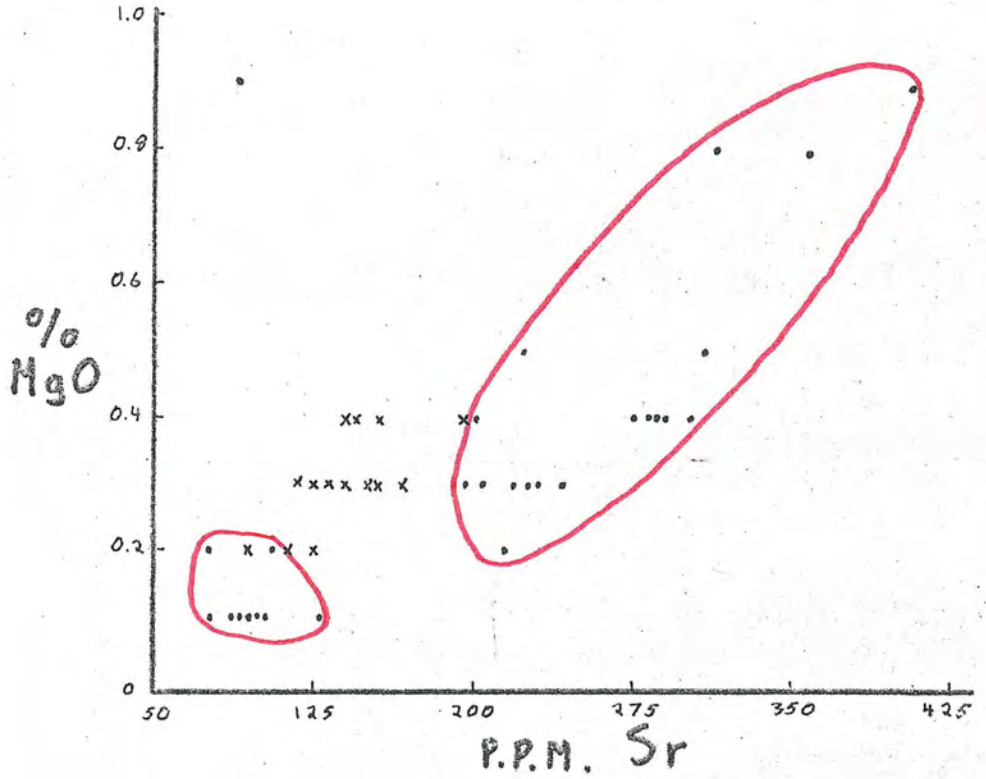
% MgO
1.0
0.8
0.6
0.4
0.2
0
50
125
200
275
350
425
P.P.M. Sr

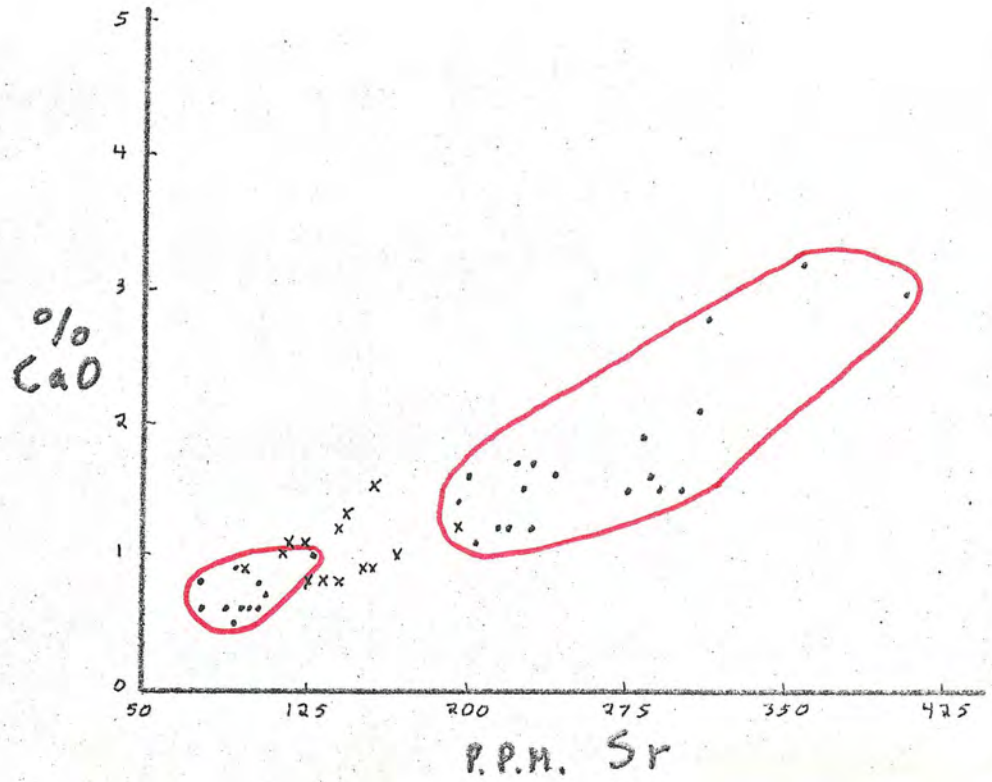
% CaO
5
4
3
2
1
0
50
125
200
275
350
425
P.P.M. Sr

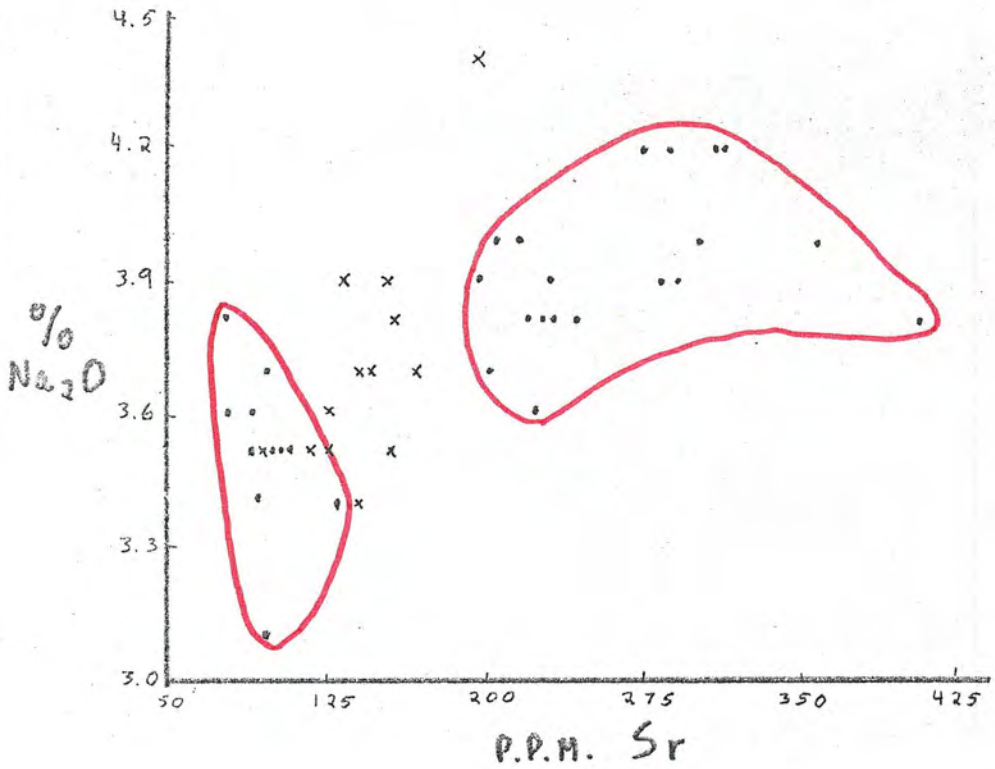
4.5
4.2
3.9
3.6
3.3
3.0
% Na_2O
50
125
200
275
350
425
P.P.M. Sr

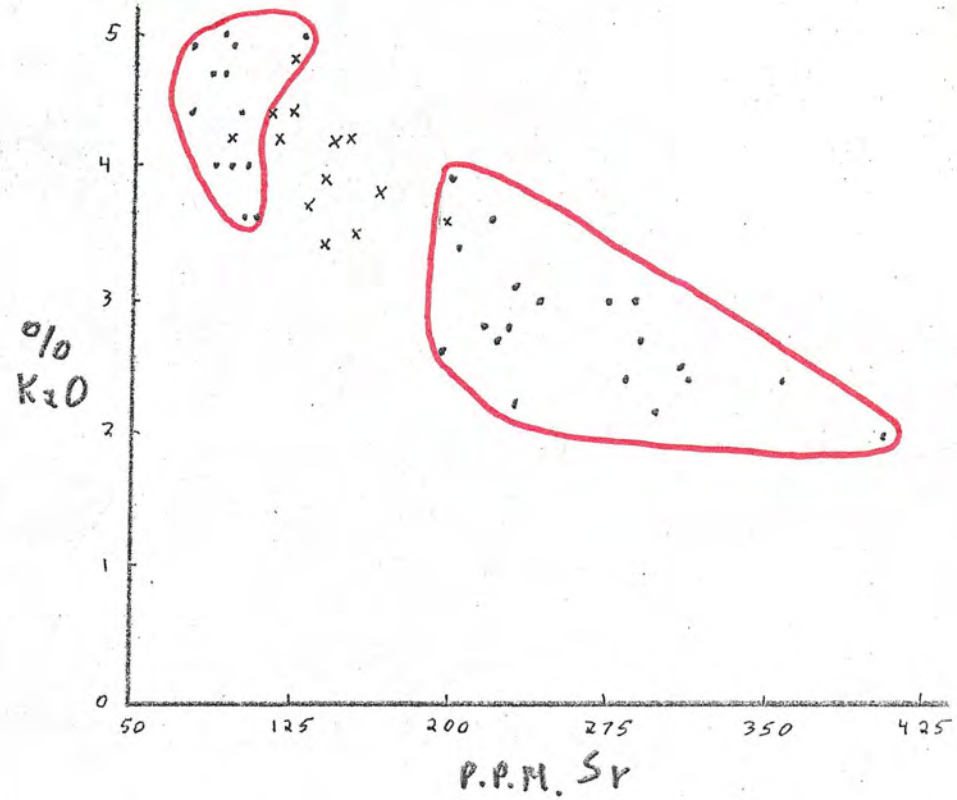
5
4
3
2
1
0
% K_2O
50
125
200
275
350
425
P.P.M. Sr

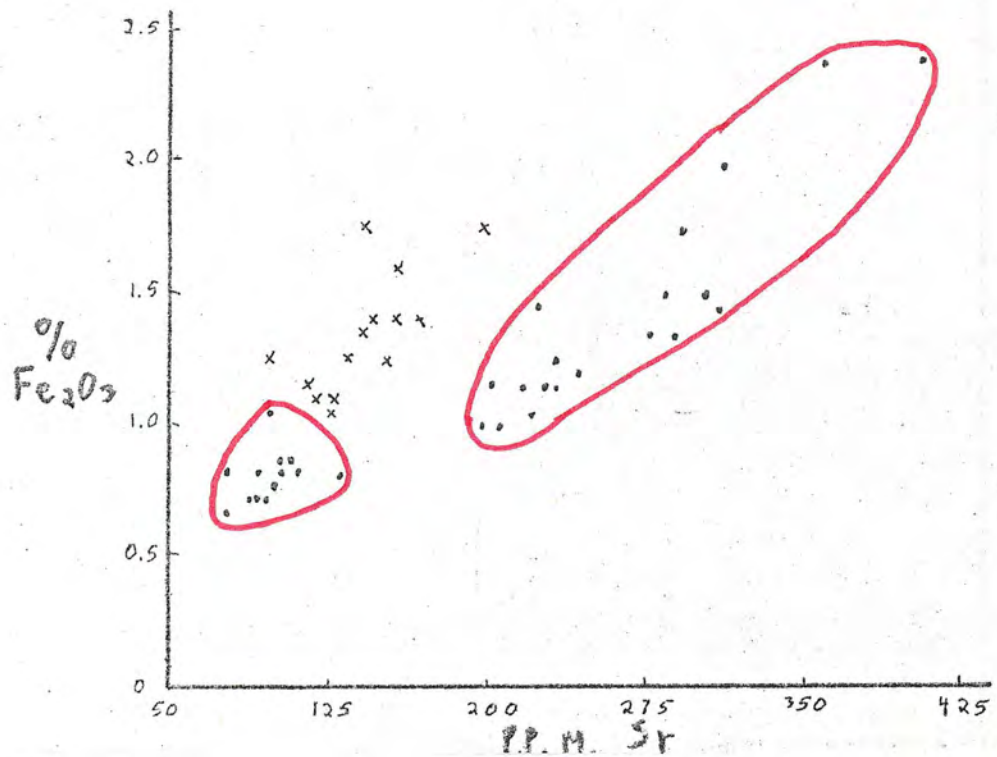
2.5
2.0
1.5
1.0
0.5
0
% Fe_2O_3
50
125
200
275
350
425
P.P.M. Sr

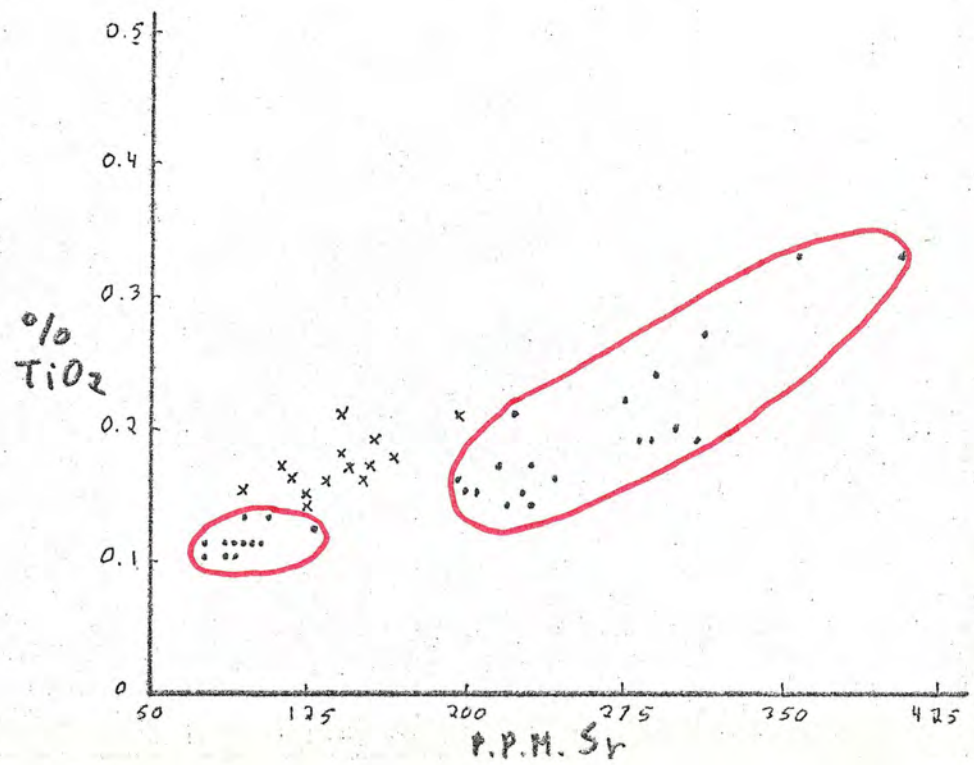
0.5
0.4
0.3
0.2
0.1
0
% TiO_2
50
125
200
275
350
425
P.P.M. Sr

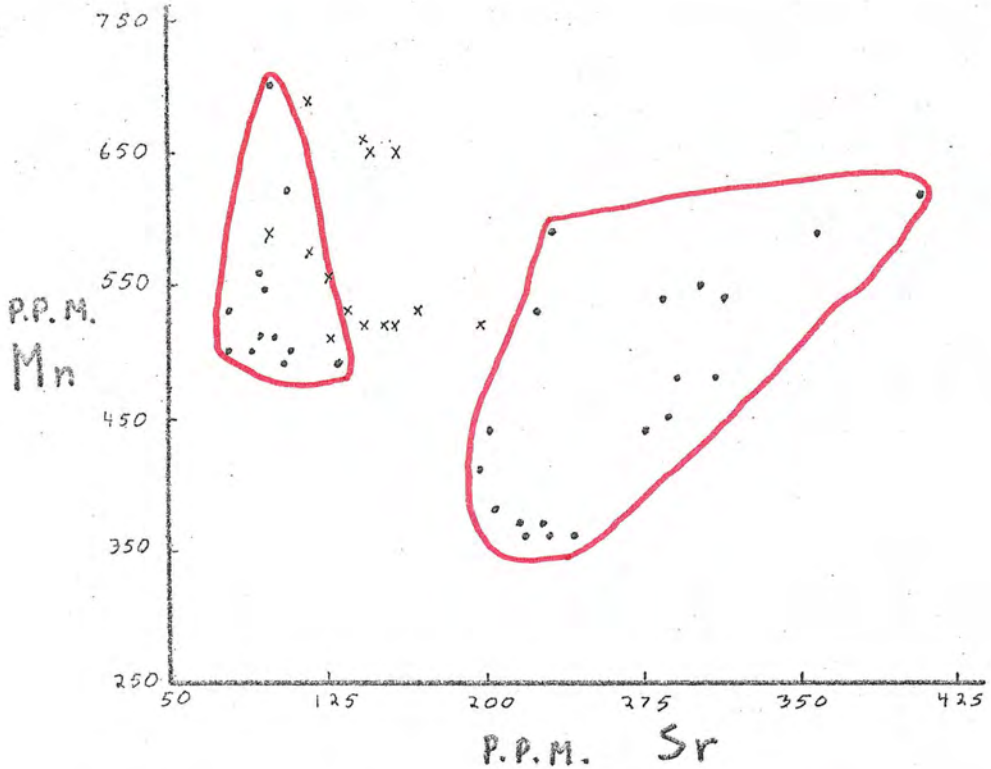
750
650
550
450
350
250
P.P.M.
Mn
50
125
200
275
350
425
P.P.M. Sr

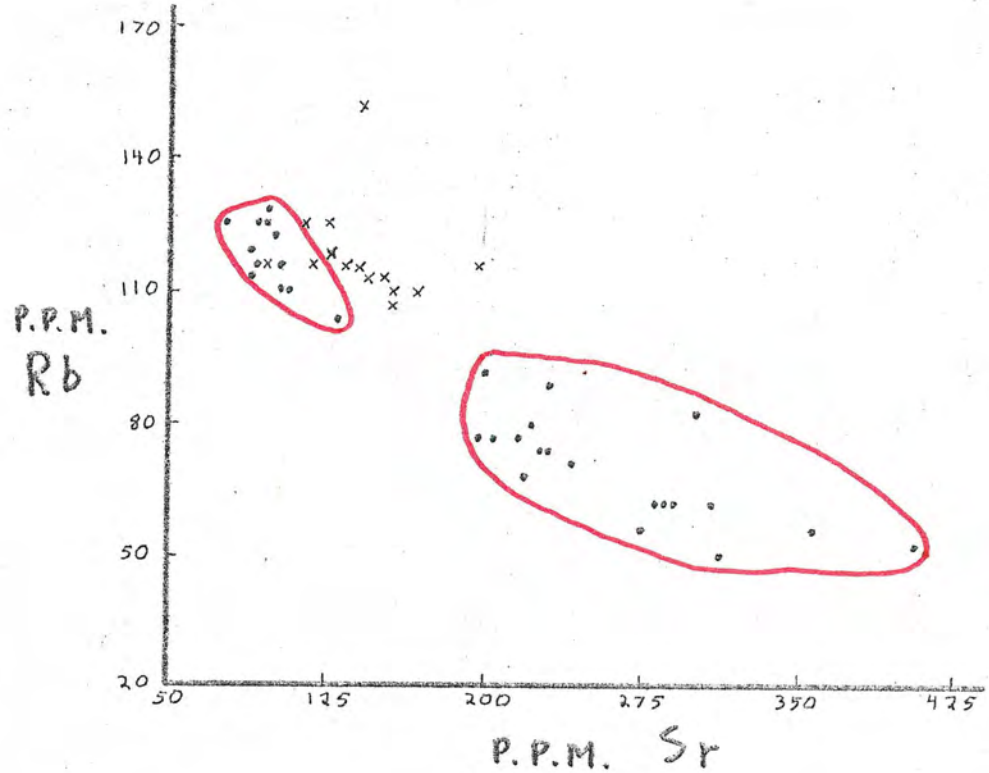
170
140
110
80
50
20
P.P.M.
Rb
50
125
200
275
350
425
P.P.M. Sr

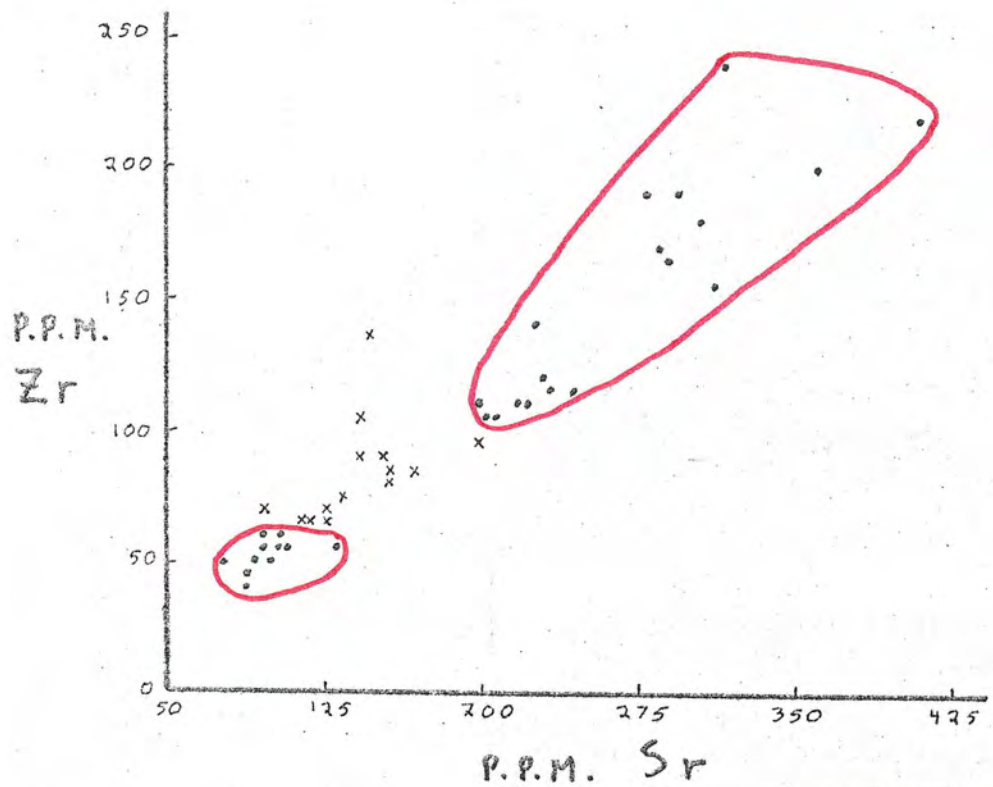
250
200
150
100
50
0
P.P.M.
Zr
50
125
200
275
350
425
P.P.M. Sr

FOR COLOR KEY TO THESE GRAPHS, SEE FIG. 17

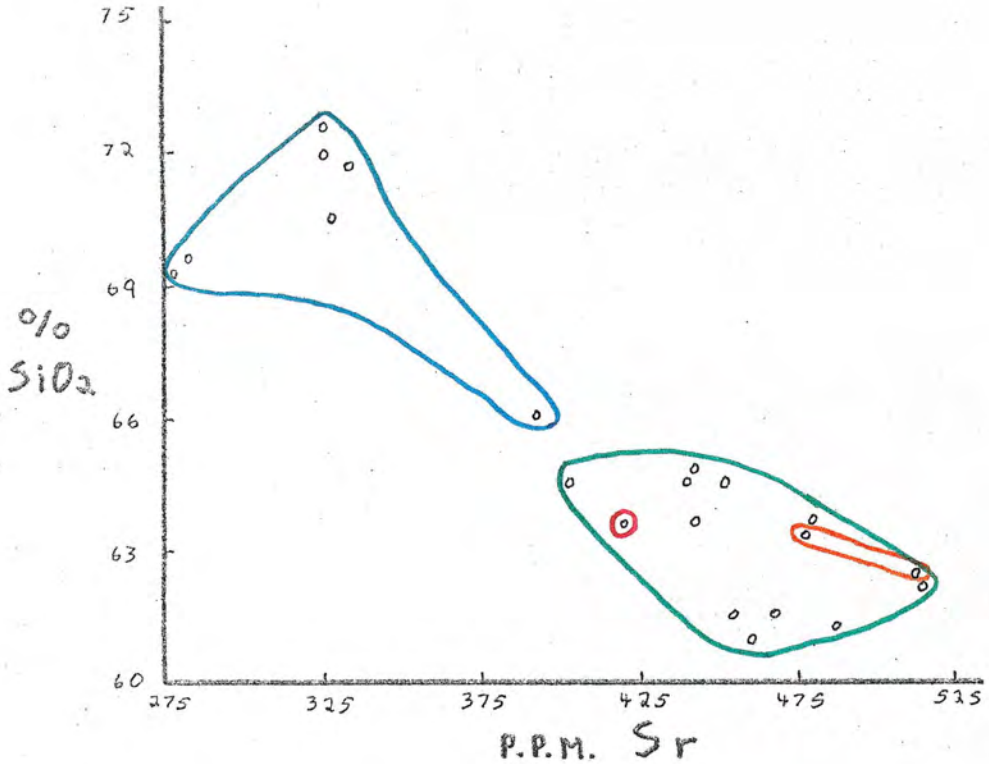

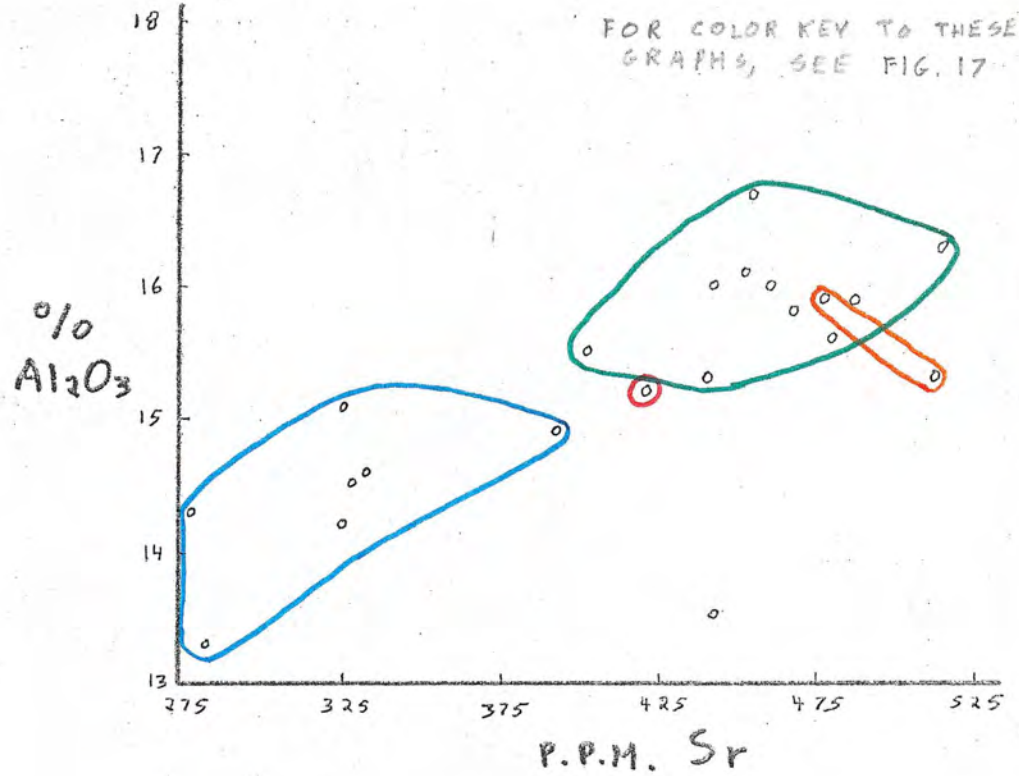

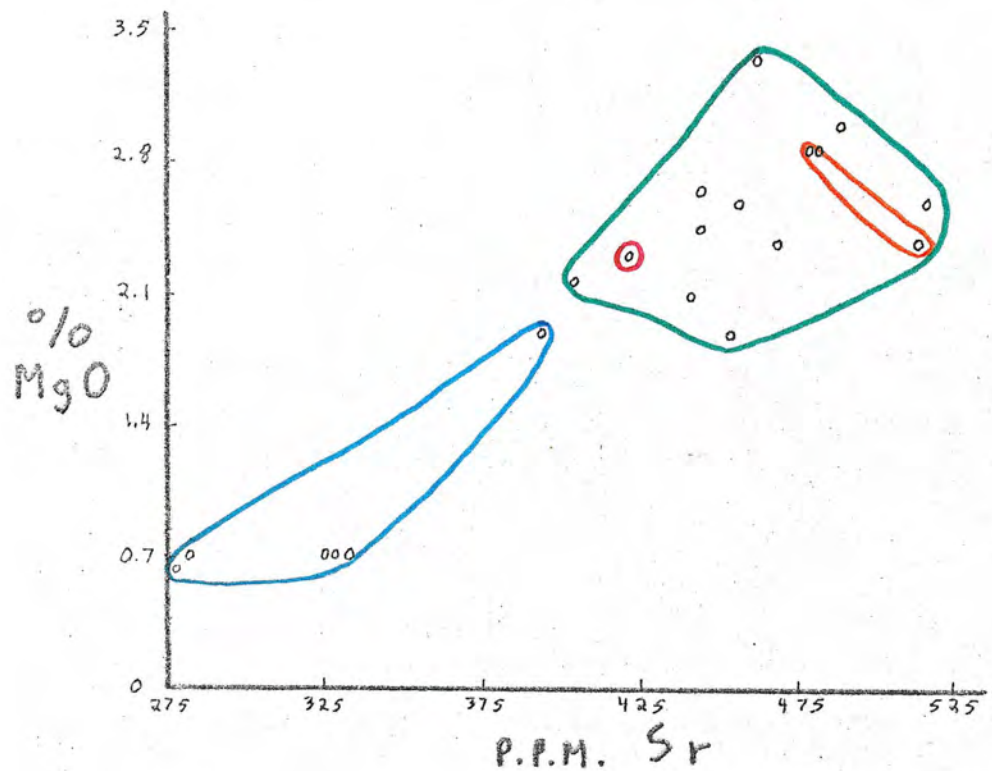

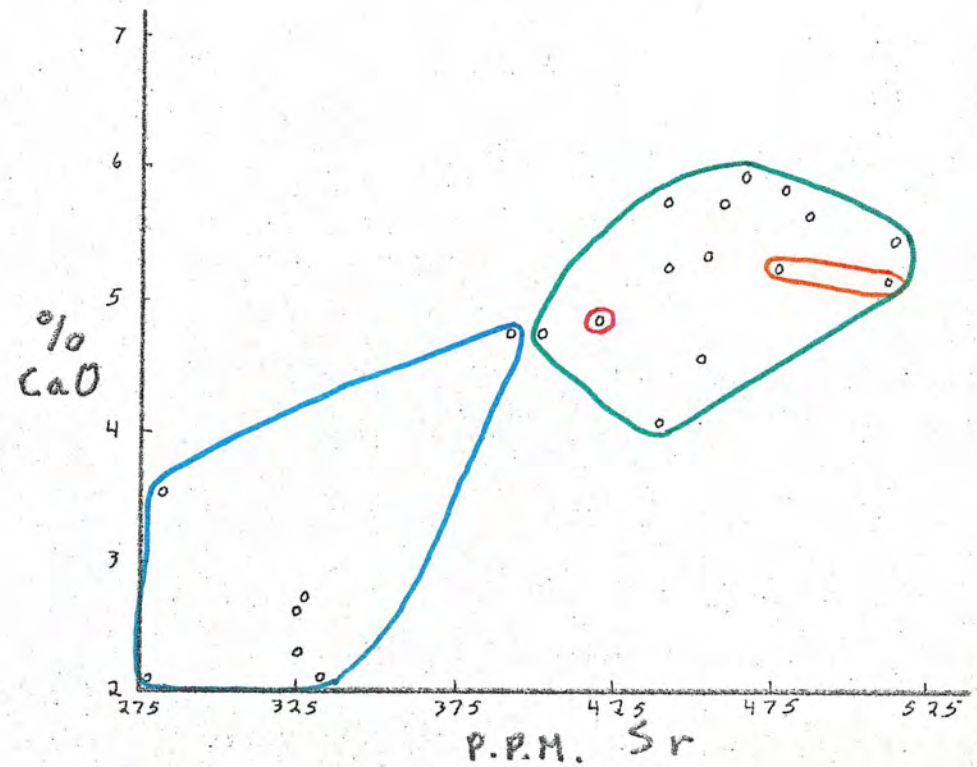

FOR COLOR KEY TO THESE GRAPHS, SEE FIG. 17

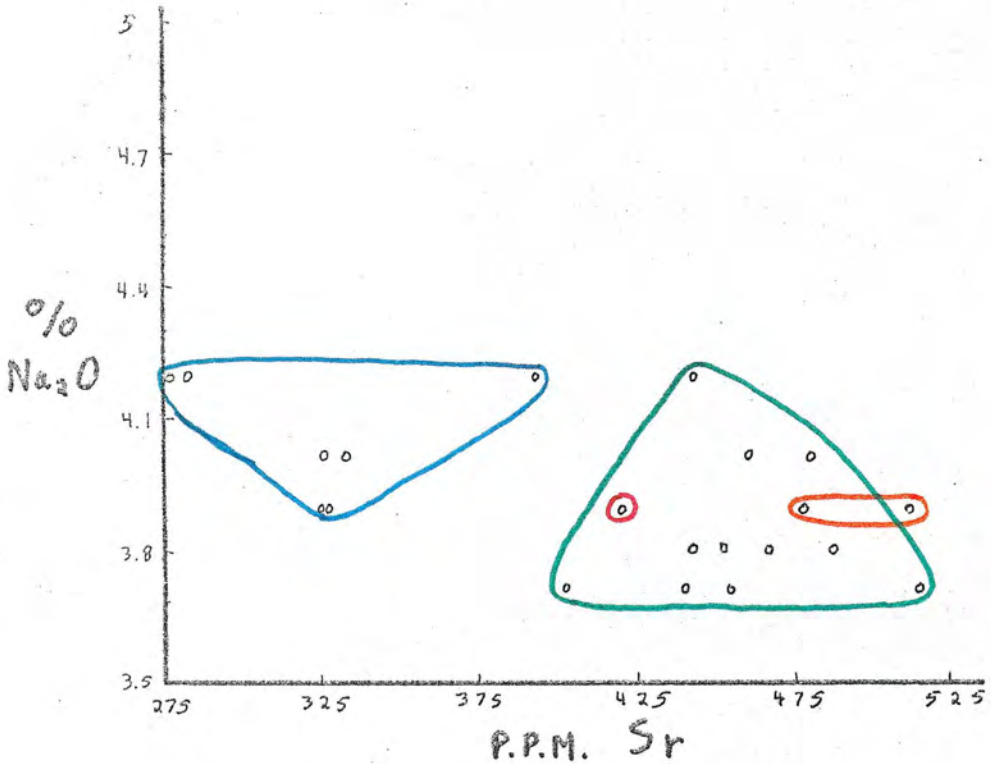

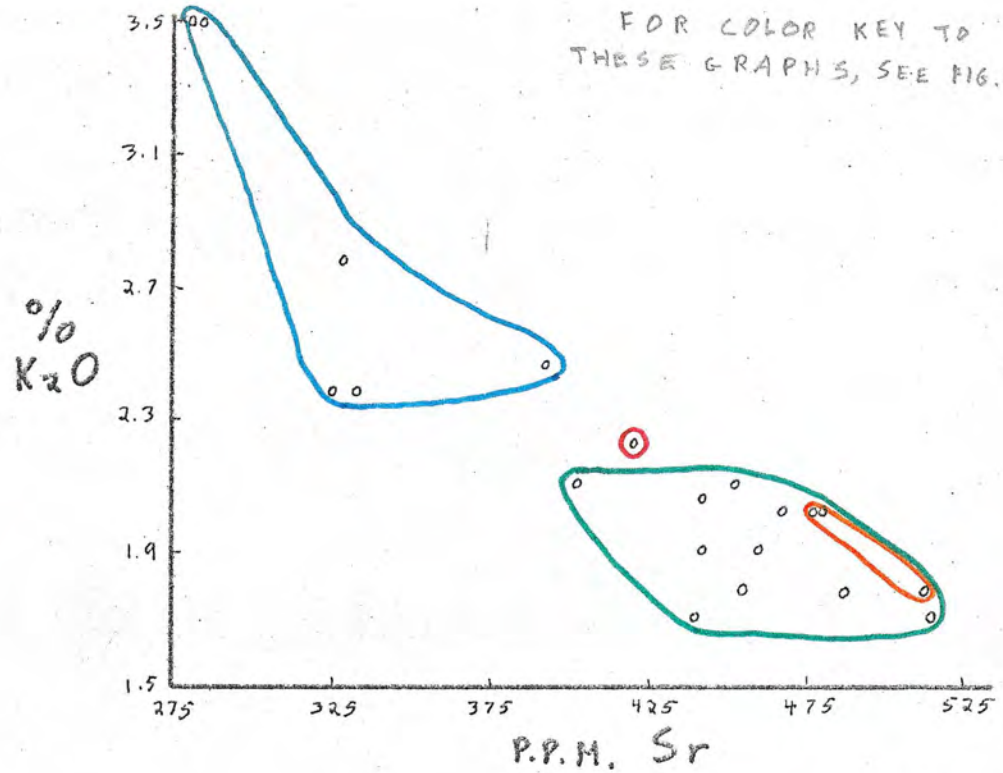

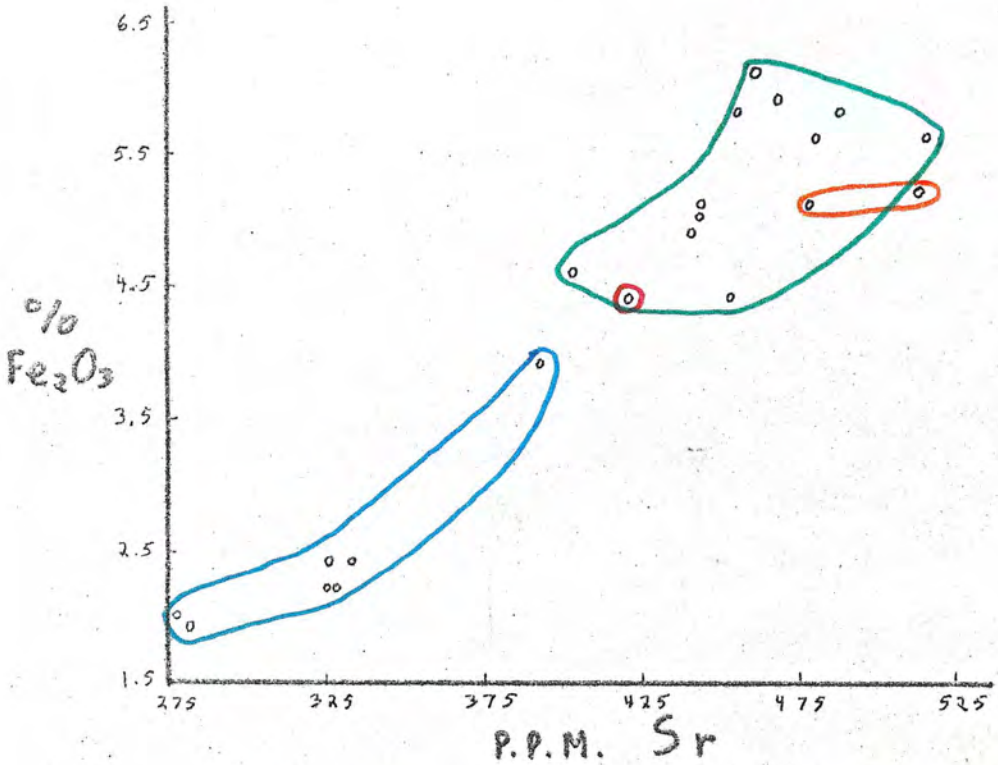

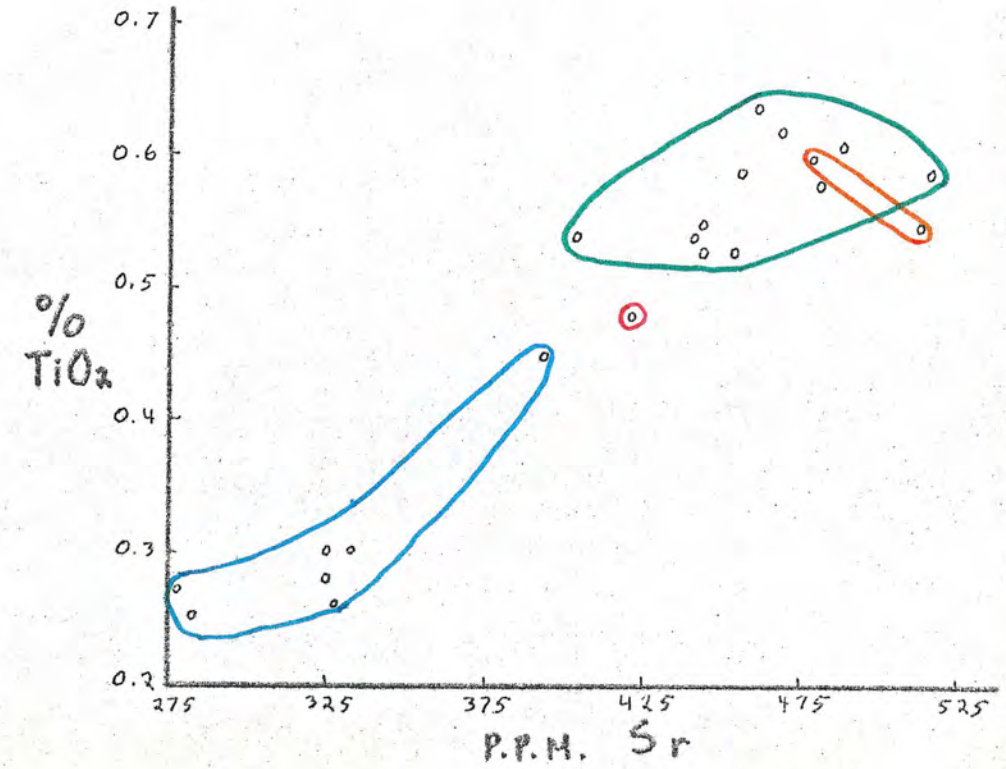

FOR COLOR KEY TO THESE GRAPHS, SEE FIG. 17

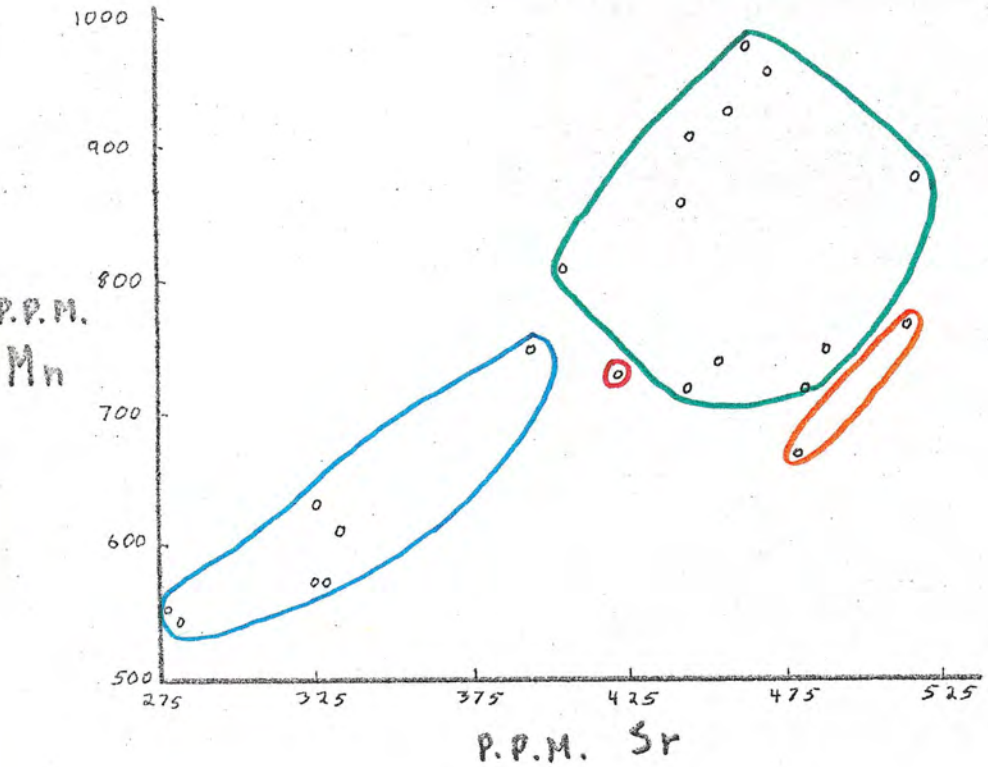

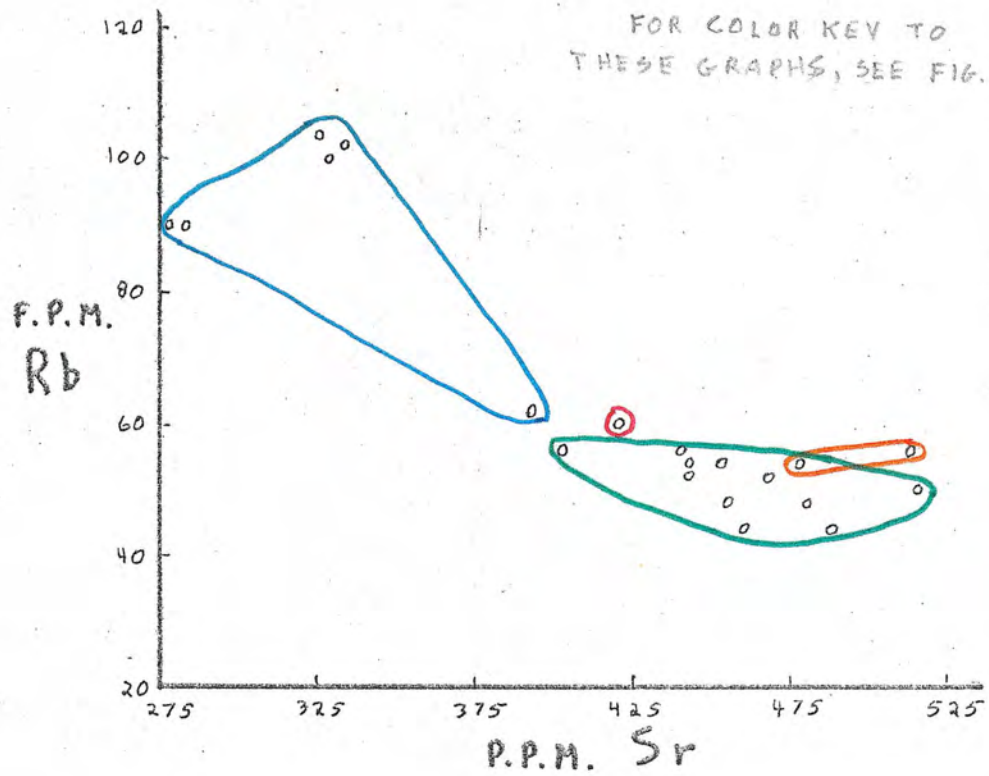

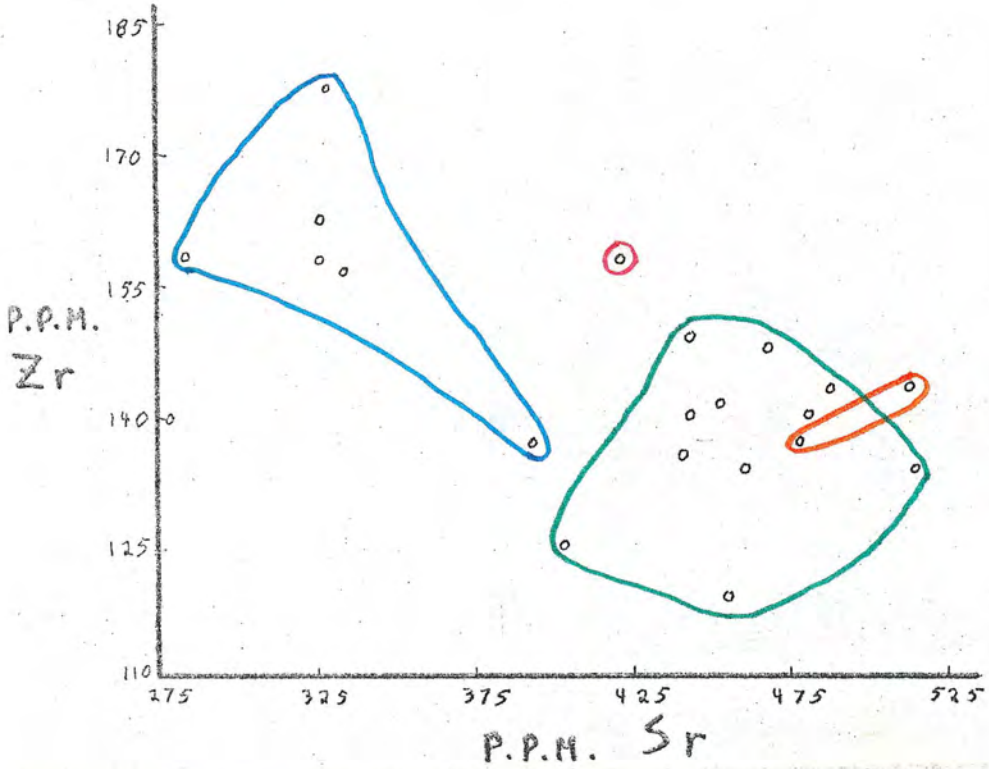

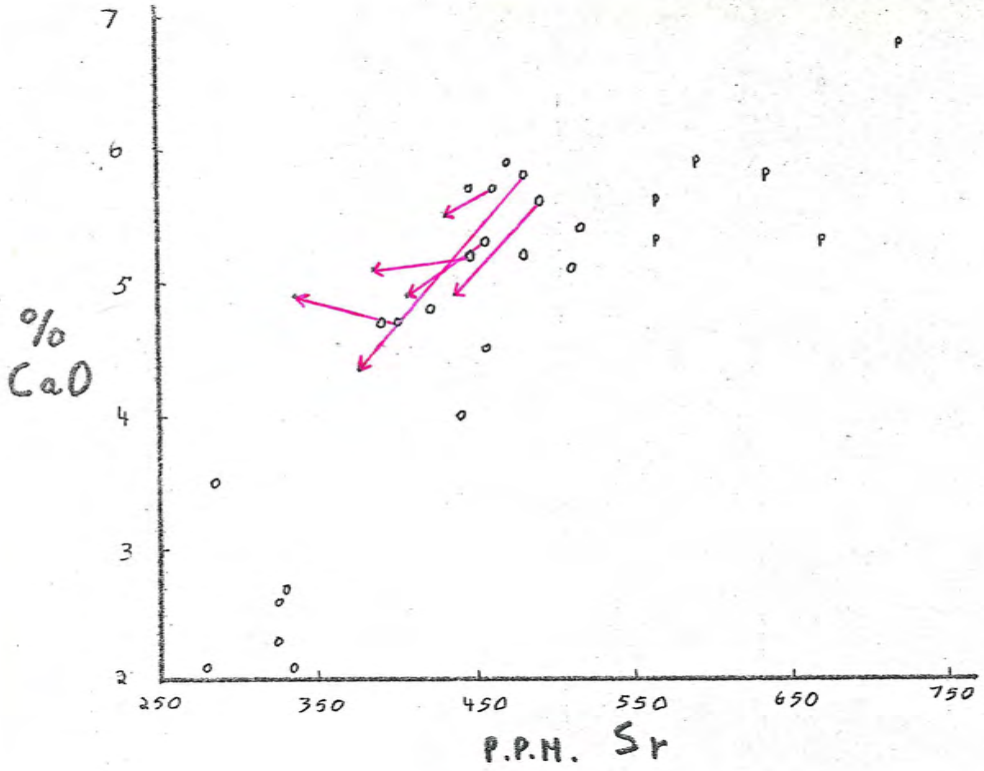
%
CaO
P.P.M. Sr

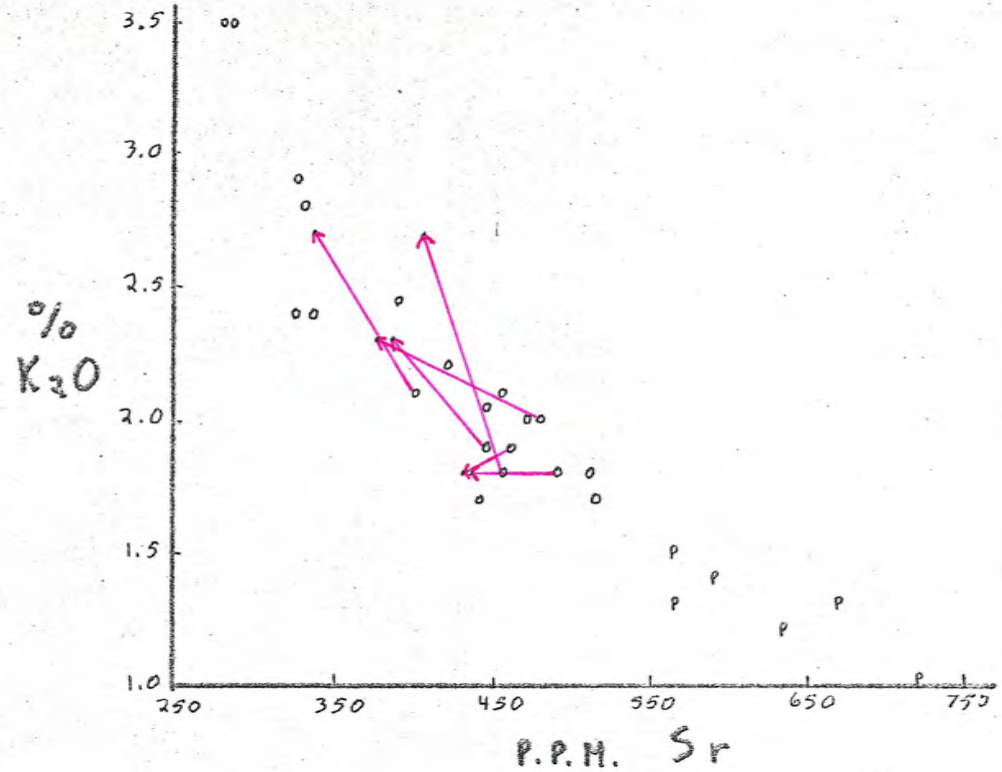
%
K_2O
P.P.M. Sr

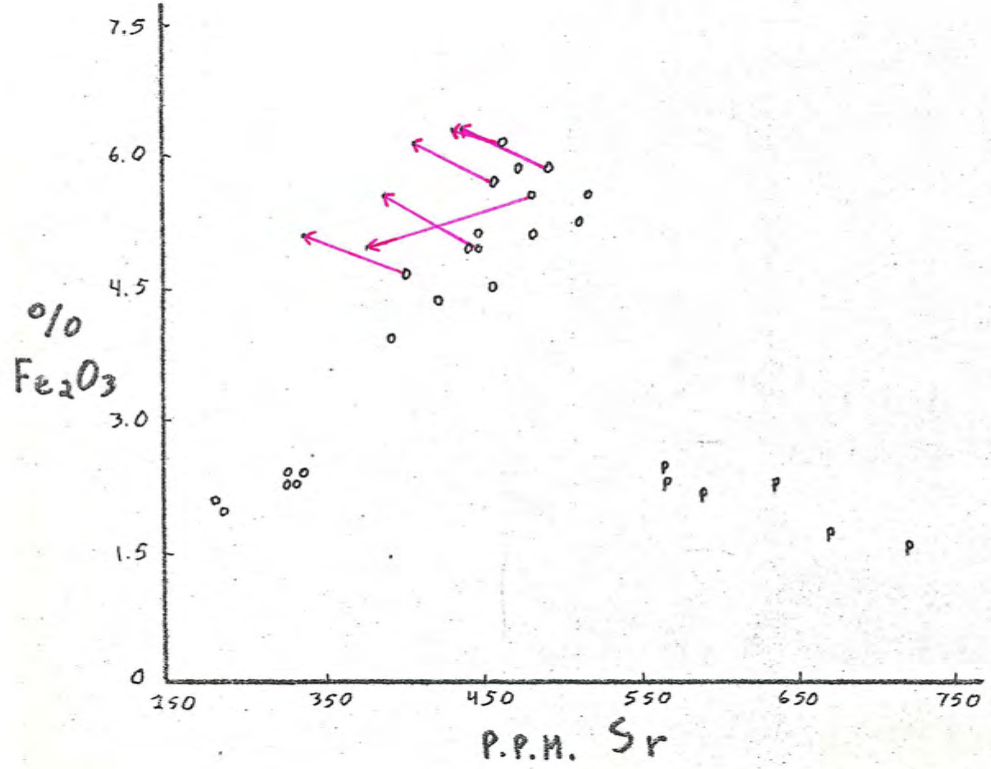
%
Fe_2O_3
P.P.M. Sr

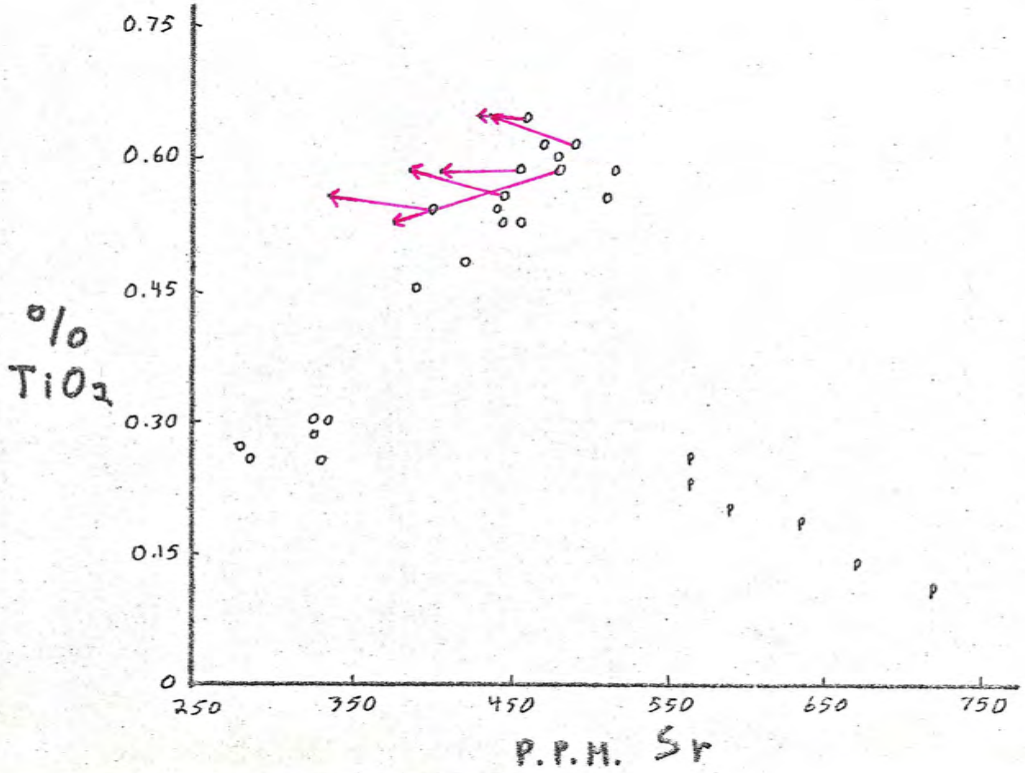
%
TiO_2
P.P.M. Sr

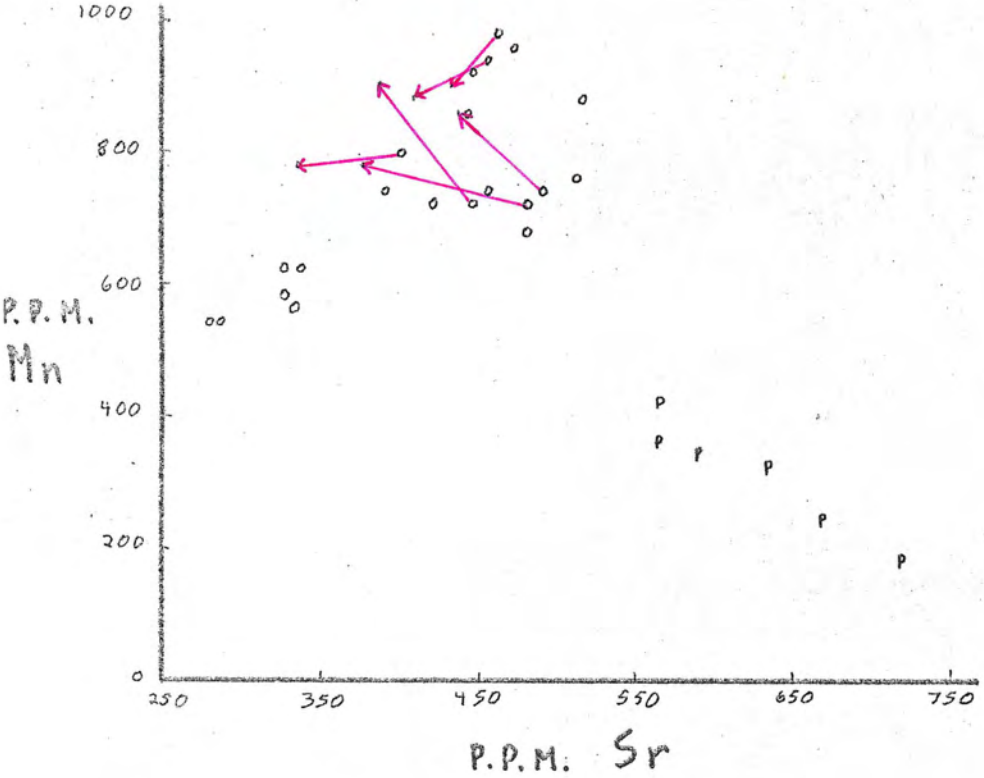
1000
800
600
400
200
0
P.P.M.
Mn
250
350
450
550
650
750
P.P.M. Sr

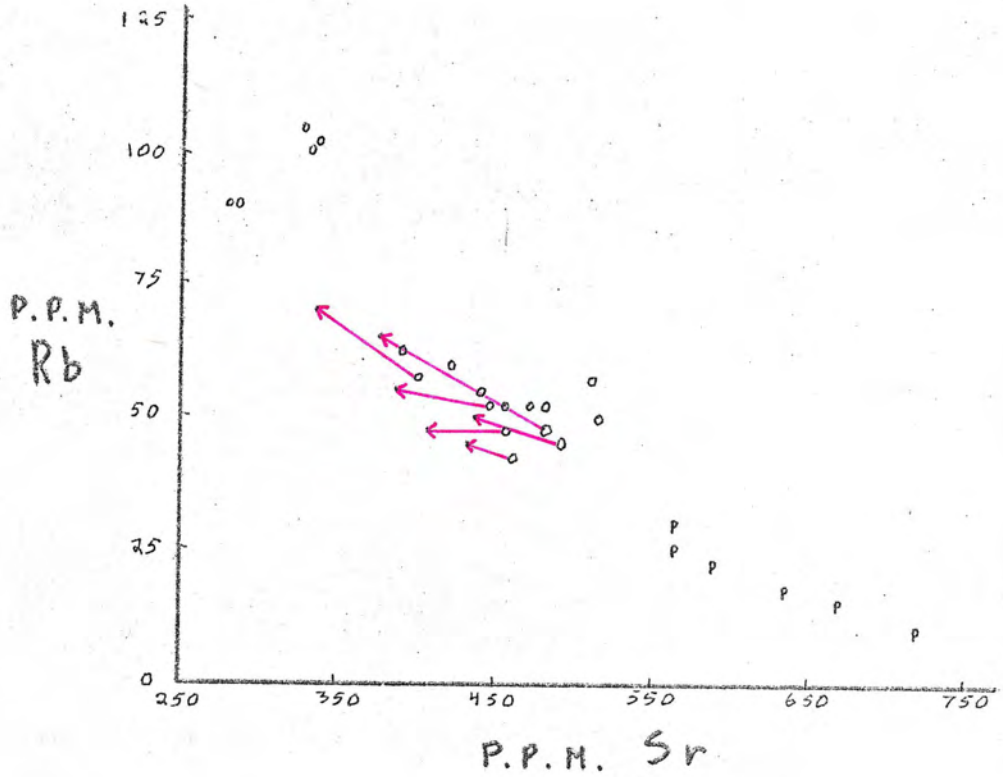
125
100
75
50
25
0
P.P.M.
Rb
250
350
450
550
650
750
P.P.M. Sr

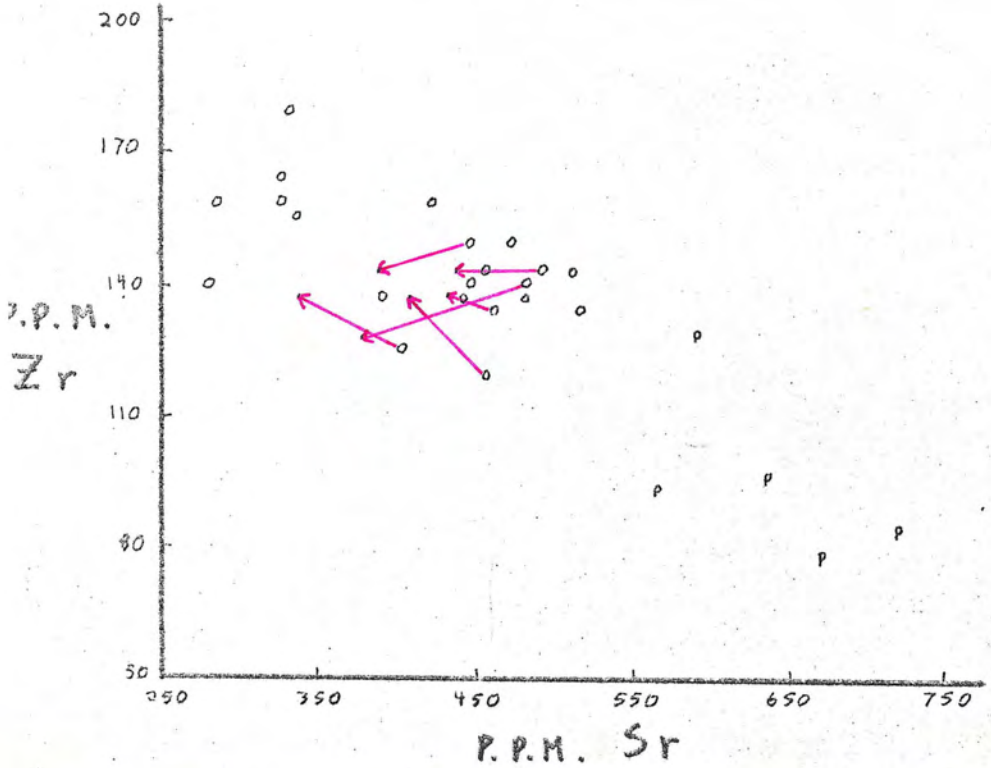
200
170
140
110
80
50
P.P.M.
Zr
250
350
450
550
650
750
P.P.M. Sr

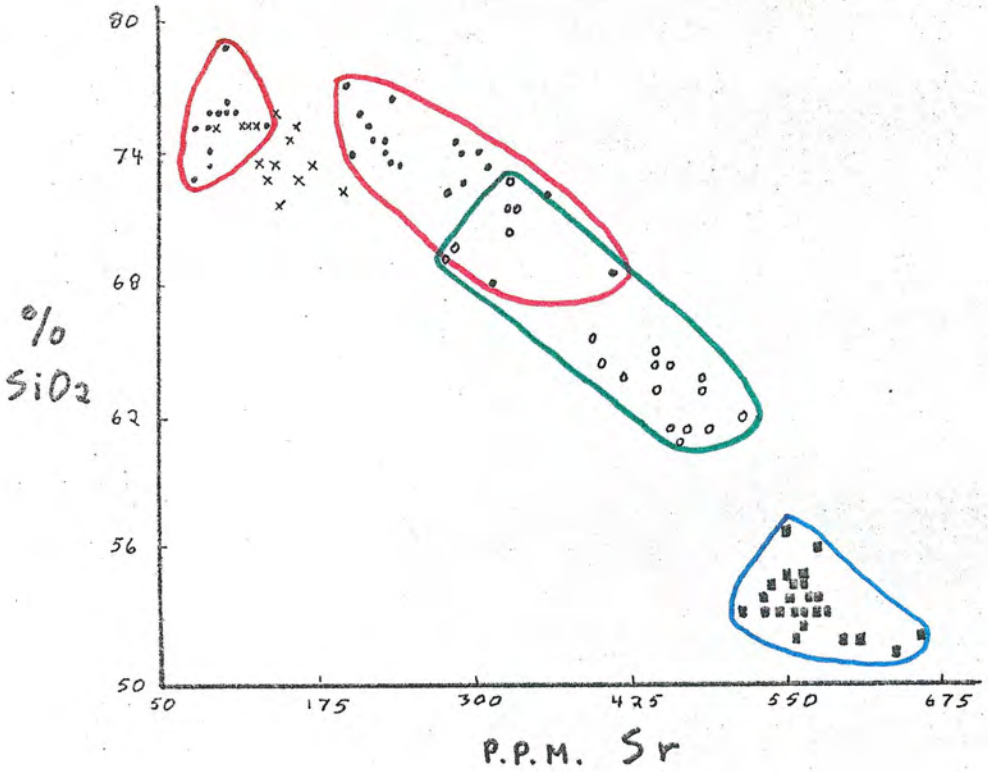
80
74
68
62
56
50
% SiO_2
50
175
300
425
550
675
P.P.M. Sr

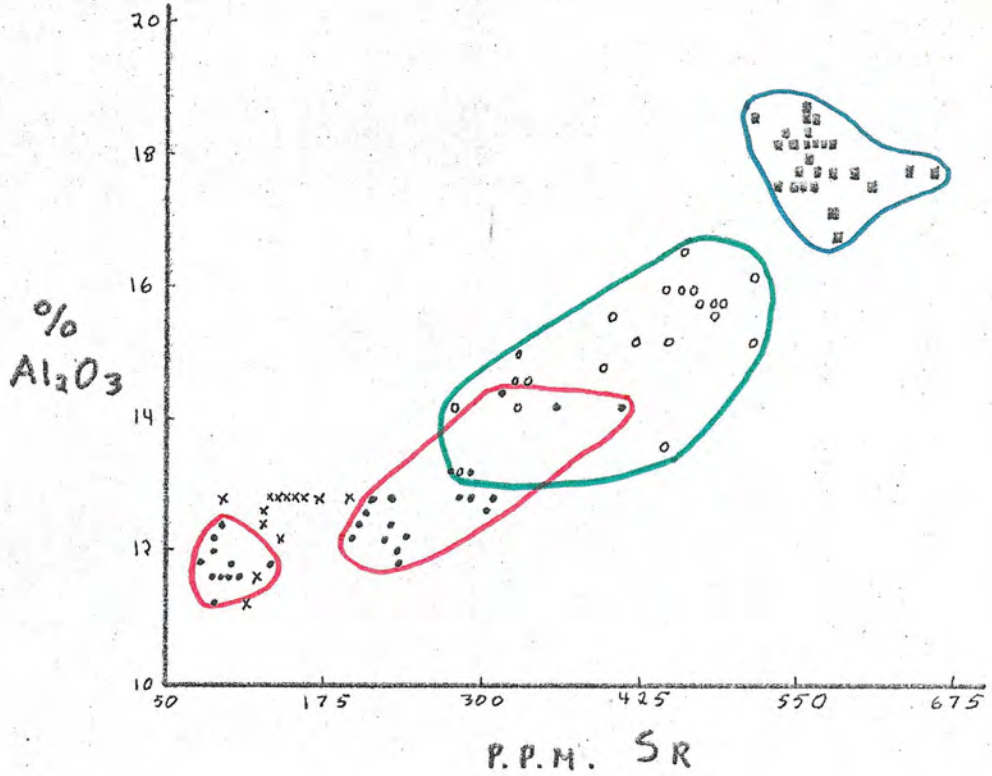
20
18
16
14
12
10
% Al_2O_3
50
175
300
425
550
675
P.P.M. SR

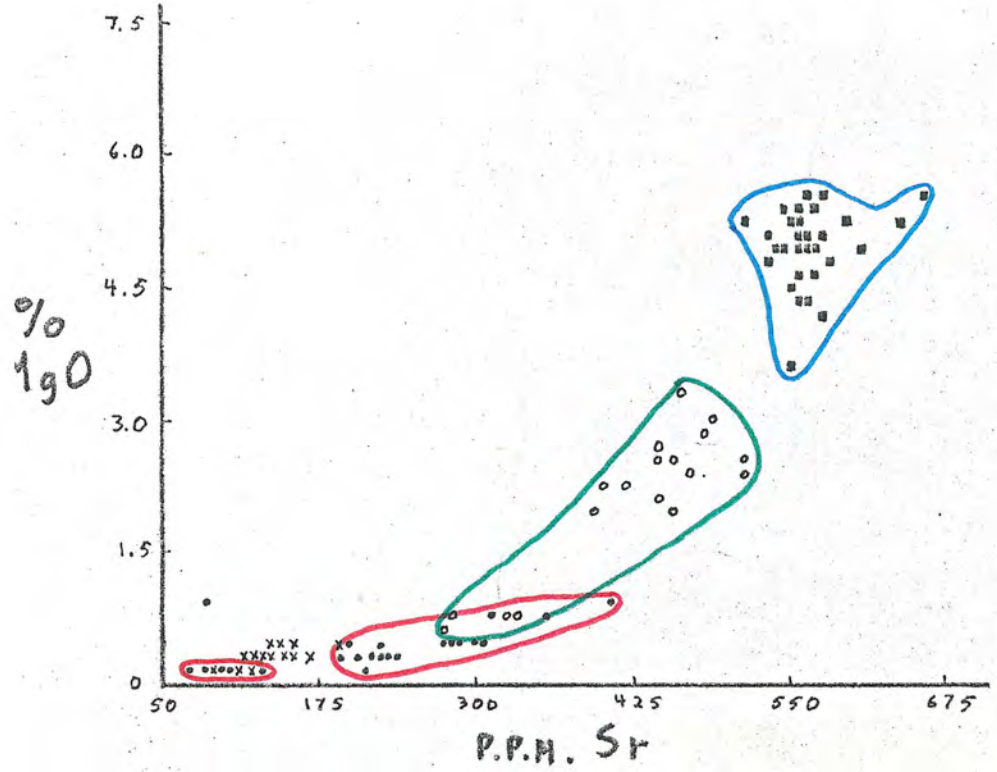
7.5
6.0
4.5
3.0
1.5
0
% MgO
50
175
300
425
550
675
P.P.M. Sr

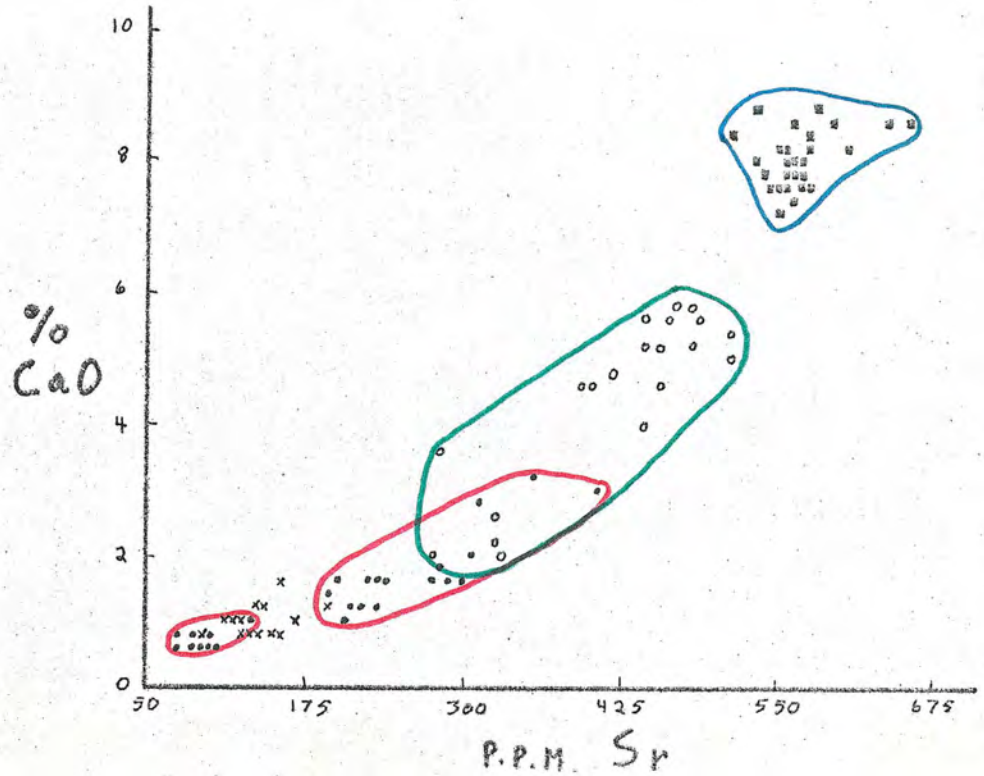
10
8
6
4
2
0
% CaO
50
175
300
425
550
675
P.P.M. Sr

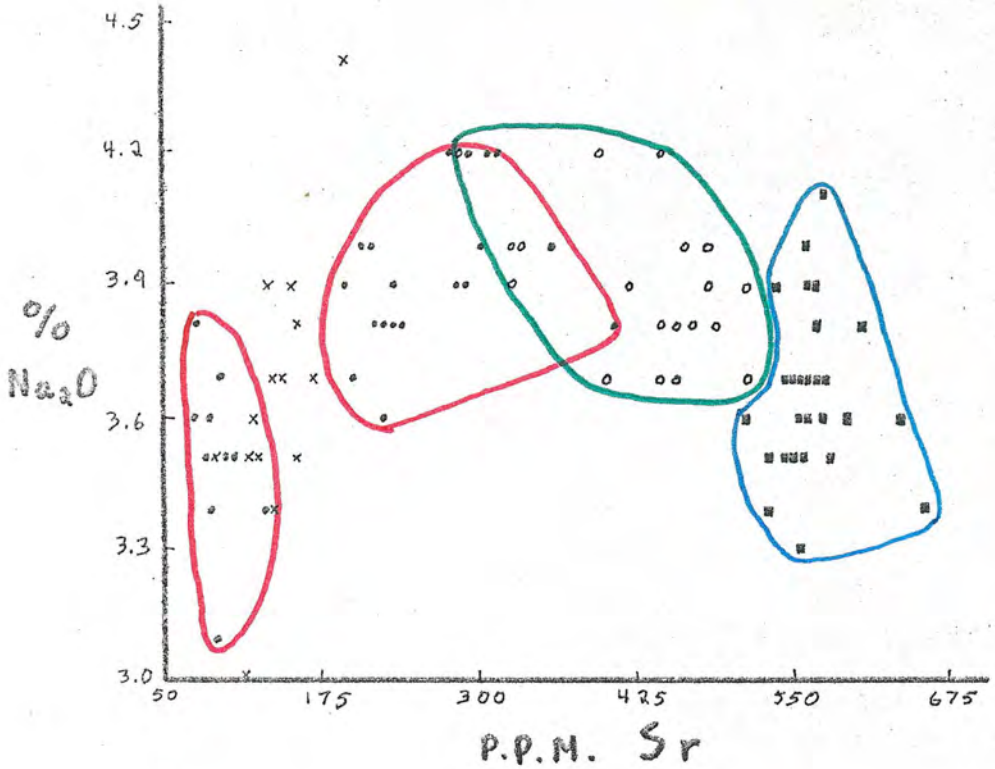
4.5
4.2
3.9
3.6
3.3
3.0
% Na_2O
50
175
300
425
550
675
P.P.M. Sr

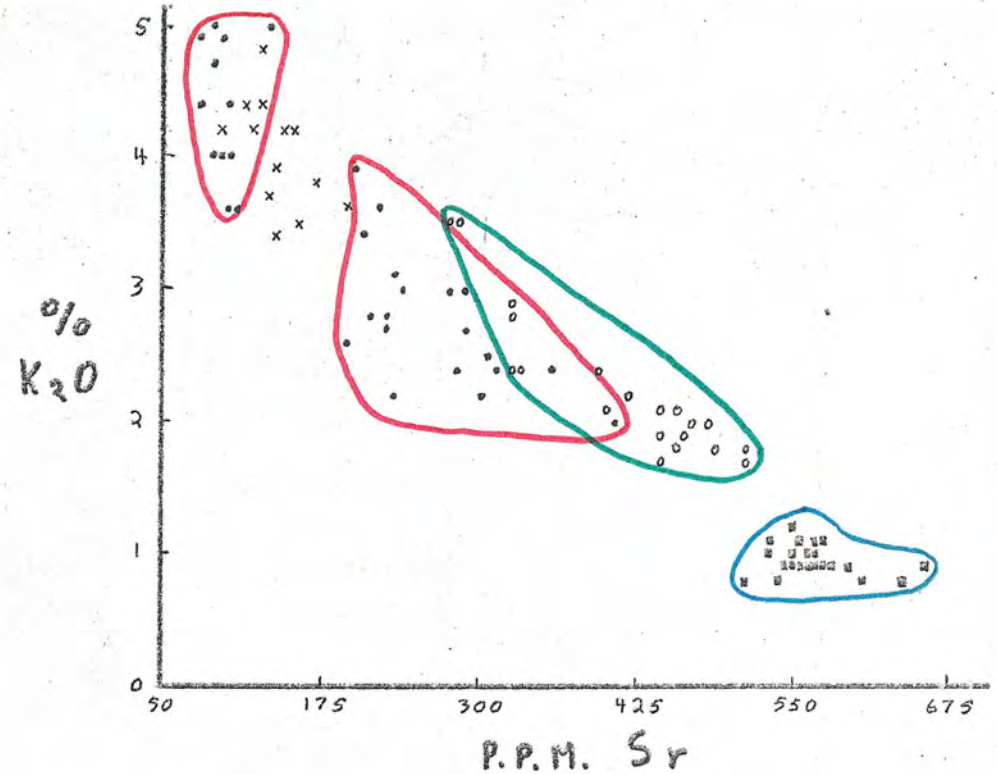
5
4
3
2
1
0
% K_2O
50
175
300
425
550
675
P.P.M. Sr

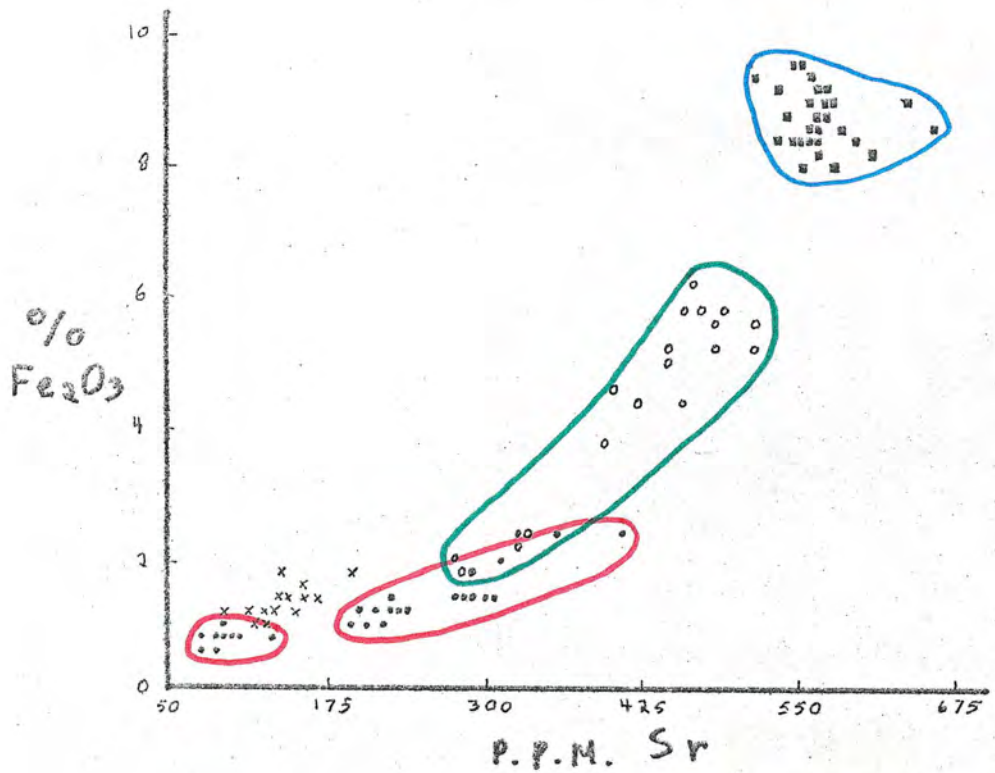
10
8
6
4
2
0
% Fe_2O_3
50
175
300
425
550
675
P.P.M. Sr

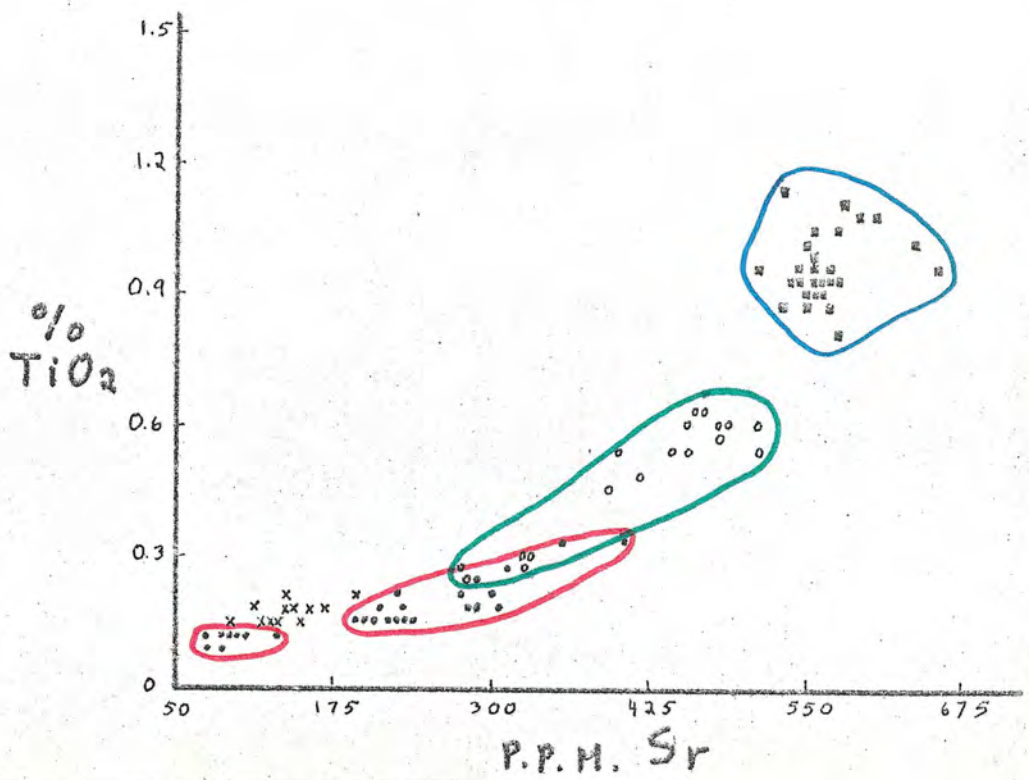
1.5
1.2
0.9
0.6
0.3
0
% TiO_2
50
175
300
425
550
675
P.P.M. Sr

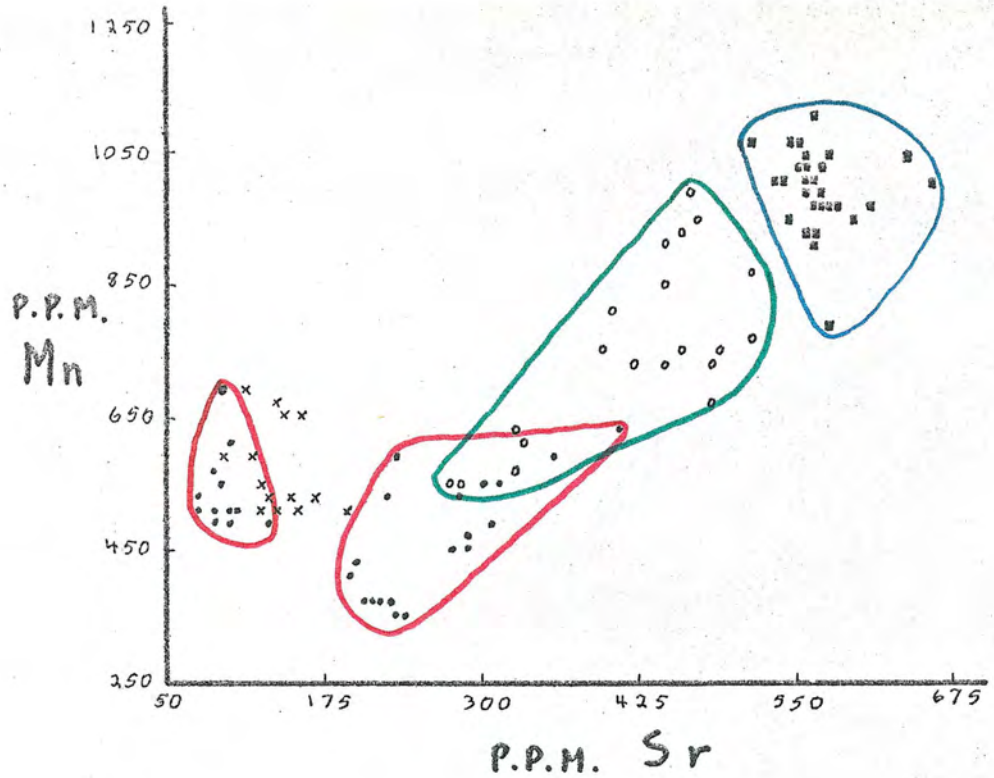
P.P.M. Mn
1250
1050
850
650
450
250
50
175
300
425
550
675
P.P.M. Sr

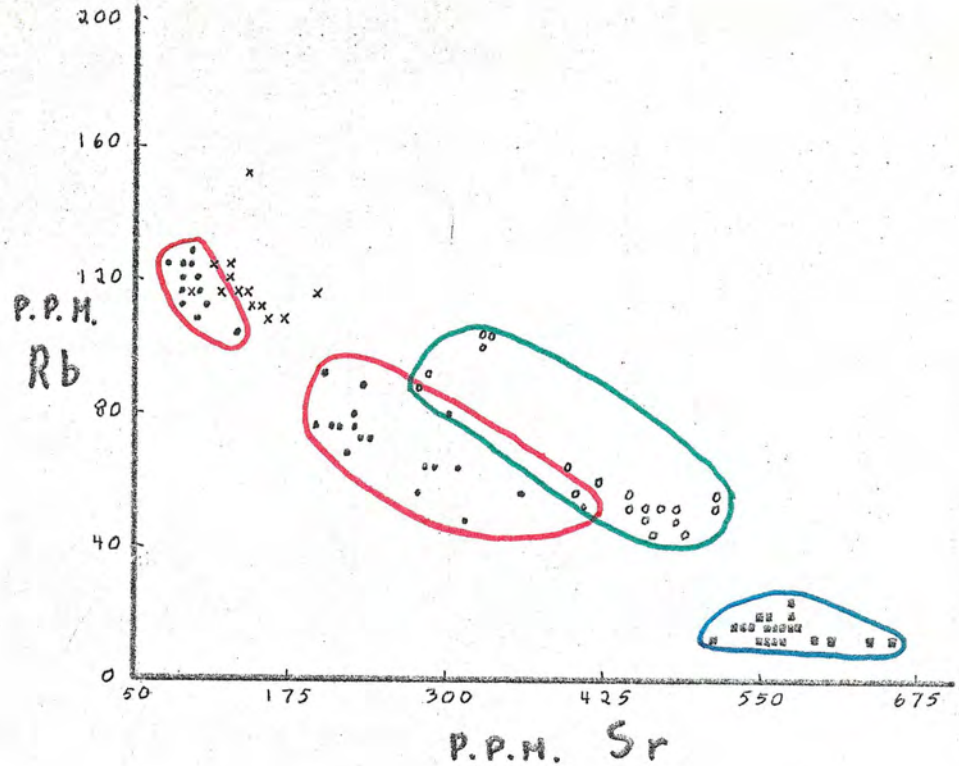
P.P.M. Rb
200
160
120
80
40
0
50
175
300
425
550
675
P.P.M. Sr

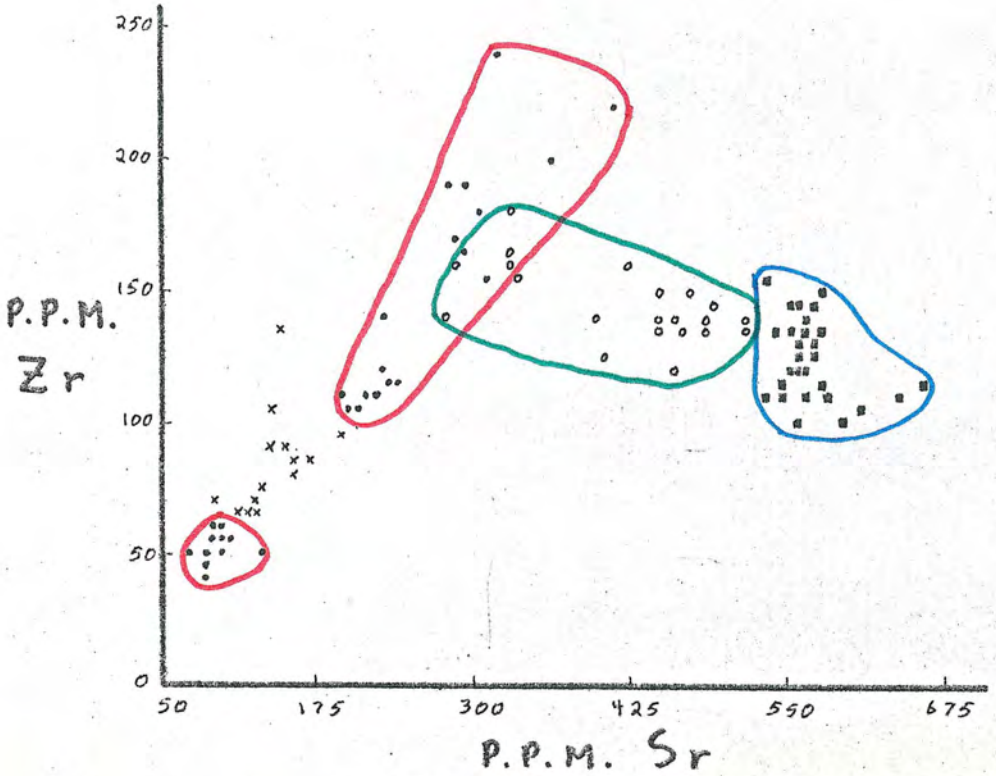
P.P.M. Zr
250
200
150
100
50
0
50
175
300
425
550
675
P.P.M. Sr

A-1-11

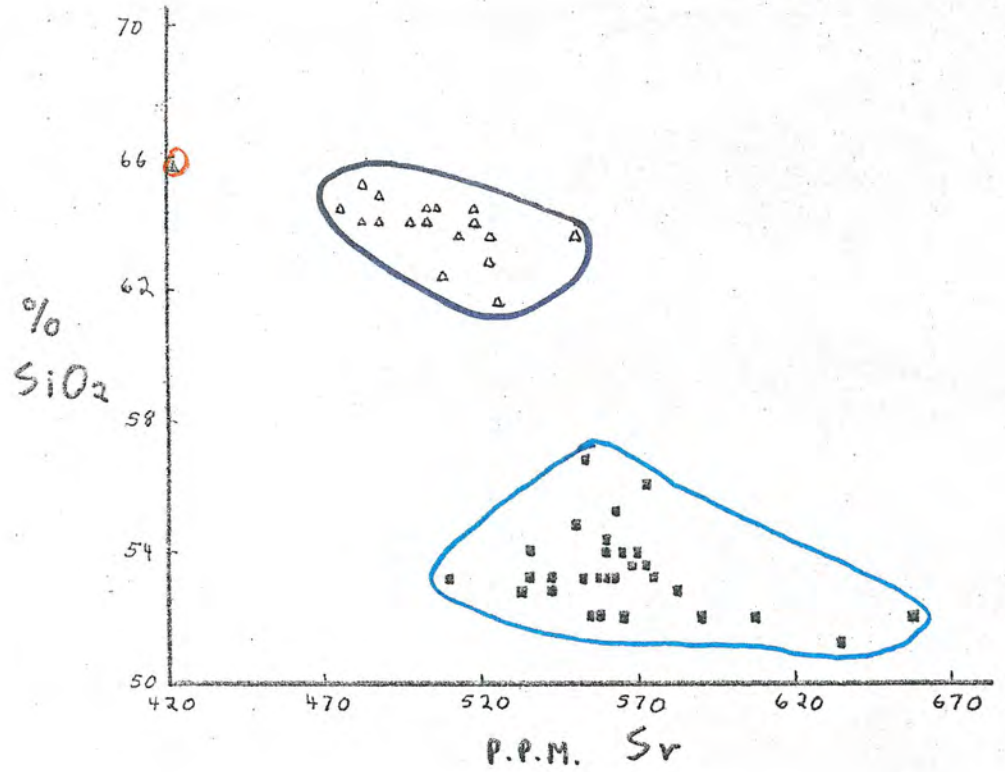
70
66
62
58
54
50
% SiO_2
420
470
520
570
620
670
P.P.M. Sr

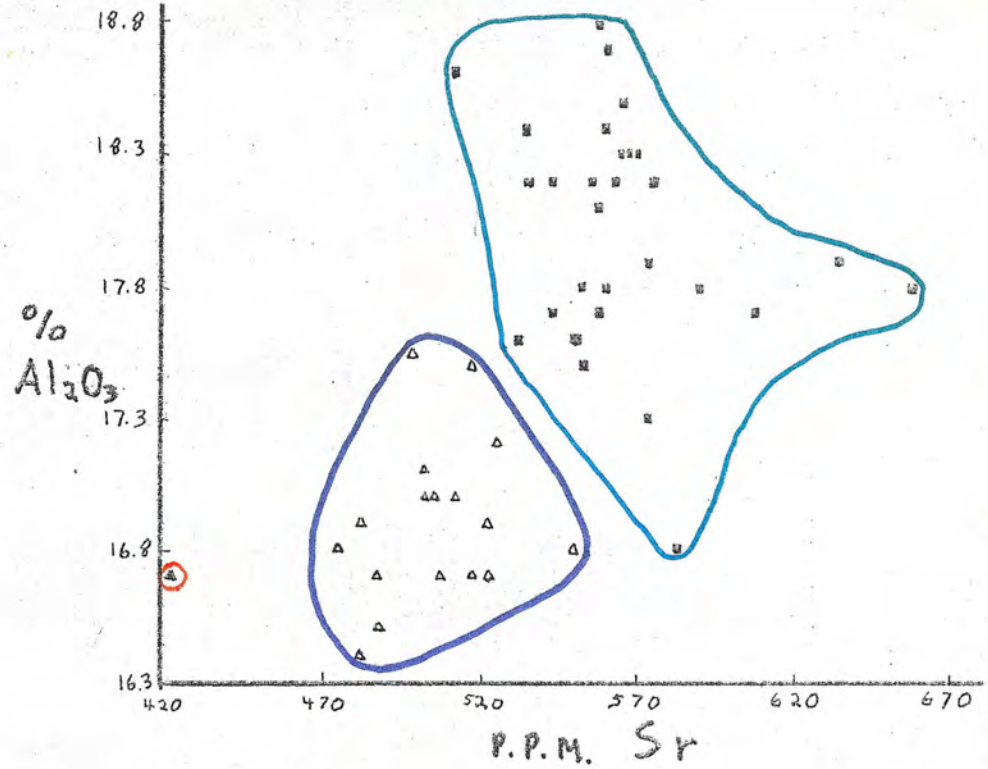
18.8
18.3
17.8
17.3
16.8
16.3
% Al_2O_3
420
470
520
570
620
670
P.P.M. Sr

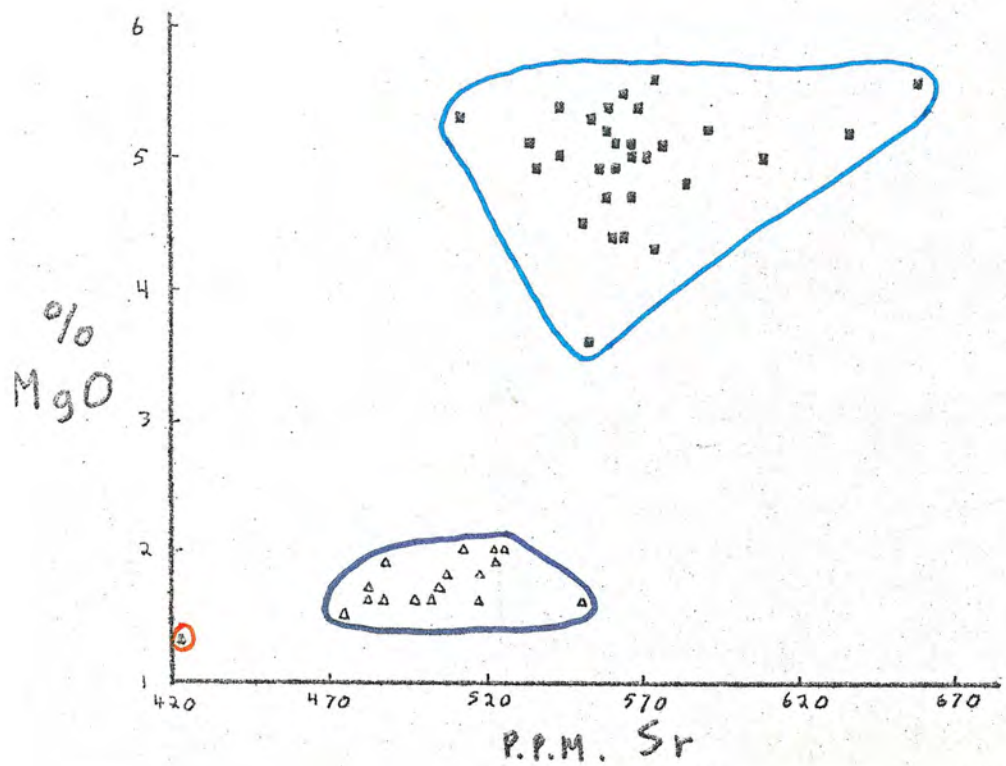
6
5
4
3
2
1
% MgO
420
470
520
570
620
670
P.P.M. Sr

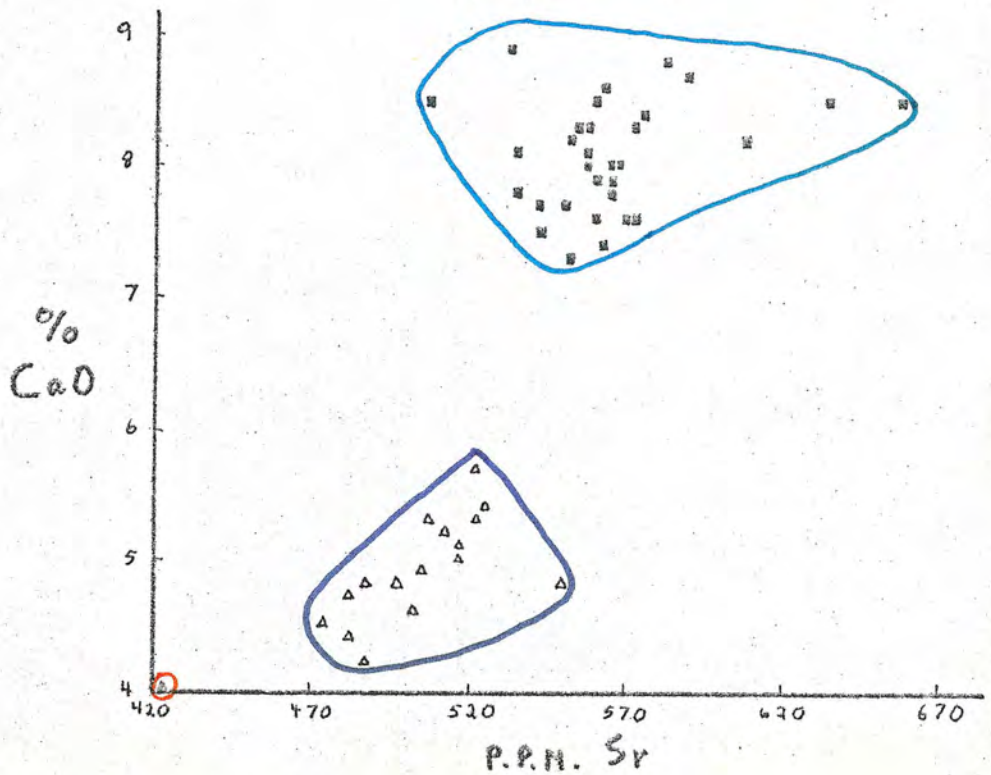
9
8
7
6
5
4
% CaO
420
470
520
570
620
670
P.P.M. Sr

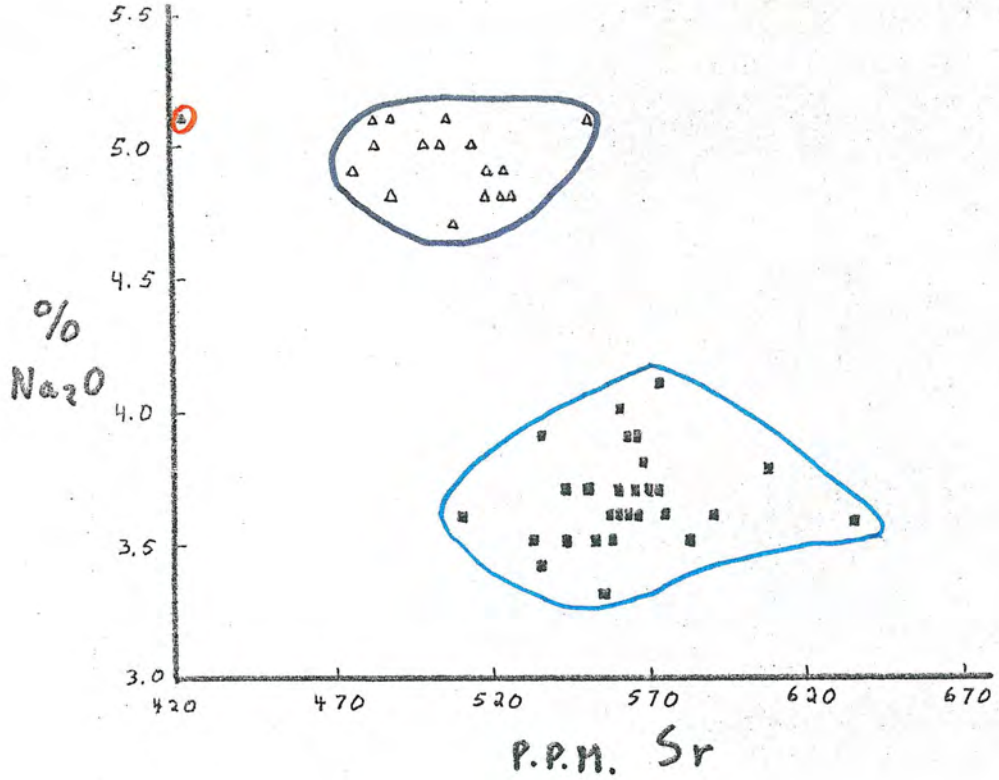
5.5
5.0
4.5
4.0
3.5
3.0
% Na_2O
420
470
520
570
620
670
P.P.M. Sr

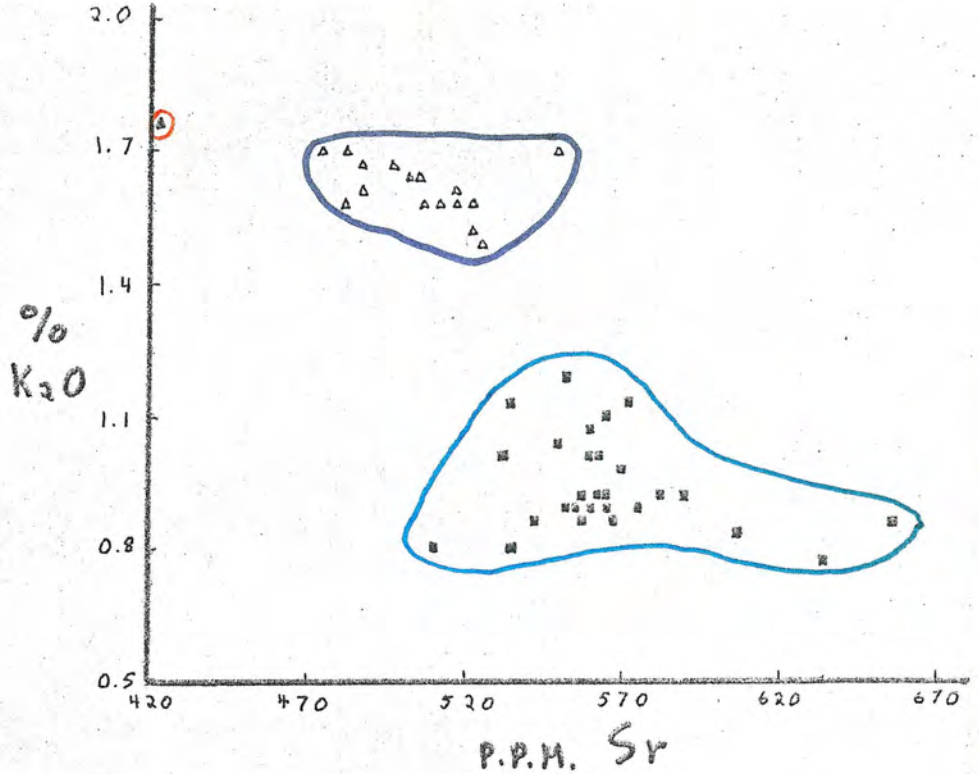
2.0
1.7
1.4
1.1
0.8
0.5
% K_2O
420
470
520
570
620
670
P.P.M. Sr

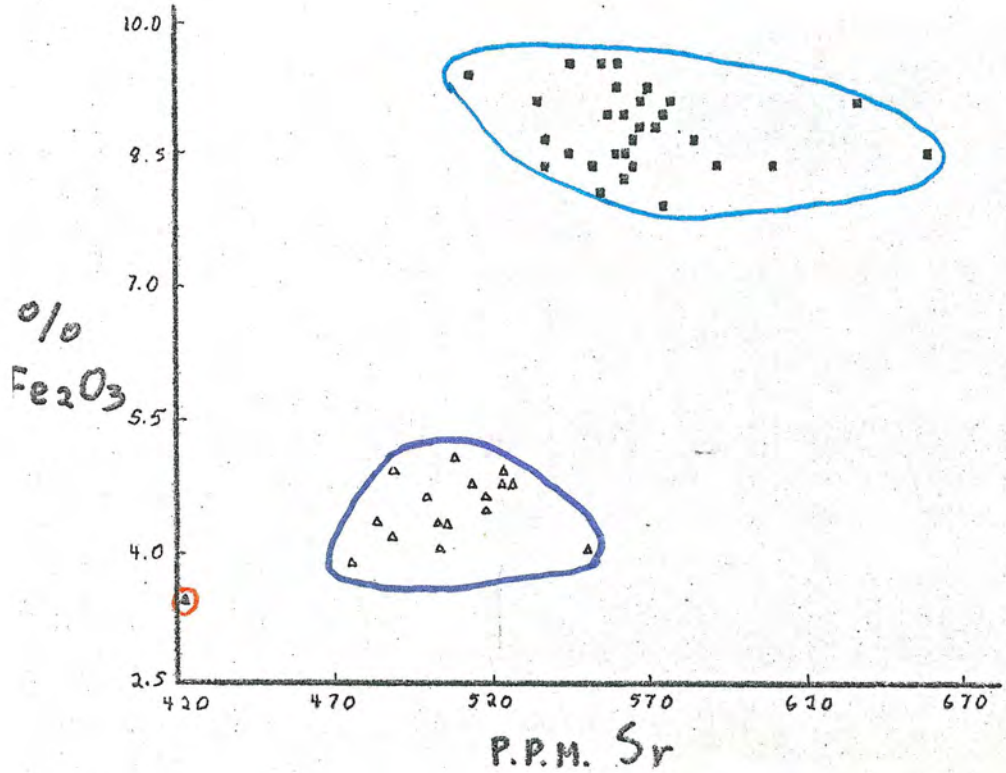
10.0
8.5
7.0
5.5
4.0
2.5
% Fe_2O_3
420
470
520
570
620
670
P.P.M. Sr

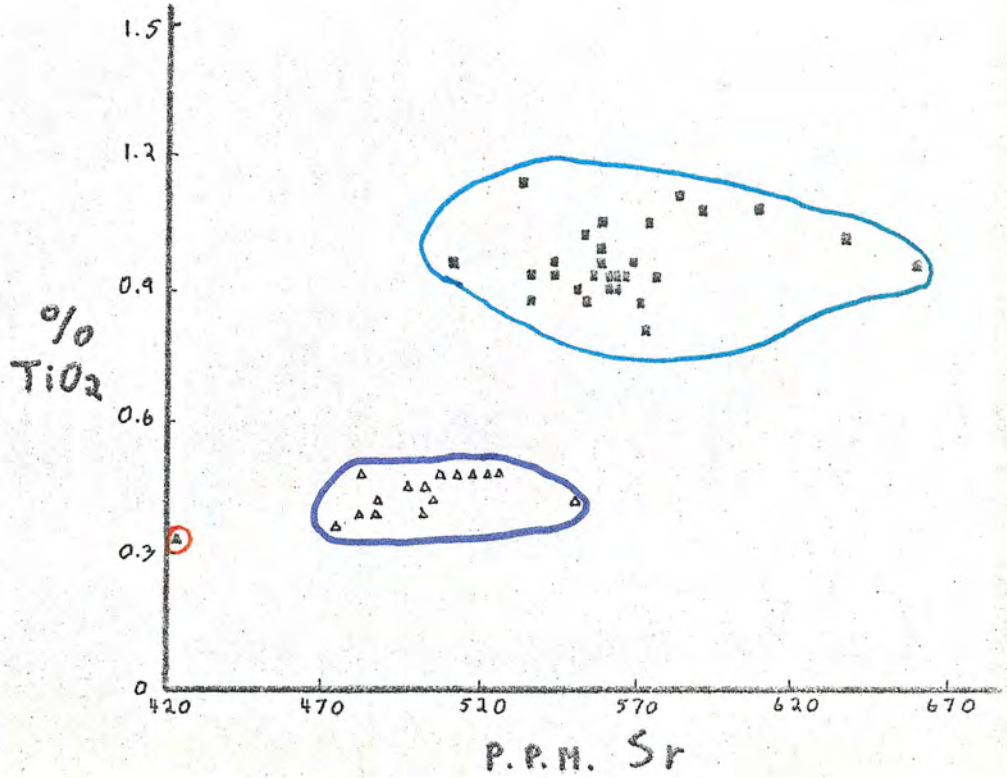
1.5
1.2
0.9
0.6
0.3
0
% TiO_2
420
470
520
570
620
670
P.P.M. Sr

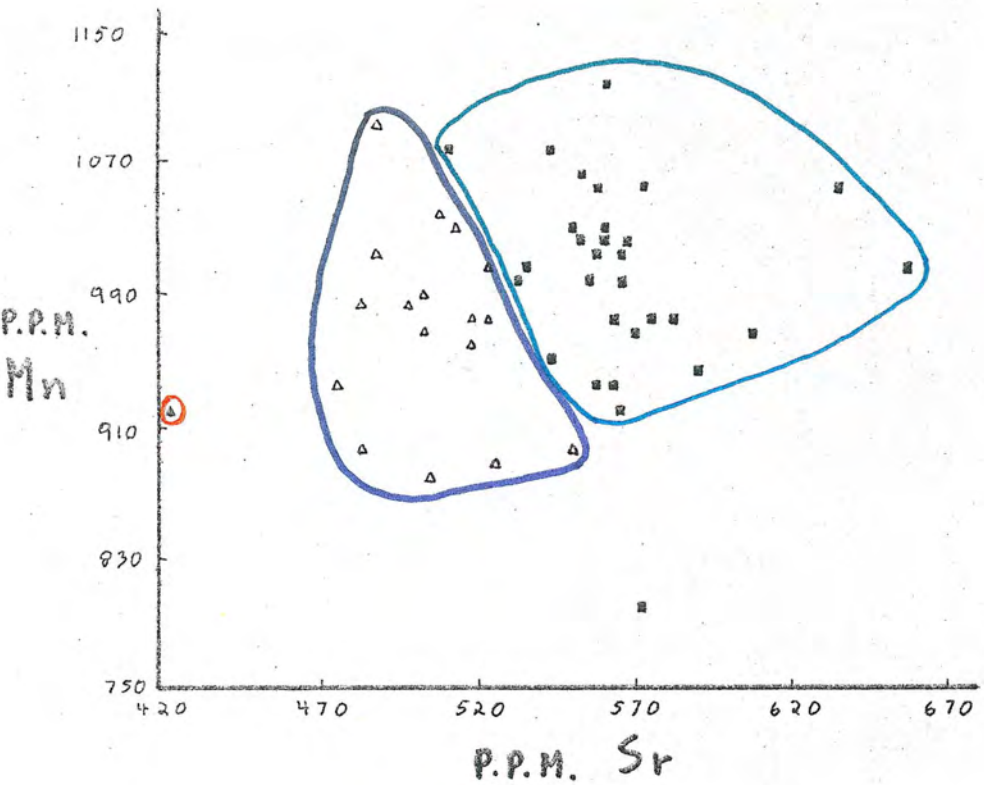
1150
1070
990
910
830
750
P.P.M.
Mn
420
470
520
570
620
670
P.P.M. Sr

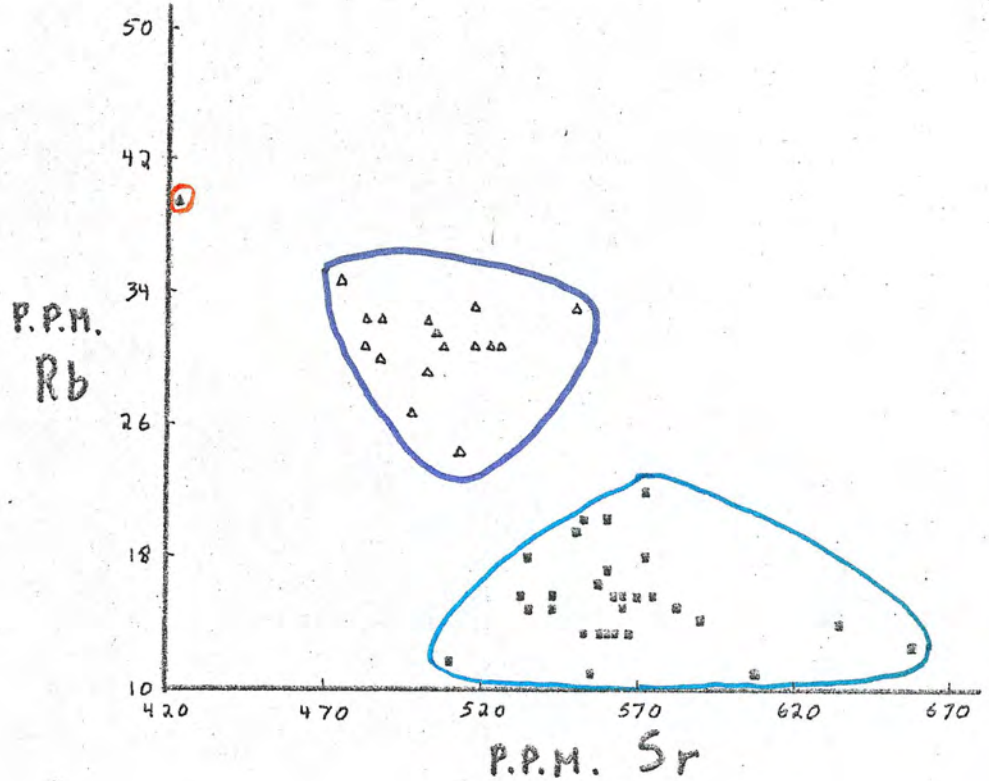
50
42
34
26
18
10
P.P.M.
Rb
420
470
520
570
620
670
P.P.M. Sr

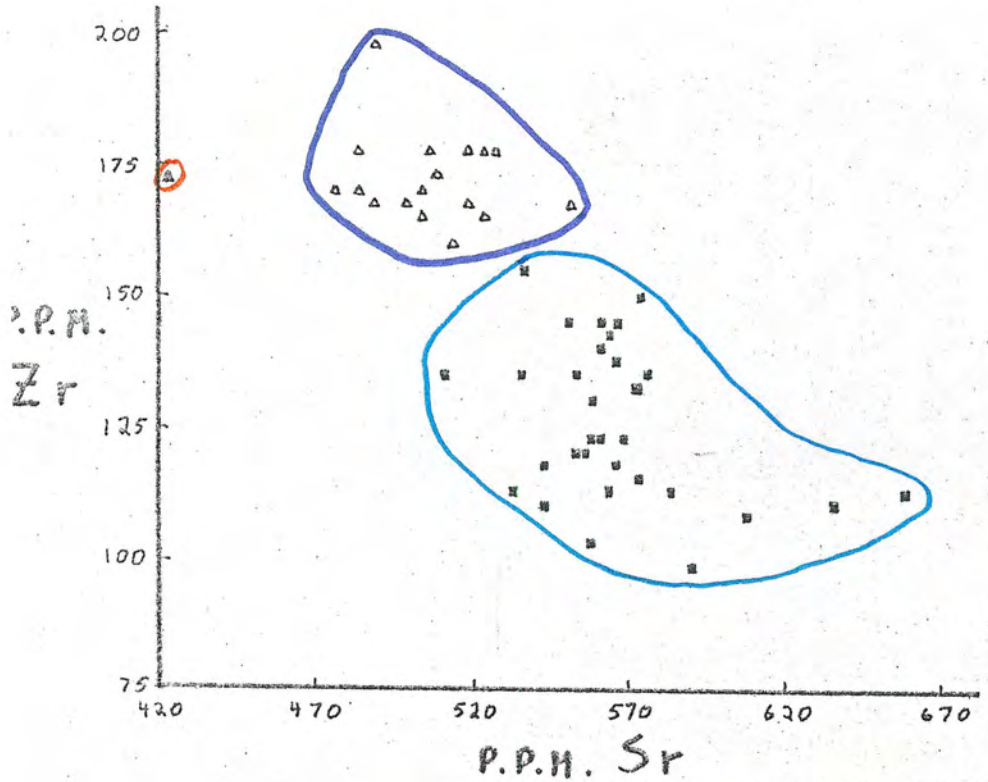
200
175
150
125
100
75
P.P.M.
Zr
420
470
520
570
620
670
P.P.M. Sr

APPENDIX II

Raw Data in Tables

STANDARD	RB	SR	ZR	NI	TI	CE	CR	MN	FE
G 1	**220**	**250**	**210**	**1.5**	**.26**	**170**	**22**	**230**	**1.96**
					.24	198	11	158	1.52
					.24	220	26	174	1.62
W 1	**22**	**190**	**100**	**78**	**1.07**	**23**	**120**	**1320**	**11.12**
	22	190	99	78	1.08	62	87	1079	10.80
	6	199	98	79	1.11	72	93	1138	10.82
	22	193	97	80	1.12	73	94	1155	10.98
	20	189	94		1.11	56	85	1062	11.14
					1.08	61	87	1129	10.87
G 2	**171**	**479**	**304**	**9.3**	**.53**	**164**	**7.9**	**262**	**2.68**
	165	485	347	8.0	.51	178	-2	240	2.88
	168	483	343	11.0	.49	290	0	239	2.86
	164	482	349	24.0	.47	232	-3	247	2.86
GSP 1	**251**	**236**	**544**	**13.5**	**.69**	**396**	**11.1**	**306**	**4.33**
	253	235	539	50	.66	404	16	314	4.37
	229	237	603	25	.70	402	12	319	4.36
					.71	353	6	294	4.19
AGV 1	**68**	**661**	**225**	**21.3**	**1.08**	**69**	**10.3**	**723**	**6.78**
	69	675	289	23	1.08	97	5	793	7.03
	69	647	277	38	1.08	203	2	634	6.93
	65	650	264	21					
	66	661	292	18					
BCR 1	**48.3**	**334**	**183**	**17**	**2.23**	**49**	**20.1**	**1353**	**13.58**
	41	327	177	16	2.46	117	20	1166	12.71
	46	328	204	32	2.49	118	20	1183	12.89
	47	323	206		2.49	114	21	1213	13.04
					2.49	114	21	1212	13.04

TABLE 1 Data for standards run as unknowns. Values from literature are shown in bold type, at the head of the column, for each standard. All concentrations are parts per million except Ti and Fe.

SAMPLE	SM 100	SM 101	SM 102	SM 103	SM 104	SM 105	SM 106	SM 107
Rock Type	Andesite	Andesite	Andesite	Andesite	Andesite	Andesite	Andesite	Andesite
SiO2 %	53.4	54.4	54.8	53.2	53.1	54.1	53.9	53.9
Al2O3 %	18.2	18.7	17.6	18.2	18.6	18.4	18.3	18.3
Fe2O3 %	9.7	8.2	8.7	8.3	8.1	8.9	8.1	8.9
MgO %	4.8	4.4	4.5	5.1	5.3	4.9	5.0	4.7
CaO %	8.1	7.9	7.7	8.4	8.4	7.8	7.6	7.9
Na2O %	3.4	3.6	3.7	3.6	3.6	3.9	3.7	3.9
K2O %	1.14	1.08	1.05	0.89	0.79	0.8	0.97	1.09
H2O %	0.9	0.9	1.0	1.5	0.8	0.9	0.5	0.5
TiO2 %	0.82	0.79	0.84	0.84	0.81	0.81	0.83	0.84
PPM Rb	17.71	20.17	19.99	15.30	11.44	15.04	15.98	15.62
PPM Sr	534.20	559.21	550.35	574.90	511.02	534.42	571.15	565.94
PPM Zr	154.94	143.94	144.97	133.87	134.67	134.13	131.36	145.82
PPM Ni	28.33	23.89	24.81	39.35	38.45	29.01	37.11	34.87
Fe2O3 %	8.38	8.55	8.38	9.05	9.44	8.71	8.79	9.10
PPM Mn	1007.00	1032.24	1032.19	971.32	1075.83	1005.18	962.65	998.46
PPM Cr	15.45	22.86	21.03	44.50	35.85	29.11	35.64	34.48
PPM Ce	102.33	108.57	115.76	96.12	87.27	106.27	91.04	101.67
TiO2 %	0.88	0.92	0.89	0.92	0.96	0.92	0.88	0.93

SAMPLE	SM 108	SM 109	SM 110	SM 111	SM 112	SM 113	SM 114	SM 115
Rock Type	Andesite	Andesite	Andesite	Andesite	Andesite	Andesite	Andesite	Andesite
SiO2 %	55.1	53.4	52.0	52.2	52.0	54.2	51.9	53.1
Al2O3 %	18.2	17.8	18.1	18.3	18.2	18.5	18.8	18.4
Fe2O3 %	8.3	8.4	9.0	8.5	8.4	8.4	8.3	8.5
MgO %	4.4	5.3	5.2	5.1	4.9	5.0	5.4	5.1
CaO %	7.4	8.2	8.1	8.0	8.3	7.8	8.0	7.6
Na2O %	3.9	3.5	3.5	3.7	3.3	3.6	3.6	3.7
K2O %	1.01	0.88	0.86	0.88	0.88	0.92	0.87	0.90
H2O %	0.8	0.8	0.8	0.9	1.2	0.9	1.1	0.5
TiO2 %	0.82	0.89	0.88	0.85	0.86	0.84	0.83	0.80
PPM Rb	15.93	13.12	13.25	14.93	11.16	15.06	13.47	13.33
PPM Sr	562.05	552.09	557.74	564.88	554.84	563.90	557.67	559.31
PPM Zr	142.29	119.42	122.63	117.76	120.51	137.32	129.04	122.05
PPM Ni	30.92	36.66	35.48	30.31	35.67	25.88	29.90	29.06
Fe2O3 %	8.65	9.57	9.31	9.12	9.01	8.82	9.48	8.97
PPM Mn	936.79	1063.99	1015.06	1014.72	995.36	915.53	1051.06	1023.92
PPM Cr	12.44	38.90	40.89	30.38	30.58	29.07	22.99	23.40
PPM Ce	91.19	101.42	85.75	94.77	84.12	94.79	81.62	94.50
TiO2 %	0.92	1.02	0.98	0.93	0.93	0.93	0.96	0.89

TABLE 2 Determinations of the top nine elements for all samples were made at Michigan Tech.

SAMPLE	SM 116	SM 117	SM 118	SM 119	SM 120	SM 121	SM 122	SM 123
Rock Type	Andesite	Andesite	Andesite	Andesite	Andesite	Andesite	Andesite	Andesite
SiO2 %	53.0	53.7	52.9	53.1	53.0	52.8	52.1	52.8
Al2O3 %	18.2	18.3	17.7	18.2	17.7	17.6	17.8	16.8
Fe2O3 %	8.2	8.3	7.2	8.2	8.2	8.7	8.2	9.8
MgO %	5.4	5.4	5.0	5.5	4.7	5.1	5.2	4.8
CaO %	7.7	8.0	7.5	8.6	8.3	8.9	8.7	8.8
Na2O %	3.7	3.8	3.5	3.6	3.5	3.5	3.6	3.5
K2O %	0.86	0.87	0.87	0.92	0.91	1.01	0.93	0.91
H2O %	0.6	0.6	0.7	0.7	1.2	0.8	1.3	0.9
TiO2 %	0.82	0.82	0.77	0.89	0.93	1.01	0.93	1.14
PPM Rb	14.68	12.90	15.41	12.95	16.30	15.84	13.79	14.68
PPM Sr	543.53	566.35	542.98	563.40	557.40	533.11	591.02	583.57
PPM Zr	116.48	122.83	110.09	111.96	102.35	111.56	98.37	111.83
PPM Ni	34.97	32.28	28.58	19.60	21.98	29.24	12.71	3.48
Fe2O3 %	9.62	9.21	8.43	8.34	8.45	9.14	8.39	8.58
PPM Mn	1079.36	1022.50	949.13	976.28	930.26	1001.87	945.77	977.85
PPM Cr	25.71	22.32	25.78	28.56	26.74	23.70	28.37	30.24
PPM Ce	84.76	78.24	82.56	99.55	87.94	82.38	94.08	78.36
TiO2 %	0.97	0.96	0.92	0.91	1.05	1.14	1.08	1.12

SAMPLE	SM 124	SM 125	SM 126	SMA 1	S 14	S 560	S 1000
Rock Type	Andesite	Andesite	Andesite	Andesite	Andesite	Andesite	Andesite
SiO2 %	52.1	52.0	51.4	56.9	53.5	54.2	56.1
Al2O3 %	17.7	17.8	17.9	17.5	17.3	17.8	17.9
Fe2O3 %	8.3	8.6	9.2	8.4			
MgO %	5.0	5.6	5.2	3.6	5.59	4.88	4.26
CaO %	8.2	8.5	8.5	7.3	8.3	8.5	7.6
Na2O %	3.8	3.4	3.6	3.5	3.7	4.0	4.1
K2O %	0.82	0.86	0.76	1.2	1.12	1.02	1.14
H2O %	1.0	1.1	0.8	1.4	0.58	0.32	0.15
TiO2 %	0.92	0.83	0.92	0.88	0.98	0.93	0.82
PPM Rb	10.69	12.44	13.94	20.30	18.24	17.23	22.31
PPM Sr	607.17	657.23	634.60	553.09	573.15	560.24	573.01
PPM Zr	107.42	113.70	109.88	136.21	115.86	140.85	150.35
PPM Ni	17.03	24.66	23.72	27.44	42.37	15.40	19.93
Fe2O3 %	8.30	8.55	9.06	8.08	8.94	8.19	7.94
PPM Mn	962.62	1008.90	1053.27	1025.30	795.66	1117.74	1052.89
PPM Cr	17.41	33.18	32.86	0.56	70.61	11.03	38.89
PPM Ce	87.86	96.12	102.00	86.98	87.74	100.20	105.13
TiO2 %	1.07	0.96	1.02	0.87	1.04	0.90	0.82

TABLE 2 Determinations of the top nine elements for all samples were made at Michigan Tech.

SAMPLE	CQ 1	CQ 4	CQ 10	CQ 11	CQ 13	CQ 14	CQ 14B	CQ 16
Rock Type	Dacite	Dacite	Dacite	Dacite	Dacite	Dacite	Dacite	Dacite
SiO2 %	63.5	61.0	61.5	64.5	64.6	64.4	61.6	62.2
Al2O3 %	16.0	16.0	16.7	15.5	16.1	15.3	15.8	16.3
Fe2O3 %	7.01	7.31	6.3	5.0	5.0	6.2	7.9	6.4
MgO %	2.48	3.35	2.6	2.2	1.9	2.1	2.4	2.6
CaO %	5.7	5.7	5.3	4.7	4.5	4.0	5.9	5.4
Na2O %	4.2	4.0	3.7	3.7	3.8	3.7	3.8	3.7
K2O %	2.07	1.89	1.8	2.1	2.1	1.7	2.0	1.7
H2O %			1.6	0.4	0.7	1.1	0.5	0.4
TiO2 %	0.68	0.7	0.6	0.5	0.5	0.4	0.6	0.5
PPM Rb	53.52	43.00	47.38	56.50	53.67	56.00	52.48	50.19
PPM Sr	442.64	460.87	454.77	401.40	453.41	440.66	467.69	514.25
PPM Zr	139.80	134.53	118.62	124.59	142.24	136.20	148.09	133.67
PPM Ni	3.88	18.84	5.51	4.98	3.93	4.62	3.69	75.72
Fe2O3 %	5.15	6.15	5.77	4.58	4.45	4.93	5.86	5.60
PPM Mn	913.43	981.51	932.15	807.05	744.29	855.69	956.06	879.33
PPM Cr	10.42	20.26	14.84	26.16	17.82	12.36	17.23	19.58
PPM Ce	21.24	25.57	57.11	54.91	35.28	12.73	38.05	60.51
TiO2 %	0.55	0.64	0.59	0.54	0.53	0.54	0.62	0.59

SAMPLE	GJ CQ 2	GJ CQ 10	GJ CQ 14	LP 1	LP 3	LP 4	LP 5	CQ 2
Rock Type	Dacite	Dacite	Dacite	Dacite	Dacite	Dacite	Dacite	Dacite
SiO2 %	61.3	64.9	63.7	71.8	72.7	70.4	71.9	65.9
Al2O3 %	15.9	13.5	15.6	14.6	15.1	14.5	14.2	14.9
Fe2O3 %	5.7	5.2	6.9	2.3	2.1	4.0	2.6	5.51
MgO %	3.04	2.63	2.85	0.7	0.7	0.7	0.7	1.88
CaO %	5.6	5.2	5.8	2.1	2.3	2.7	2.6	4.7
Na2O %	3.8	3.8	4.0	4.0	3.9	3.9	4.0	4.2
K2O %	1.8	1.9	2.0	2.4	2.4	2.8	2.9	2.45
H2O %	1.2	0.8	0.6	2.0	0.6	1.2	0.7	
TiO2 %	0.65	0.57	0.62	0.2	0.3	0.3	0.3	0.55
PPM Rb	44.85	52.74	47.18	102.04	104.26	100.03	104.74	62.62
PPM Sr	487.67	443.44	480.98	333.46	326.06	328.03	324.60	391.34
PPM Zr	142.88	149.41	139.44	156.12	162.64	177.78	158.54	137.66
PPM Ni	19.67	20.39	22.06	61.53	64.23	63.82	82.23	11.27
Fe2O3 %	5.83	5.01	5.56	2.40	2.36	2.20	2.20	3.88
PPM Mn	745.05	722.37	722.16	610.38	628.07	565.38	570.39	746.10
PPM Cr	7.20	10.92	6.38	-0.13	1.26	-0.44	-2.42	7.74
PPM Ce	96.92	133.44	109.82	15.01	57.50	22.47	30.45	18.42
TiO2 %	0.61	0.53	0.58	0.30	0.30	0.26	0.28	0.45

TABLE 2 Determinations of the top nine elements for all samples were made at Michigan Tech.

SAMPLE	CQ 3	CQ 5	LL 1	LL 2	CQ 6			
Rock Type	Dacite	Dacite	Dacite	Dacite	Dacite			
SiO2 %	69.6	69.3	63.2	62.3	63.6			
Al2O3 %	13.3	14.3	15.9	15.3	15.2			
Fe2O3 %	4.61	4.0	7.3	6.0	6.7			
MgO %	0.71	0.64	2.9	2.4	2.32			
CaO %	3.5	2.1	5.2	5.1	4.8			
Na2O %	4.2	4.2	3.9	3.9	3.9			
K2O %	3.49	3.5	2.0	1.8	2.22			
H2O %		0.9	0.3	0.3				
TiO2 %	0.42	0.3	0.7	0.6	0.68			
PPM Rb	90.73	89.24	53.15	56.3	60.06			
PPM Sr	282.51	277.63	478.21	512.19	420.85			
PPM Zr	157.82	139.48	136.97	142.33	158.52			
PPM Ni	6.31	2.19	89.10	66.57	9.12			
Fe2O3 %	1.89	2.03	5.14	5.23	4.40			
PPM Mn	542.43	548.29	671.76	769.33	726.55			
PPM Cr	-2.53	0.71	44.64	12.62	8.75			
PPM Ce	24.40	47.41	115.00	119.68	141.32			
TiO2 %	0.25	0.27	0.60	0.55	0.48			

SAMPLE								
Rock Type								
SiO2 %								
Al2O3 %								
Fe2O3 %								
MgO %								
CaO %								
Na2O %								
K2O %								
H2O %								
TiO2 %								
PPM Rb								
PPM Sr								
PPM Zr								
PPM Ni								
Fe2O3 %								
PPM Mn								
PPM Cr								
PPM Ce								
TiO2 %								

TABLE 2 Determinations of the top nine elements for all samples were made at Michigan Tech.

SAMPLE	GJCQ 2 GM	GJCQ 2 PH	GJCQ10 GM	GJCQ10 PH	GJCQ14 GM	GJCQ14 PH	CQ 4 GM	CQ 4 PH
Rock Type	Groundmass	Phenocryst	Groundmass	Phenocryst	Groundmass	Phenocryst	Groundmass	Phenocryst
SiO2 %								
Al2O3 %								
Fe2O3 %								
MgO %								
CaO %	4.9	6.8	5.1	5.9	4.3	5.6	5.5	5.8
Na2O %								
K2O %	1.8	1.0	2.3	1.4	2.3	1.5	1.8	1.2
H2O %								
TiO2 %								
PPM Rb	49.52	9.70	55.22	22.90	65.13	29.35	45.04	17.99
PPM Sr	437.47	720.17	383.49	592.03	376.90	564.31	432.20	635.18
PPM Zr	143.54	83.21	141.56	127.69	128.13	93.45	137.92	94.99
PPM Ni	23.95	11.96	30.59	12.71	33.35	15.78	19.88	21.62
Fe2O3 %	6.27	1.49	5.60	2.05	4.96	2.23	6.33	2.31
PPM Mn	866.29	182.00	906.34	334.71	777.18	352.13	899.78	316.51
PPM Cr	12.98	5.11	7.75	-10.37	11.03	-5.51	12.83	1.72
PPM Ce	101.36	99.57	97.53	102.12	98.39	80.16	101.13	103.75
TiO2 %	0.64	0.11	0.59	0.20	0.53	0.23	0.65	0.18

SAMPLE	CQ 10 GM	CQ 10 PH	CQ 11 GM	CQ 11 PH				
Rock Type	Groundmass	Phenocryst	Groundmass	Phenocryst				
SiO2 %								
Al2O3 %								
Fe2O3 %								
MgO %								
CaO %	4.9	5.3	4.9	5.3				
Na2O %								
K2O %	2.7	1.3	2.7	1.3				
H2O %								
TiO2 %								
PPM Rb	48.55	14.21	69.18	25.93				
PPM Sr	404.15	669.16	337.36	566.89				
PPM Zr	136.09	75.99	136.19	93.31				
PPM Ni	29.97	8.64	23.68	14.10				
Fe2O3 %	6.12	1.63	5.04	2.41				
PPM Mn	873.81	237.53	786.35	416.04				
PPM Cr	3.13	-1.19	20.06	1.46				
PPM Ce	89.76	93.44	117.30	97.09				
TiO2 %	0.59	0.13	0.56	0.26				

TABLE 2 Determinations of the top nine elements for all samples were made at Michigan Tech.

SAMPLE	ALM 2	ALM 3	ALM 4	CA 5	CA 6	OL 3	OL 4	OL 5
Rock Type	Pum Frag	Pum Frag	Pum Frag	Pum Frag	Pum Frag	Pum Frag	Pum Frag	Pum Frag
SiO2 %	73.7	75.7	73.5	73.4	74.0	77.20	73.90	68.5
Al2O3 %	12.8	11.6	11.6	12.0	12.6	12.30	12.80	14.3
Fe2O3 %	2.1	0.7	1.0	1.9	1.5	1.00	2.00	3.0
MgO %	0.5	0.2	0.1	0.3	0.4	0.30	0.50	0.9
CaO %	2.1	0.6	0.9	1.7	1.5	1.40	1.70	3.0
Na2O %	4.2	3.1	3.4	3.8	4.0	3.90	3.60	3.8
K2O %	2.5	4.0	5.0	3.1	2.2	2.60	2.70	2.0
H2O %	2.1	2.8		2.0	1.7	1.90	2.00	2.0
TiO2 %	0.3	0.1	0.1	0.2	0.2	0.20	0.30	0.4
PPM Rb	62.43	128.03	116.61	89.36	81.98	76.31	79.82	53.22
PPM Sr	307.50	94.48	90.01	230.15	299.47	196.49	223.81	404.44
PPM Zr	153.51	59.22	48.37	113.10	182.24	112.26	142.45	220.76
PPM Ni	15.93	28.68	30.48	8.52	9.02	4.44	3.21	3.96
Fe2O3 %	1.47	1.04	0.80	1.27	1.49	1.01	1.43	2.38
PPM Mn	482.30	699.91	564.63	591.45	545.52	406.65	533.43	620.29
PPM Cr	1.29	1.65	6.49	-0.27	0.41	1.54	-0.39	5.68
PPM Ce	67.13	65.57	34.82	35.54	64.49	22.97	29.37	72.21
TiO2 %	0.19	0.13	0.11	0.17	0.20	0.16	0.21	0.33

SAMPLE	OL 6	OL 7	RS 2	SAX 4	SC 2	SC 3	SC 4	SC 5
Rock Type	Pum Frag	Pum Frag	Pum Frag	Pum Frag	Pum Frag	Pum Frag	Pum Frag	Pum Frag
SiO2 %	76.7	74.90	68.2	75.3	72.80	76.00	72.10	74.90
Al2O3 %	11.6	12.90	14.4	11.9	11.80	12.50	13.30	12.30
Fe2O3 %	0.6	1.50	3.6	1.3	2.50	1.30	2.80	1.80
MgO %	0.1	0.40	0.8	0.2	0.10	0.30	0.40	0.30
CaO %	0.80	1.90	2.8	0.8	0.60	1.10	1.50	1.20
Na2O %	3.50	3.90	4.2	3.6	3.80	4.00	4.20	3.80
K2O %	4.00	2.40	2.4	4.4	4.90	3.40	3.00	3.60
H2O %	2.00	2.10	1.9	2.3	2.20	2.10	2.00	1.60
TiO2 %	0.10	0.20	0.4	0.2	0.20	0.20	0.30	0.20
PPM Rb	114.97	62.54	49.42	125.36	123.52	76.18	56.25	69.04
PPM Sr	100.77	281.09	311.05	75.52	76.35	203.81	273.62	220.40
PPM Zr	56.47	168.48	237.80	48.19	50.00	105.78	189.81	111.24
PPM Ni	4.89	4.95	7.10	6.97	1.82	1.21	3.47	3.13
Fe2O3 %	0.84	1.48	1.99	0.81	0.67	1.01	1.34	1.07
PPM Mn	617.32	538.02	540.09	502.05	533.08	375.31	441.38	364.55
PPM Cr	5.12	3.05	-2.77	-2.56	4.13	3.92	-8.11	-2.46
PPM Ce	62.27	73.21	189.54	51.80	53.71	96.99	150.09	94.18
TiO2 %	0.11	0.19	0.27	0.11	0.10	0.15	0.22	0.14

TABLE 2 Determinations of the top nine elements for all samples were made at Michigan Tech.

SAMPLE	SC 6	SC 7	SC 9	SC 10	SC 11	SC 12	SC 13	SFU 1
Rock Type	Pum Frag	Pum Frag	Pum Frag	Pum Frag	Pum Frag	Pum Frag	Pum Frag	Pum Frag
SiO2 %	72.80	75.70	75.70	75.00	75.50	75.30	72.20	76.5
Al2O3 %	12.80	11.90	12.10	12.40	12.90	12.30	14.20	11.8
Fe2O3 %	2.30	0.90	1.40	1.10	1.50	0.40	2.50	1.0
MgO %	0.40	0.10	0.10	0.10	0.20	0.10	0.80	0.3
CaO %	1.60	0.60	0.50	0.60	1.20	0.60	3.20	1.2
Na2O %	4.20	3.50	3.60	3.70	4.00	3.50	4.00	3.9
K2O %	3.00	4.40	4.70	4.90	2.80	4.70	2.40	2.2
H2O %	2.30	3.00	1.90	1.80	1.80	2.10	1.60	2.1
TiO2 %	0.30	0.10	0.10	0.10	0.20	0.10	0.40	0.2
PPM Rb	63.36	120.80	125.14	125.84	77.52	113.18	54.64	72.76
PPM Sr	287.97	97.23	90.17	95.54	214.06	85.77	359.02	228.43
PPM Zr	166.52	51.86	52.10	55.31	108.96	45.34	197.93	115.96
PPM Ni		5.65	4.28	5.78	2.57	5.42	3.89	3.37
Fe2O3 %	1.36	0.74	0.71	0.71	1.13	0.71	2.42	1.17
PPM Mn	454.44	506.02	507.34	546.77	370.74	498.01	592.65	357.62
PPM Cr	-3.92	-5.68	0.31	-7.83	-5.19	2.96	-2.59	-3.44
PPM Ce	131.07	47.26	60.54	54.71	88.86	63.02	156.06	102.25
TiO2 %	0.19	0.11	0.10	0.11	0.17	0.11	0.33	0.14

SAMPLE	SFU 2	SFU 3	SFU 4	TOT 7	XE 1	XE 2	XE 3	XE 4
Rock Type	Pum Frag	Pum Frag	Pum Frag	Pum Frag	Pum Frag	Pum Frag	Pum Frag	Pum Frag
SiO2 %	74.2	73.5	74.7	73.90	74.2	75.0	75.9	78.7
Al2O3 %	12.4	12.2	12.4	13.30	11.3	11.9	11.6	11.6
Fe2O3 %	1.6	1.7	1.4	3.40	0.5	1.4	0.6	0.5
MgO %	0.4	0.3	0.3	0.40	0.9	0.1	0.2	0.1
CaO %	1.6	1.6	1.5	1.50	0.6	1.0	0.7	0.6
Na2O %	3.7	3.8	3.8	3.90	3.5	3.4	3.5	3.5
K2O %	3.9	3.0	2.8	2.70	4.0	5.0	3.6	3.6
H2O %	2.2	2.4	1.2	1.90	3.0	2.3	1.8	2.4
TiO2 %	0.2	0.2	0.2	0.30	0.1	0.1	0.1	0.1
PPM Rb	91.17	72.35	74.54	62.29	119.14	103.89	110.71	108.72
PPM Sr	199.55	239.73	224.41	290.01	87.84	129.84	108.04	102.91
PPM Zr	106.43	115.13	119.24	190.99	38.50	49.34	56.93	60.49
PPM Ni	2.13	5.38	5.20	2.51	17.42	17.97	18.54	20.48
Fe2O3 %	1.16	1.22	1.14	1.74	0.70	0.82	0.87	0.80
PPM Mn	439.24	357.16	372.35	479.78	504.54	489.90	503.85	493.16
PPM Cr	-4.37	-6.49	-3.39	-1.54	-10.03	-10.22	-3.07	-5.84
PPM Ce	74.61	86.66	94.07	150.52	24.43	50.77	60.49	57.11
TiO2 %	0.15	0.16	0.15	0.24	0.10	0.12	0.13	0.11

TABLE 2 Determinations of the top nine elements for all samples were made at Michigan Tech.

SAMPLE	ALM 1	CA 4	SFU 5	SFU 6		CA 3	OL 1	OL 8
Rock Type	Pum Frag	Pum Frag	Pum Frag	Pum Frag		Bulk Pum	Bulk Pum	Bulk Pum
SiO2 %		74.6				73.2	75.20	75.20
Al2O3 %	13.4	12.8				12.3	11.50	11.30
Fe2O3 %	0.9	1.8	0.9	1.4		1.8	1.30	1.50
MgO %	1.8	0.5	0.3	0.3		0.4	0.30	0.20
CaO %	1.2		1.3	1.5		1.2	1.10	1.00
Na2O %	4.2	3.9	3.9	3.7		3.4	3.50	3.00
K2O %	3.4		2.5	2.8		3.4	4.20	4.40
H2O %	2.3	2.3				2.2	3.20	2.20
TiO2 %	0.2	0.2	0.1	0.2		0.2	0.20	0.20
PPM Rb	52.06	86.07	77.67	81.12		150.68	114.71	125.78
PPM Sr	411.93	282.45	213.17	226.57		138.74	116.23	114.53
PPM Zr	214.72	200.14	119.47	106.26		103.81	67.29	65.93
PPM Ni	18.99	10.80	1.09	2.18		14.01	5.27	6.07
Fe2O3 %	3.24	1.64	1.11	1.19		1.74	1.10	1.17
PPM Mn	685.18	552.08	355.44	351.93		664.12	580.43	693.73
PPM Cr	7.35	-3.53	2.62	-8.22		5.98	3.88	0.64
PPM Ce	74.85	38.00	98.87	89.96		15.38	15.50	5.23
TiO2 %	0.37	0.21	0.14	0.16		0.21	0.16	0.17

SAMPLE	SAX 1	SC 1	SJO 1	SJO 2	SJO 5	TOT 1	TOT 2	TOT 3
Rock Type	Bulk Pum	Bulk Pum	Bulk Pum	Bulk Pum	Bulk Pum	Bulk Pum	Bulk Pum	Bulk Pum
SiO2 %	75.1	73.40	71.60	72.80	75.20	72.40	73.40	75.00
Al2O3 %	12.5	12.40	12.90	12.90	12.80	12.90	12.90	12.90
Fe2O3 %	1.6	1.80	2.00	1.80	1.50	2.40	2.00	1.80
MgO %	0.2	0.30	0.40	0.40	0.20	0.40	0.30	0.30
CaO %	1.1	0.80	1.30	1.50	0.90	1.20	1.00	0.90
Na2O %	3.5	3.60	3.70	3.50	3.50	4.40	3.70	3.80
K2O %	4.4	4.80	4.20	3.50	4.20	3.60	3.80	3.50
H2O %	2.1	1.70	3.00	2.40	2.50	2.00	1.60	1.80
TiO2 %	0.1	0.10	0.20	0.10	0.20	0.30	0.20	0.20
PPM Rb	118.02	125.87	113.13	106.11	115.43	116.23	108.98	109.75
PPM Sr	123.29	124.17	142.81	154.47	96.39	196.30	165.74	155.91
PPM Zr	71.04	66.47	133.26	81.83	69.05	92.67	86.09	84.76
PPM Ni	0.14	3.06	5.76	6.29	6.09	16.13	5.35	12.86
Fe2O3 %	1.05	1.12	1.38	1.59	1.23	1.77	1.42	1.38
PPM Mn	512.07	559.38	651.63	646.81	587.23	518.09	532.13	519.23
PPM Cr	-5.15	-0.36	-1.05	5.01	3.92	-8.02	-0.09	-1.36
PPM Ce	56.92	72.89	25.40	45.42	63.51	59.52	68.51	70.67
TiO2 %	0.14	0.15	0.17	0.19	0.15	0.21	0.18	0.17

TABLE 2 Determinations of the top nine elements for all samples were made at Michigan Tech.

SAMPLE	TOT 4	TOT 5	TOT 6		AL 1	AL 2	AL 3	AL 4
Rock Type	Bulk Pum	Bulk Pum	Bulk Pum		Air Pum	Air Pum	Air Pum	Air Pum
SiO2 %	74.40	72.60	75.80		62.0	63.1	62.6	72.7
Al2O3 %	12.90	12.80	12.80		17.2	15.2	17.6	11.8
Fe2O3 %	1.50	2.10	1.50		6.7	5.6	5.8	1.5
MgO %	0.30	0.30	0.30		0.9	1.2	0.9	0.3
CaO %	0.90	0.80	0.80		4.0	3.9	3.5	1.6
Na2O %	3.90	3.90	3.70		4.1	4.4	4.5	2.7
K2O %	4.20	3.70	3.90		1.8	2.3	2.4	3.9
H2O %	2.40	2.30	1.60		1.6	3.6	3.6	5.0
TiO2 %	0.20	0.20	0.20		0.5	0.4	0.4	0.3
PPM Rb	111.90	116.54	116.13		93.01	96.61	51.68	151.70
PPM Sr	150.23	131.48	138.33		524.10	398.27	468.31	199.31
PPM Zr	88.56	74.90	89.37		215.06	174.85	174.27	127.82
PPM Ni	9.60	7.24	4.85		11.03	9.38	0.60	5.45
Fe2O3 %	1.26	1.24	1.33		3.41	3.41	2.92	1.68
PPM Mn	520.73	527.36	517.72		844.60	769.83	1034.80	483.75
PPM Cr	7.58	-1.41	-0.56		9.31	7.53	4.81	-0.17
PPM Ce	81.15	58.83	68.24		77.05	34.81	38.00	37.21
TiO2 %	0.16	0.16	0.18		0.43	0.41	0.32	0.22

SAMPLE	AL 5	SJO 3	SJO 4					
Rock Type	Air Pum	Air Pum	Air Pum					
SiO2 %	70.8	71.70	74.20					
Al2O3 %	13.8	13.60	12.70					
Fe2O3 %	2.4	1.90	1.70					
MgO %	0.4	0.5	0.10					
CaO %	2.4	1.80	1.10					
Na2O %	3.7	3.00	3.70					
K2O %	3.4	3.70	3.80					
H2O %	2.1	3.80	3.60					
TiO2 %	0.3	0.20	0.10					
PPM Rb	183.80	121.48	108.36					
PPM Sr	295.81	207.33	125.53					
PPM Zr	119.95	118.41	45.12					
PPM Ni	6.30	7.44	6.49					
Fe2O3 %	1.69	2.03	0.85					
PPM Mn	505.28	578.29	574.09					
PPM Cr	-0.65	-1.08	2.16					
PPM Ce	14.65	33.24	21.00					
TiO2 %	0.21	0.24	0.11					

TABLE 2 Determinations of the top nine elements for all samples were made at Michigan Tech.

SAMPLE	S 550	S 800	S 802	S 1003	S 1004	S 1005	S 1023	S 1101
Rock Type	Dacite	Dacite	Dacite	Dacite	Dacite	Dacite	Dacite	Dacite
SiO2 %	64.4	64.1	64.3	64.0	64.8	63.8	61.8	63.92
Al2O3 %	17.0	16.9	17.0	17.1	16.7	16.9	17.2	17.54
Fe2O3 %								
MgO %	1.67	1.7	1.56	1.57	1.58	2.03	1.97	1.62
CaO %	4.9	4.7	4.6	4.6	4.2	5.3	5.4	4.8
Na2O %	5.1	5.1	5.0	5.0	5.1	4.8	4.8	4.99
K2O %	1.64	1.59	1.64	1.63	1.66	1.53	1.48	1.68
H2O %	0.26	0.34	0.2	0.31	0.41	0.25	0.2	0.15
TiO2 %	0.45	0.48	0.42	0.4	0.39	0.53	0.53	0.43
PPM Rb	31.65	32.73	32.36	28.98	32.36	30.81	30.66	27.05
PPM Sr	504.56	482.93	502.39	501.98	487.55	521.54	524.92	496.71
PPM Zr	177.51	170.79	171.24	164.46	166.88	177.15	178.23	167.87
PPM Ni	3.85	5.24	2.72	1.77	9.96	6.25	1.26	6.85
Fe2O3 %	4.27	4.36	4.31	4.05	4.19	4.95	4.77	4.54
PPM Mn	879.95	982.91	987.04	966.77	1013.45	975.44	888.88	978.70
PPM Cr	11.77	-2.21	2.36	-3.44	16.16	7.12	-0.69	-2.43
PPM Ce	143.03	145.51	137.51	144.29	152.85	144.36	125.76	137.28
TiO2 %	0.42	0.47	0.44	0.40	0.38	0.49	0.49	0.45

SAMPLE	S 1102	S 1103	S 1104	S 1105	S 1106	S 1125	S 1229	S 1511
Rock Type	Dacite	Dacite	Dacite	Dacite	Dacite	Dacite	Dacite	Dacite
SiO2 %	63.6	62.5	65.0	62.8	64.0	64.3	63.86	63.5
Al2O3 %	16.8	16.7	16.4	16.7	16.5	16.8	17.5	17.0
Fe2O3 %								
MgO %	1.61	1.85	1.62	1.93	1.88	1.48	1.65	1.97
CaO %	4.8	5.3	4.4	5.7	4.8	4.5	4.99	5.2
Na2O %	5.1	4.7	5.0	4.9	4.8	4.9	4.89	5.0
K2O %	1.7	1.58	1.7	1.58	1.6	1.7	1.59	1.58
H2O %	0.25	0.36	0.30	0.34	0.25	0.42	0.16	0.8
TiO2 %	0.46	0.51	0.41	0.55	0.42	0.36	0.43	0.49
PPM Rb	33.51	30.50	30.51	31.18	30.24	35.20	31.04	24.66
PPM Sr	550.18	508.68	482.83	522.66	486.76	475.78	518.03	512.60
PPM Zr	167.64	173.21	178.47	165.49	197.42	169.16	167.49	158.83
PPM Ni	10.08	11.82	15.01	11.48	7.26	12.12	8.42	4.35
Fe2O3 %	3.98	5.11	4.28	4.81	4.84	3.88	4.61	4.69
PPM Mn	893.22	1035.44	890.62	1009.17	1094.52	931.44	973.90	1031.50
PPM Cr	7.20	10.59	16.91	13.17	4.80	2.13	3.43	9.37
PPM Ce	142.39	116.90	124.04	132.33	149.12	138.86	134.35	119.97
TiO2 %	0.42	0.48	0.40	0.47	0.43	0.36	0.47	0.47

TABLE 2 Determinations of the top nine elements for all samples were made at Michigan Tech.

SAMPLE	S 1669	S 1115		RS 1	S 1118	CQ 15	OL 2	LP 2
Rock Type	Dacite	1902 pumice		Bulk pumice	Andesite	Dacite float	Granite	Xenolith
SiO2 %	64.3	65.7		70.8	54.9	56.0	76.9	54.6
Al2O3 %	16.7	16.7		12.6	17.4	16.4	12.5	15.2
Fe2O3 %				3.8		8.5	1.90	9.7
MgO %	1.83	1.35		0.2	5.58	4.8	0.3	3.4
CaO %	5.1	4.0		3.6	7.7	7.1	0.8	8.6
Na2O %	4.8	5.1		3.7	3.7	3.4	3.6	3.6
K2O %	1.62	1.76		1.9	1.14	1.2	4.4	1.4
H2O %	0.38	0.72		1.8	0.5	0.7	1.2	1.0
TiO2 %	0.48	0.35		0.4	0.97	0.8	0.3	1.0
PPM Rb	33.19	39.54		107.75	21.84	24.30	156.03	31.74
PPM Sr	517.47	421.70		166.56	662.33	555.87	73.07	601.04
PPM Zr	177.12	172.38		59.83	168.72	119.41	182.27	106.17
PPM Ni	5.85	4.27		20.23	40.63	12.60	8.06	67.29
Fe2O3 %	4.48	3.43		0.97	8.57	7.83	1.40	7.78
PPM Mn	961.01	915.58		467.44	1013.82	1073.22	415.48	977.97
PPM Cr	-4.48	2.41		1.06	74.79	61.72	-4.73	16.46
PPM Ce	119.73	143.36		75.15	99.64	33.62	38.42	117.79
TiO2 %	0.48	0.34		0.14	0.90	0.86	0.25	0.83

SAMPLE	S 1120	S 1401			SO 1A	SO 1B	SO 2	SO 3
Rock Type	Inclusion	Basement			Andesite	Andesite	Andesite	Andesite
SiO2 %	59.0	55.8			59.8	63.6	54.3	57.2
Al2O3 %	18.0	15.9			18.2	16.8	18.0	16.6
Fe2O3 %					5.2	5.1	7.9	8.5
MgO %	3.0	4.7			1.6	1.6	3.9	3.1
CaO %	7.0	7.6			5.0	4.8	7.6	6.9
Na2O %	4.4	3.5			3.7	4.1	3.5	3.4
K2O %	1.28	2.02			3.0	1.9	1.3	2.2
H2O %	0.25	0.75			1.5	1.2	0.7	1.2
TiO2 %	0.84	0.9			0.6	0.5	0.8	0.8
PPM Rb	24.44	56.50			61.62	32.15	25.13	42.92
PPM Sr	544.87	331.06			416.77	420.68	597.25	457.83
PPM Zr	140.70	147.06			216.27	223.33	159.17	176.15
PPM Ni	6.87	46.58			26.41	25.09	47.80	20.95
Fe2O3 %	6.85	9.93			4.32	4.76	7.87	6.37
PPM Mn	946.44	1262.89			774.70	782.50	933.47	936.81
PPM Cr	7.40	62.38			5.71	3.40	85.09	15.53
PPM Ce	112.39	101.66			65.53	51.59	53.70	62.14
TiO2 %	0.85	0.95			0.52	0.56	0.90	0.76

TABLE 2 Determinations of the top nine elements for all samples were made at Michigan Tech.